Role of the H^+-Activated Ovarian Cancer G Protein-Coupled Receptor 1 (OGR1) in the Renal Handling of Calcium and Magnesium

Dissertation

zur

Erlangung der naturwissenschaftlichen Doktorwürde

(Dr. sc. nat.)

vorgelegt der Mathematisch-naturwissenschaftlichen Fakultät

der Universität Zürich

von

Chahira BENABBAS

Aus Algerien

Promotionskomitee:

Prof. Dr. Carsten A. WAGNER

Prof. Dr. Jürg BIBER

Prof. Dr. Johannes LOFFING

Prof. Dr. Dominique Eladari

Zürich 2009

TABLE OF CONTENTS

SUMMARY

Calcium and magnesium are of central importance for multiple essential physiological functions including muscle contraction and relaxation, neuronal excitability, bone formation, and enzymatic activity. Consequently, the body calcium and magnesium concentrations are tightly controlled by the intestine, kidney, and bone. It is well known that acid-base homeostasis affects the renal handling of the divalents calcium and magnesium, thus, chronic metabolic acidosis is associated with the development of hypercalciuria, hypermagnesuria, hypocalcemia, and hypomagnesemia. However, the molecular sensor triggering the renal wasting of calcium and magnesium during this disturbance of acid-base balance has remained unknown.

The Ovarian cancer G-protein coupled Receptor 1 OGR1 (GPR68) is activated by extracellular protons and stimulates intracellular inositol-tris-phosphate (IP_3) production and intracellular Ca^{2+} rises. Interestingly, we detected OGR1 mRNA expression in the kidney in most nephron segments including the thick ascending limb and distal tubule, major sides of regulated calcium and magnesium reabsorption. The aim of the present project, therefore, was to investigate the physiological role of OGR1 which has remained elusive to date. Focusing mainly on the kidney we tested for a potential role of this proton sensor receptor in the renal calcium and magnesium handling, and evaluated its contribution to altered calcium and magnesium excretion during chronic metabolic acidosis.

In the first part of my PhD project, we investigated the potential role of OGR1 in acid-base and electrolyte homeostasis during NH_4Cl-induced metabolic acidosis using OGR1 deficient mice.

Ogr1$^{-/-}$ mice demonstrated that OGR1 is dispensable for normal acid-base status and adaptation to an acute (1 day NH_4Cl) or chronic (7 days NH_4Cl) acid-load. Interestingly, during acidosis, wild-type mice developed renal calcium and magnesium losses which were absent from *Ogr1*$^{-/-}$ mice. Bone morphology and in vitro reabsorptive activity of osteoclasts from *Ogr1*$^{+/+}$ and *Ogr1*$^{-/-}$ mice were similar. We also found that OGR1 does not regulate expression levels of the major renal proteins involved in regulated renal

calcium and magnesium reabsorption, calbindin-D_{28K}, TRPV5 and TRPM6. Ablation of OGR1, however, prevented the internalization of TRPV5 from the luminal membrane during acidosis. Our data suggest that stimulation of OGR1 is responsible for the internalization of the TRPV5 calcium channel and urinary calcium wasting during metabolic acidosis. Therefore, OGR1 may represent a novel target for the treatment of renal osteodystrophy.

Under normal conditions, analysis of different urinary electrolytes in the *Ogr1*$^{-/-}$ mice did not show any differences compared to the wild-type animals, however, urinary magnesium excretion was strongly reduced, and a tendency to a lower urinary calcium excretion was observed in the *Ogr1*$^{-/-}$ mice. Therefore we aimed in the second part of this project to further investigate the contribution of OGR1 to the regulation of renal calcium and magnesium handling using different calcium and magnesium diets.

Ogr1$^{-/-}$ mice showed an altered renal excretion of magnesium after 2 and 7 days high calcium diet, and 7 days low calcium diet. Similarly, ablation of OGR1 altered urinary magnesium excretion when animals were treated with high magnesium diet for 7 days. Interestingly, we demonstrated that loss of OGR1 affected TRPM6 magnesium channel mRNA expression in the kidney in response to 2 and 7 days low and high calcium diets. However, normal intestinal TRPM6 mRNA expression was found in the *Ogr1*$^{-/-}$ mice during the same conditions. These preliminary results suggest that OGR1 may be involved in the renal regulation of the magnesium channel TRPM6 and therefore may have a role in the renal regulation of Mg^{2+} balance. Thus, whereas the presented data demonstrated that OGR1 affects active magnesium reabsorption, future experiments will have to investigate the exact mechanism by which OGR1 affects TRPM6 expression in the kidney.

Finally, using different calcium and magnesium diets, preliminary results demonstrated that loss of OGR1 lead to significant changes in the urinary Ca^{2+} excretion, suggesting that OGR1 could also be also involved in renal calcium handling.

In summary, using OGR1 deficient mice, we demonstrate in contrast to all expectations that there is no obvious role for OGR1 in osteoclast activation in vivo and no role in maintaining or controlling systemic acid-base status and renal acid excretion. However, we show that OGR1 is responsible for

increasing renal calcium and magnesium excretion during acidosis and that stimulation of OGR1 is responsible for the internalization of the TRPV5 calcium channel and urinary calcium wasting during metabolic acidosis. And finely, we demonstrate that OGR1 may be involved in the control of the renal handling of magnesium and calcium.

DEUTSCHE ZUSAMMENFASSUNG DER DOKTORARBEIT

Kalzium und Magensium sind von zentraler Bedeutung für eine Vielzahl von physiologischen Vorgängen, u.a. Muskelkontraktion und –relaxation, neuronale Erregbarkeit, Knochenbildung oder Enzymfunktion. Die Konzentration von Kalzium und Magnesium werden daher sehr genau kontrolliert und reguliert sowohl durch den Dünndarm, die Niere als auch Knochen. Die Tatsache, dass der Säure-Basenstatus die Ausscheidung von Kalzium und Magneisum beeinflusst, ist seit langem bekannt. Metabolische Azidose ist mit der Entwicklung von Hyperkalziurie, Hypermagnesurie, Hypokalzämie und Hypomagnesämie verbunden. Der genaue molekulare Mechanismus durch den ein gestörter Säure-Basenhaushalt die vermehrte Ausscheidung von Kalzium und Magnesium durch die Niere verursacht ist bislang allerdings unbekannt.

Der OGR1 Rezeptor (GPR68, Ovarian cancer G protein coupled receptor 1) wird durch extrazelluläre Protonen aktiviert und stimuliert die intrazelluläre Produktion von Inositoltriphosphat (IP_3) sowie einen Anstieg des intrazellulären Kalziums. Wir konnten OGR1 mRNA Expression in der Niere in den meisten Nephronabschnitten detektieren inklusive der dicken aufsteigenden Henle'schen Schleife und dem distalen Konvolut, wichtigen Nephronabschnitte der regulierten Reabsorption von Kalzium und Magnesium. Es war daher das Ziel der vorliegenden Arbeit die physiologische Rolle von OGR1, die bislang gänzlich unbekannt ist, zu untersuchen. Wir haben uns dabei vorallem auf die Niere konzentriert und eine mögliche Rolle von OGR1 in der Ausscheidung von Kalzium und Magnesium und deren Veränderungen während metabolischer Azidose untersucht.

Im ersten Teil der Arbeit untersuchten wir die mögliche Rolle von OGR1 in der Säure-Basen- und Elektrolythomöostase unter basalen Bedingungen und während einer mit NH_4Cl induzierten metabolischen Azidose in OGR1 defizienten Mäusen. *Ogr1*$^{-/-}$ Mäuse zeigten, dass OGR1 für einen normalen Säure-Basenstatus und für die Adaptation an eine akute (1 Tag NH_4Cl) oder chronische (7 Tage NH_4Cl) Säurebeladung nicht benötigt wird. Allerdings entwickelten die Wildtypmäuse einen vermehrten renalen

Kalzium- und Magnesiumverlust, der in *Ogr1*$^{-/-}$ Mäusen nicht eintrat. Knochendichte und in vitro Reabsorptionskapazität von Osteoklasten war bei *Ogr1*$^{+/+}$ und *Ogr1*$^{-/-}$ Mäusen ähnlich. Ausserdem konnten wir auch zeigen, dass OGR1 nicht die Expression der wichtigsten renalen Proteine (Calbindin-D_{28K}, TRPV5 und TRPM6), die an der Kalzium- und Magnesiumresorption beteiligt sind, verändert. Die genetische Ausschaltung von OGR1 verhinderte aber die Internalisierung des TRPV5 Kalziumkanals während metabolischer Azidose in den Knock-out Mäusen. Unsere Daten deuten daher darauf hin, dass die Stimulation von OGR1 (mit)verantwortlich ist für die Internalisierung von TRPV5 und damit für den renalen Kalziumverlust. OGR1 könnte daher ein neues Ziel für die Behandlung der renalen Osteodystrophie darstellen.

Unter normalen Bedingungen zeigte die Urinanalyse in den *Ogr1*$^{-/-}$ Mäusen keine Veränderungen im Vergleich zu Wildtypmäusen ausser dass die renale Ausscheidung von Magnesium stark reduziert war und Kalzium eine Tendenz zu niedrigerer Ausscheidung zeigte. Wir versuchten daher im zweiten Teil der Arbeit den Beitrag von OGR1 zur Regulation der renalen Kalzium- und Magnesiumausscheidung mit Hilfe verschiedener Kalzium- und Magnesiumdiäten weiter zu untersuchen. *Ogr1*$^{-/-}$ Mäuse zeigten eine veränderte Magnesiumausscheidung nach 2 und 7 Tagen Hochkalziumdiät und 7 Tagen Niedrigkalziumdiät. Aehnlich verursachte die genetische Ausschaltung von OGR1 auch eine veränderte Magnesiumausscheidung bei einer Hochmagnesiumdiät für 7 Tage. Wir konnten zeigen, dass die Abwesenheit von OGR1 die Expression des Magnesiumkanals TRPM6 in der Niere verändert, interessanterweise auch nach 2 und 7 Tagen Kalziumdiäten. Im Darm blieb die Expression von TRPM6 normal. Diese vorläufigen Ergebnisse deuten an, dass OGR1 den TRPM6 Kanal reguliert und damit eine wichtige Rolle in der Kontrolle der renalen Magnesiumausscheidung haben könnte. Weitere Experimente sind notwendig um den genauen Mechanismus über den OGR1 TRPM6 reguliert aufzudecken. Darüberhinaus zeigten die verschiedenen Kalzium- und Magnesiumdiäten auch eine veränderte Kalziumausscheidung, ein möglicher Hinweis darauf, dass OGR1 eventuell auch die Ausscheidung von Kalzium beeinflusst.

Zusammenfassend lässt sich sagen, dass wir zeigen können, dass OGR1 im Gegensatz zu allen Erwartungen keine Rolle spielt in der Aktivierung von Osteoklasten in vivo und in vitro und auch keine wichtige Funktion hat in der Regulation der renalen Säure-Basenausscheidung und des systemischen Säure-Basenhaushaltes. Wir zeigen aber, dass OGR1 verantwortlich ist für die vermehrte renale Kalzium- und Magnesiumausscheidung während Azidose und dass die Stimulation von OGR1 zur Internalisierung von TRPV5 führt. Ausserdem zeigen wir, dass OGR1 eventuell an der Kontrolle der renalen Kalzium- und Magnesiumausscheidung beteiligt ist.

1. INTRODUCTION

Acid-base status affects the renal handling of calcium and magnesium (35; 50; 54; 55; 103). Clinical disorders such as distal renal tubular acidosis and renal failure result in chronic metabolic acidosis often associated with increased renal calcium and magnesium loss. In addition, hypercalciuria in these states may contribute to loss of calcium from bone resulting in the development of metabolic bone disease, such as osteopenia and osteoporosis, and often causes renal calcification and deterioration of kidney function (56). Nijenhuis *et al*. reported that chronic metabolic acidosis is associated with decreased renal expression of the epithelial calcium and magnesium channels TRPV5 and TRPM6 leading to the development of hypercalciuria and hypomagnesemia (54). However, the molecular pH sensor that triggers these renal calcium and magnesium loss has not been identified to date.

Recently, OGR1 (ovarian cancer G-protein-coupled receptor 1, GPR68) has been described as a proton sensing receptor (5), OGR1 mRNA expression is wide-spread in most organs including major organs involved in maintaining calcium and magnesium homeostasis such as bone and kidney. Therefore, OGR1 represent an interesting candidate to be a part of the mechanism that translates the acid-base status to regulation of gene expression or transporter function in response to changes in systemic acid-base balance.

2. NOVEL G PROTEIN-COUPLED RECEPTORS

G-protein-coupled receptors (GPCR) form the largest gene family in the human genome; these receptors have a common structural feature of a seven-helical transmembrane region. Actually, around 865 GPCR genes have been identified (1), about 367 of these genes have been described to be receptors for endogenous ligands (2), however, many GPCRs are still considered as orphan receptors.

Recently, the proton sensing mechanism has been described as a new action mode of GPCRs activation, thus a new subfamily of GPCRs has been

identified to be activated by increasing extracellular H^+-concentrations. OGR1 (Ovarian Cancer G protein-coupled receptor 1, GPR68), GPR4 and TDAG8 (T cell death-associated gene 8) belong to this new subfamily (4; 5; 7; 8).

OGR1 was initially cloned from an ovarian cancer cell line (8), but its expression is not restricted to cancer cells; OGR1 mRNA is expressed in several tissues, including the kidney, spleen, testis, intestine, brain, heart, and lung (Fig 6; 8). Moreover, immunohistochemistry revealed that the OGR1 protein is expressed in active osteoblasts in rat bone sections (5).

GPR4 receptor is widely expressed in many tissues including the kidney, spleen, testis, intestine, brain, heart, liver, lung, pancreas and fat tissue (Fig 8; 9). Moreover, Northern blot analysis showed that the TDAG8 mRNA is mainly expressed in lymphoid tissues including, the spleen, thymus, lymph nodes and peripheral blood leukocytes (12; 13; 14).

3. PROTON SENSING RECEPTORS AND LYSOLIPIDS

OGR1, GPR4 and TDAG8 were initially described as receptors for sphingosylphosphorylcholine (SPC), lysophosphatidylcholine (LPC), and psychosine (18; 17; 9; 56). In 2000, Xu *et al* reported OGR1 to be a high affinity receptor for SPC, thus SPC was shown to elicit intracellular calcium transients and ERK activation in OGR1 transfected cells (18) this paper is today retracted. Similarly, GPR4 has been described as receptor for SPC and LPC (9), however, this publication is also today retracted.

The original publications describing GPR4, OGR1, as receptors for LPC or SPC have now been mostly retracted, and the first studies exploring receptors of this family as pH sensors in physiology have appeared. Therefore to date these receptors are considered as proton-sensing receptors.

4. GPCRS AS PROTON-SENSING RECEPTORS

Ludwig *et al.* (5) showed that at pH 7.8, OGR1 was inactive, but activated fully inositol-tris-phosphate (IP_3) accumulation at pH 6.8. Moreover, site directed mutagenesis showed that histidine residues at the extracellular surface of OGR1 are involved in pH sensing (5).

Similarly, GPR4, and TDAG8 showed a number of highly conserved histidine residues that appear to be part of the ligand-binding pocket involved in pH sensing (5, 7). The proton sensibility of the three receptors OGR1, GPR4 and TDAG8 was also confirmed by Radu *et al* (15).

Similarly, G2A a member of GPCRS mainly expressed in hematopoetic tissues and cells including the spleen, thymus, T-lymphocytes, B-lymphocytes, monocytes, and macrophages (10; 11) has been described by Murakami and co-workers (6) as another proton sensing receptor; they demonstrated that transient expression of this receptor caused inositol-tris-phosphate (IP_3) formation at pH 7.6.

However, the pH dependent stimulation of G2A could not be confirmed (15-15-1); Radu and co-workers proposed that lack of many histidine residues at the extracellular surface, defined to be involved in the pH sensing mechanism of OGR1, could be the cause for insensitiveness of G2A to acidic pH.

4.1 Proton sensing mechanism of OGR1

Recently, Ludwig *et al*. (5) used an OGR1 3D model, based on the high similarity to rhodopsin. They predicted that extracellular histidine residue at position 17 (N-terminal), 20 (N-terminal), 84 (first outer loop), 169 (second outer loop) and 269 (helix VII proximity to the third outer loop) might be involved in the proton-sensing mechanism (Fig. 1). Thus, the substitution of histidines with phenylalanine in these positions of the OGR1 receptor resulted in the failure to stimulate inositol-tris-phosphate (IP_3) response at pH 6.8; however, the activity was recovered at a more acidic pH (5). The mutation of several histidine residues shifted the concentration-response curve for extracellular protons to the right. Based on these studies, Ludwig *et al*. suggested that under alkaline conditions, the inactive state of the receptor is stabilized by the hydrogen bonding between the histidine residues. However, under acidic conditions, the hydrogen bonds are destabilized leading to the activation of the receptor (5).

In OGR1 expressing cells, $CuCl_2$ inhibited the proton induced response, probably by stabilizing the unprotonated state of histidine residues (5), In

addition, the mutation of the histidine at position 245 in OGR1 located in transmembrane helix VI facing the lipid environment, resulted in a marked reduction in the proton sensing response, suggesting that this position may be important for overall structural integrity (5).

a **b**

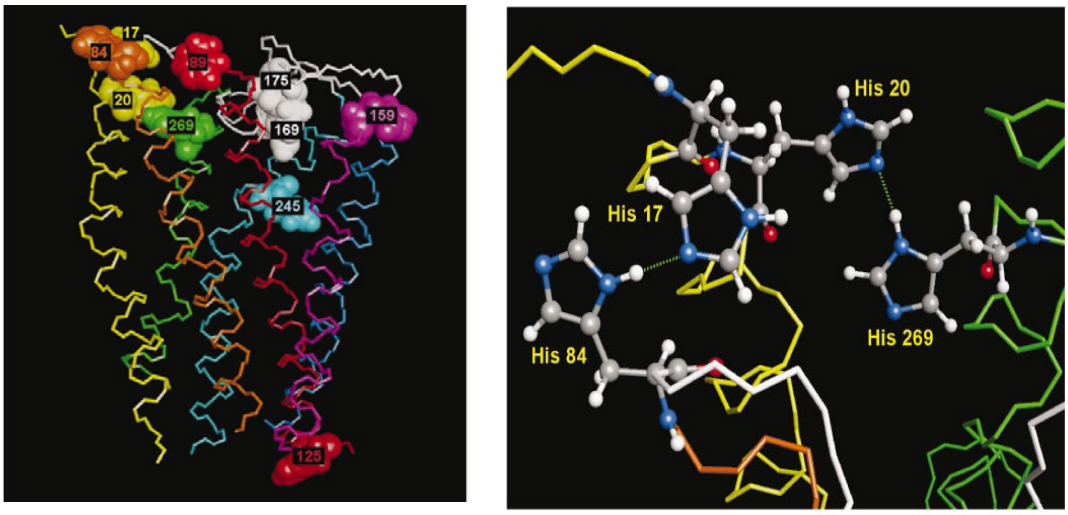

Fig. 1 (a) Backbone of the OGR1 model with all histidine residues highlighted. (b) Close up view of the predicted interactions between H17 and H84, and between H20 and H269. Taken from: Ludwig *et al*. 2003 (5).

OGR1 SIGNALING PATHWAYS

The activation of the proton sensor receptor OGR1 occurs in the physiological range of extracellular pH (5), and its EC_{50} is around pH 7.4. Experiments in OGR1 transfected cells showed that the proton stimulation of OGR1 results in the activation of phospholipase C via pertussis toxin sensitive G-proteins and increases in intracellular calcium concentrations (5). Moreover, Bektas *et al* (19) showed increased phosphorylation of ERK1/2 MAPK kinases in cells overexpressing OGR1. The proton-dependent increase in the inositol-tris-phosphate response was also observed in human preosteoblasts and MG63 human osteosarcoma cells (5), in addition to the human medulloblastoma tissue and its corresponding neuronal cell line (23) where OGR1 was shown to be expressed. These results suggest that OGR1 is a sensor of extracellular pH and its stimulation leads to the activation of distinct intracellular signaling cascades.

5. POTENTIAL PHYSIOLOGICAL AND PATHOPHYSIOLOGICAL ROLES

Acidification of the extracellular or interstitial space is described to occur under many physiological and pathophysiological states, including tumors, inflammation, ischemia, arthritis, and exercise. Although our knowledge of proton sensing GPCRs is preliminary, circumstantial evidences suggests different potential roles in multiple physiological and pathophysiological circumstances.

6.1 OGR1 in tumors

It is well known that tumors have a more acidic extracellular pH than the normal tissues. In some cases the pH has been described to drop to 5.8 (20). This acidification is the result of the poorly organized vasculature of tumors which lead to a hypoxic environment. Although the extracelullar pH is low, the intracellular pH is normal because tumor cells stimulate proton efflux (21), thus preventing cellular acidosis and apoptosis.

Interestingly, high abundance of OGR1 mRNA has been found in different human tumors (22; 23; 24). Therefore, regulation of the intracellular pH by this proton sensing receptor could represent a mechanism of survival and invasiveness in tumors.

6.2 OGR1 in bone

Metabolic acidosis increases urinary calcium concentration without increasing intestinal calcium absorption, leading to bone calcium loss. However, it has been unclear how bone cells detect the increase in proton concentration.

Recently, Ludwig *et al.* showed that OGR1 is expressed and functional in osteoblasts (5). On the other hand, Yang and coworkers demonstrated that OGR1 is expressed early during osteoclastogenesis and plays an important role in osteoclast differentiation (25). Komarova *et al* reported that osteoclasts express OGR1 and that OGR1 would couple extracellular acidification to increases of intracellular calcium. They demonstrated that acidosis acts directly on osteoclasts to induce elevation of intracellular calcium leading to stimulation of bone resorption (26). Similarly, Frick *et al* (2009) showed that acid induced bone resorption in vitro may involve OGR1, and described OGR1 as a prime candidate for an osteoblast proton sensor (27).

In organ culture of bone, acidic conditions have been shown to induce cyclooxygenase-2 (COX-2) expression and prostaglandin E_2 (PGE_2) production, resulting in stimulation of bone calcium release (28). Interestingly, it has been shown that the OGR1 / G_q / phospholipase C / protein kinase C pathway regulates osteoblastic COX-2 expression and PGE_2 formation in response to acidic pH (28). Taken together, these data suggest that OGR1 may play an important role in pH sensing mechanisms in bone.

6.3 OGR1 in vascular smooth muscle

Systemic or local acidosis may cause vasodilation of systemic arterial beds, however, pulmonary arteries are resistant to the vasodilator effect of acidosis (29). Extracellular and intracellular pH have been shown to be

responsible for the vasoldilation of systemic arteries induced by acidosis (29; 30)

Recent studies demonstrated an important role of the ATP sensitive potassium channels in the acidosis induced vasodilation (30; 31; 32). Intracellular histidine residues have been shown to participate in the activation of the channel in response to intracellular acidosis (33). This potassium channel activation is one of the mechanisms of the intracellular pH effect on vasodilation. On the other hand, the mechanism by which extracellular pH induces relaxation of vascular smooth muscle cells remains unclear.

Recently, OGR1 mRNA was found to be expressed in human aortic smooth muscle cells (34). Acidic extracellular pH has been shown to induce inositol-tris-phosphate production, a transient elevation in intracellular calcium concentration, and cAMP accumulation in these cells (34). In addition, Tumora *et al* demonstrated that siRNA against OGR1 abrogated acid induction PGI2 formation. PGI2 is a vasodilating factor and may be involved in mediating the acidosis induced vasorelaxation (34).

6. PHYSIOLOGY OF CALCIUM AND MAGNESIUM HOMEOSTASIS

Calcium and magnesium play an important role in different physiological functions of the body, including, neural excitability, bone formation, muscle contraction and relaxation, and enzymatic activity (35). Therefore, the body concentration of these divalent is tightly controlled.

Calcium and magnesium are absorbed in the intestine, filtered and reabsorbed in the kidney, and stored in bone. Thus, their absorption and reabsorption by these organs is mediated by a passive paracelullar transport mechanism that connect the luminal compartment to the blood, and an active transcellular transport mechanism which involves the passage across the apical and the basolateral membranes of cells along the nephron or intestine (Fig. 2; 36)

In the kidney, the epithelial calcium channel TRPV5 (Transient receptor potential cation channel, subfamily V, member 5) is responsible for the luminal calcium influx (Fig. 2A) and the connecting tubule (CNT) of the nephron. The Ca^{2+} is then transported from the apical to the basolateral membrane by the Ca^{2+} binding protein calbindin-D_{28K}, and taken into the blood via the Na/Ca^{2+} exchanger (NCX1) and PMCA1b (36). However, in the intestine (duodenum), the apical Ca^{2+} influx is mediated by TRPV6 channels (transient receptor potential cation channel, subfamily V, member 6), then Ca^{2+} is transported from the apical to the basolateral membrane by the Ca^{2+} binding protein calbindin-D_{9K}, and taken into the blood via the plasma membrane Ca^{2+} - ATPase PMCA1b (36).

The epithelial Mg^{2+} transport in the renal distal convoluted tubules and the intestine is mediated by the epithelial magnesium channel TRPM6 (transient receptor potential cation channel, subfamily M, member 6) (Fig. 2B). However, the molecular identity of different players that transport the Mg^{2+} from the apical to the basolateral membrane and then to the blood remains unknown.

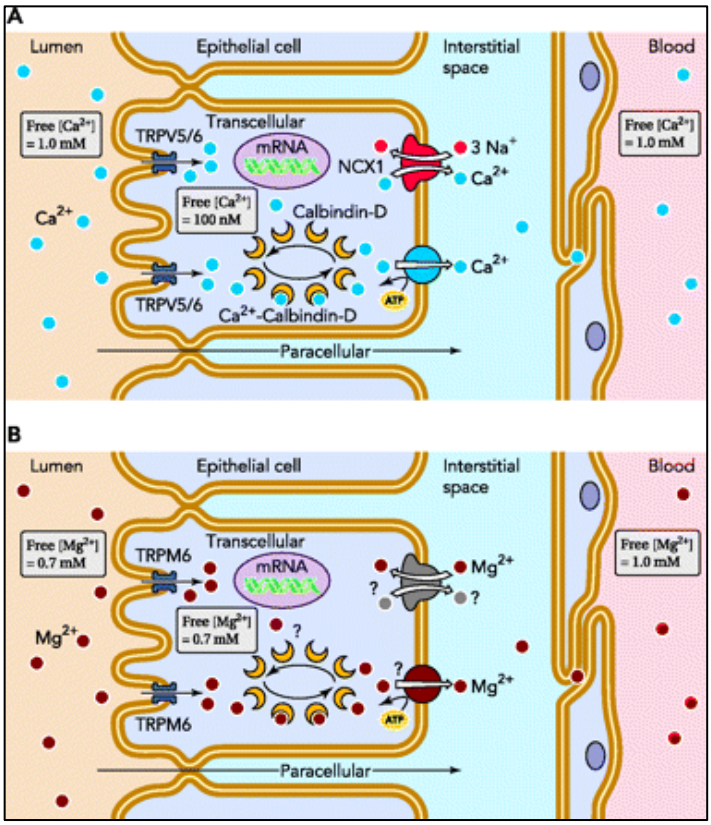

Fig. 2 Transcellular Ca^{2+} and Mg^{2+} transport across renal and intestinal epithelia. Taken from: Hoenderop JG *et al.* 2008 (36). Detailed description in the text.

7.1 Mechanisms of renal calcium reabsporption

The kidney plays an important role in the regulation of body calcium balance. About 45% of the free ionized form of plasma Ca^{2+} is filtered in the kidney through the glomerulus, approximately 65% of the filtered Ca^{2+} is passively reabsorbed in the proximal tubule (96; 97), and 20% in the thick ascending loop of Henle (TAL) through tight junction proteins including claudin16 via a passive paracellular pathway (98; 71). It is important to note that the calcium reabsorption in proximal tubule and thick ascending loop of Henle (TAL) is not regulated and depends on the gradients created by NaCl and H_2O reabsorption (37; 38). Finally, 15% of filtered Ca^{2+} is actively reabsorbed in the distal part of the nephron including, the late part of distal convoluted tubule (DCT2), and the connecting tubule (CNT) (Fig. 3; 99) where active calcium reabsorption is tightly regulated.

The mechanism of active calcium reabsorption in DCT2 and CNT has been described to be divided into three steps (Fig. 3; 36): first, passive Ca^{2+} influx across the apical membrane via apically localized epithelial Ca^{2+} channel TRPV5, then cytosolic diffusion of Ca^{2+} to the basolateral membrane bound to vitamin D_3-sensitive calcium-binding proteins (calbindin-D_{28K}), and finally active transport of Ca^{2+} to the blood across the basolateral membrane by Na^+/ Ca^{2+} exchanger (NCX1) and Ca^{2+}-ATPase (PMCA1b) (39) (Fig. 3)

Different factors have been shown to be involved in the regulation of active calcium reabsorption in the distal part of the nephron (DCT2 and CNT). Indeed, parathyroid hormone (PTH) plays an important role in the regulation of Ca^{2+} homeostasis. Changes in calcium plasma concentration are sensed in the parathyroid gland by the parathyroid Ca^{2+} sensing receptor and lead to the secretion of PTH (100). It is important to note that both DCT2 and CNT segments express the PTH receptors (101). PTH hormone has been shown to increase the expression of TRPV5, calbindin-D_{28K}, and NCX1 (102; 40, 41) in DCT2 and CNT, thus absence of PTH in parathyroidectomized rats resulted in decreased active Ca^{2+} reabsorption and development of hypocalcemia.

Moreover, several studies showed that the active form of vitamin D (1,25-$(OH)_2$ Vitamin D_3) has a role in the Ca^{2+} homeostasis regulation (40; 42; 43; 44; 49), and experiments on vitamin D knockout models showed a

significant downregulation of TRPV5, calbindin-D_{28K}, and NCX1 mRNA in the kidney (49).

Similarly, expression of TRPV5, NCX1, PMCA1b, and calbindin-D_{28K} has also been shown to be increased by estrogen (46; 47), indeed, increased urinary calcium excretion and formation of renal stone are observed in women after menopause. This demonstrates the role of estrogens in the regulation of the active Ca^{2+} transport in the distal convoluted tubule. In addition, other studies reported that calcitonin also increases the active calcium transport in DCT and CNT (45).

The dietary Ca^{2+} plays also an important role in the regulation of transport proteins participating in the renal active calcium reabsorption, indeed in the 1α-OHase knockout mice (mice lacking the 25-hydroxyvitamin D_3-1α-hydroxylase enzyme which is responsible for the 1,25-$(OH)_2$ vitamin D_3 synthesis in the kidney), high dietary Ca^{2+} intake resulted in the normalization of the decreased TRPV5, NCX1, and calbindin-D_{28K} expression in the kidney (49), similarly, dietary calcium levels regulated TRPV5 expression in the vitamin D receptor knockout mice (107). These results demonstrate that dietary Ca^{2+} has a role in the regulation of calcium transport proteins expression in the kidney independently of the 1,25-$(OH)_2$ vitamin D_3.

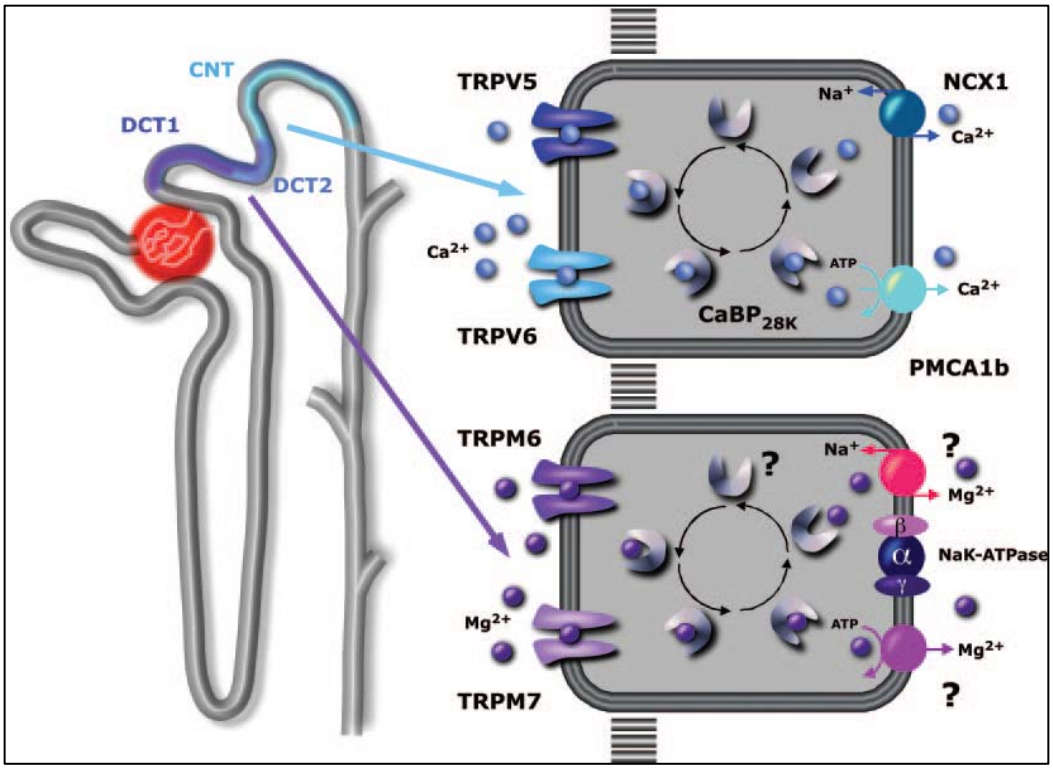

Fig. 3 Transcellular Ca^{2+} and Mg^{2+} transport across renal epithelia. Taken from: Hoenderop JG *et al* 2005 (38).

7.2 Mechanisms of renal magnesium reabsorption

Magnesium is an important divalent for different metabolic functions including neural excitability, muscular relaxation, and bone formation. The kidney plays a crucial role in controlling the magnesium homeostasis; however the exact mechanisms that regulate the renal magnesium handling are partially understood. About 80% of the total plasma magnesium filters through the glomerulus (50), consequently, 10 to 20% of the filtered Mg^{2+} is reabsorbed in the proximal tubule (PT), and around 50 to 70% is reabsorbed through tight junction proteins including claudin-16 via a passive paracellular pathway in the thick ascending loop of Henle (TAL) (50; 76). Finally, 10% of the filtrated Mg^{2+} is actively reabsorbed in the distal part of the nephron specifically the superficial distal convoluted segment (DCT) where the final urinary magnesium excretion is determined (Fig. 3; 50; 51; 52).

Little is known about the mechanism of active magnesium reabsorption in the distal convoluted tubule segment, the apically localized epithelial Mg^{2+} channel TRPM6 mediates passive entry of Mg^{2+} across the apical membrane in DCT (Fig. 3), however, transport proteins enabling the cytosolic diffusion of Mg^{2+} to the basolateral membrane (Mg^{2+} binding proteins) and its active transport across the basolateral membrane to the blood (putative Na^{+}/ Mg^{2+} exchangers or ATP dependent Mg^{2+} pumps) remain unknown (Fig. 3).

The epithelial magnesium channel TRPM6 has been described to be regulated by different factors. The epidermal growth factor EGF is expressed in the DCT along with the Mg^{2+} channel TRPM6 and has been shown to increase the activity of TRPM6 resulting in increased magnesium reabsorption in the DCT (104). Additionally, Groenestege *et al* (105) demonstrated that magnesium restriction as well as 17β-Estradiol increased expression of TRPM6 mRNA in the DCT which leads to increased Mg^{2+} reabsorption (105). However, parathyroid hormone (PTH) and vitamin D_3 have been shown to increase Mg^{2+} transport only in a DCT cell culture model but not *in vivo* (50; 106).

7. ACID-BASE HOMEOSTASIS AND RENAL HANDLING OF CALCIUM AND MAGNESIUM

Several studies demonstrated that acid–base balance affects renal handling of Ca^{2+} and Mg^{2+} (35; 50; 54; 55; 103). Renal Ca^{2+} and Mg^{2+} excretion is significantly increased during chronic metabolic acidosis (35; 50); however, chronic metabolic alkalosis results in decreased urine Ca^{2+} and Mg^{2+} excretion (35; 50). Recently, Bindels *et al* (54) proposed a molecular mechanism that may explain the renal calcium and magnesium excretion during disturbances of acid–base status. They showed that chronic metabolic acidosis decreased TRPV5 mRNA abundance and immunostaining intensity in the kidney, and enhanced calciuresis; however, chronic metabolic alkalosis increased the renal expression of TRPV5 mRNA and reduced urine Ca^{2+} excretion. Similarly, chronic metabolic acidosis decreased TRPM6 mRNA expression in the kidney, and increased urine excretion of Mg^{2+}, whereas chronic metabolic alkalosis increased renal TRPM6 mRNA expression, and reduced urinary Mg^{2+} excretion.

Other recent studies demonstrated that exposure of cells expressing the epithelial calcium channel TRPV5 to an acidic extracellular environment pH around 6.5, resulted in the internalization of TRPV5 from the plasma membrane leading to a decreased channel activity (83). However, exposure of the same cells to an alkaline extracellular milieu (pH 8) induced recruitment of TRPV5 to the plasma membrane and increased TRPV5 activity (83).

In addition, Yeh *et al* (82) showed that acidification of the extracellular milieu reduced the channel conductance of TRPV5, and described the glutamate at position 522 in the pore helix of TRPV5 as an extracellular pH sensor of the channel. They proposed that the binding of protons to the sensor results in a conformational change of the pore helix of TRPV5 and reduces the channel activity at the apical membrane of the cell which is the cause of the calcium wasting observed during chronic metabolic acidosis (82)

Taken together, these results suggest that regulation of Ca^{2+} and Mg^{2+} transport proteins may contribute to the effects of acid base status on divalent handling in the kidney.

8. MOUSE MODELS USED IN THIS PROJECT

8.1. OGR1 deficient mice

OGR1 deficient mice were purchased from Lexington (Ca, USA) by Novartis under the agreement that these mice could be used in collaborative projects and were provided to the Institute of Physiology under this agreement. OGR1 deficient mice (*Ogr1*$^{-/-}$) were generated by replacing the first exon of OGR1 by a cassette expressing LacZ. All attempts to detect Beta-galactosidase staining in OGR1 deficient mice, however, failed in our hands as well as in the hands of Novartis, possibly due to very low expression.

9.2. NH_4Cl-induced metabolic acidosis in *Ogr1*$^{-/-}$ and wild-type mice

Ammonium chloride (NH_4Cl) is known to be an efficient chemical used to induce systemic metabolic acidosis in animals, different methods of NH_4Cl administration have been described in several experimental studies (55; 54; 58; 59; 60; 61; 62; 63; 64; 65; 66). The NH_4Cl loading produces a metabolic acid load after metabolism in the liver.

In the present project, we used two models of NH_4Cl-induced metabolic acidosis animals, in the first; acute metabolic acidosis was induced using 0.28M of NH_4Cl in drinking water for 1 day with 1% sucrose added to control and NH4Cl-receiving groups. However, the second group of animals received 2 g NH_4Cl added to 100 g of food for 7 days in order to induce chronic metabolic acidosis. This amount of NH_4Cl gives an equivalent NH_4Cl load as compared to drinking water but prevents the induction of dehydration due to reduced water intake (Nowik, Wagner, unpublished results).

9.3 Acetazolamide- induced metabolic acidosis in *Ogr1*$^{-/-}$ and wild-type mice

In an alternative model of chronic metabolic acidosis, *Ogr1*$^{-/-}$ and wild type mice were treated for 7 days with the carbonic anhydrase inhibitor

acetazolamide that was added to mouse chow (20 mg/kg per d). Acetazolamide treatment causes metabolic acidosis by inducing urinary bicarbonate wasting due to inhibition of proximal tubular bicarbonate reabsorption (Fig. 4; 73; 74). This type of metabolic acidosis is characterized by high urinary pH and high net anion excretion and may give a hint as to distinguish between the effects of urinary and systemic pH. (75).

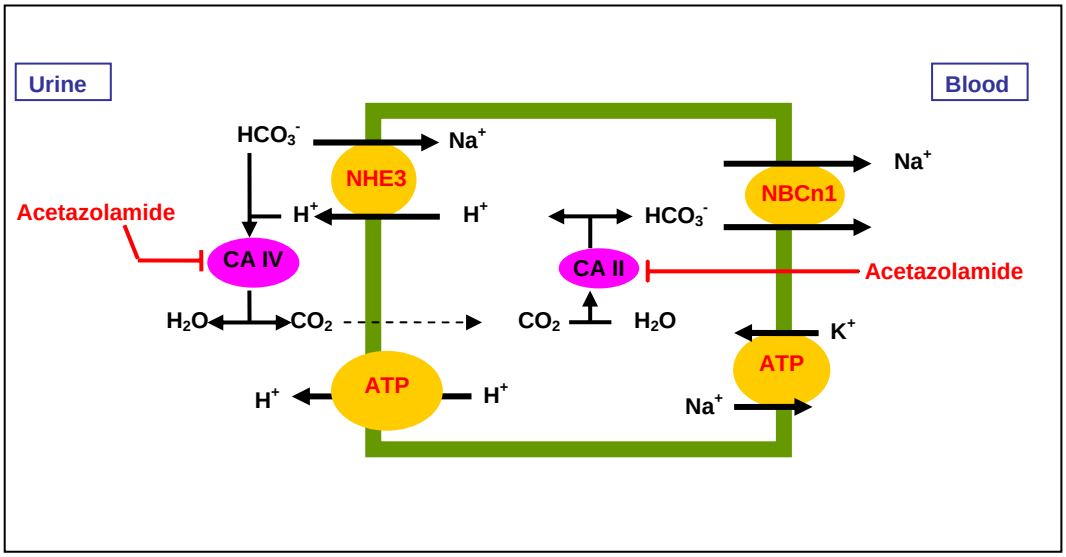

Fig. 4 Bicarbonate absorption in the proximal tubule: Modified from: Wagner *et* al 2006 (106). Bicarbonate absorption in the proximal tubule is mediated by the concerted action of the apical Na^+/ H^+ exchanger (NHE3), the vacuolar H^+ ATPase and the extracellular and cytosolic carbonic anhydrase (CAII and CAIV), and is taken into the blood via the basolateral Na^+/ HCO_3^- cotransporter (NBCe1).

10. AIM OF THE PROJECT

It is well known that systemic acid-base homeostasis affects the renal handling of the divalents calcium and magnesium. Chronic metabolic acidosis has been associated with decreased renal expression of the epithelial calcium and magnesium channels TRPV5 and TRPM6 which may contribute to the development of hypercalciuria and –magnesuria and the subsequent hypocalcemia and -magnesemia. However, the molecular sensor(s) triggering the renal wasting of calcium and magnesium during this disturbance of acid-base balance remain(s) unknown.

Recently, Ludwig *et al.* (5) described the Ovarian cancer G-protein coupled Receptor OGR1 (GPR68) as a proton sensing receptor, they reported that its activation by protons lead to the inositol-tris-phosphate (IP_3) formation, and elevation of intracellular calcium concentration. Interestingly, using quantitative real-time PCR, we detected OGR1 mRNA expression in the kidney and intestine, major sides of regulated calcium, magnesium, and acid-base transport. Therefore, the primary goal of the present project was to investigate the physiological role of OGR1 focusing on kidney and intestine. For this purpose, we decided to:

1. Explore the tissue distribution of OGR1 in different organs, and its cellular and sub-cellular localization especially in the kidney.
2. Investigate for a potential role of OGR1 in the regulation of the local pH and acid-base transporters in the kidney, and explore the regulation of OGR1 expression in different levels.
3. Investigate the potential contribution of OGR1 to the altered calcium and magnesium excretion observed during chronic metabolic acidosis.
4. Investigate the role of OGR1 in the renal calcium and magnesium handling under normal conditions.

11. MATERIALS AND METHODS

11.1. Animals

OGR1 deficient mice (*Ogr1*$^{-/-}$) were generated by replacing the first exon of OGR1 by a cassette expressing LacZ and purchased from Lexington Inc (Ca, USA). Experiments were performed on *Ogr1*$^{-/-}$ and *Ogr1*$^{+/+}$ male mice of 12-14 weeks of age, 25–30 g.

All experiments were according to Swiss Animal Welfare laws and approved by the local veterinary authority (Veterinäramt Zürich).

11.2. Genotyping of mice

Ogr1$^{+/-}$ mice were bred with *Ogr1*$^{+/-}$ mice (C57BL/6J background). The resulting offspring was genotyped by PCR (5 min at 95^{0}C, 39 cycles of 30 sec at 94^{0}C, 30 sec at 65^{0}C, 45 sec at 72^{0}C) on genomic tail DNA using two sets of primers. One set of primers (5'-ACCACCAGTGATGCCTAGATCCTGA-3', and 5'-AAGATGACCACGGTGCTGAGCACCA-3') amplifies an 827 base pair segment. The other primer set (5'-AAGATGACCACGGTGCTGAGCACCA-3' and 5'-CCATTCGACCACCAAGCGAAACATC-3') amplifies a segment of 1kb , thus identifying the wild-type allele by the presence of a 827 base pair PCR product, and the knockout allele by the presence of 1 kb PCR product (Fig. 5).

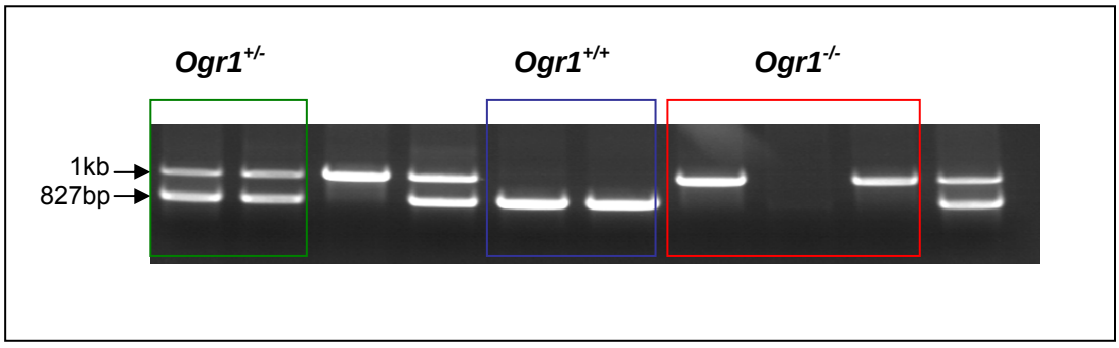

Fig. 5 Mice genotyping: PCR analysis showing the identification of the *Ogr1*$^{-/-}$ knockout mice (PCR product of 1 kb), wild-type mice (PCR product of 827 base pair) and *Ogr1*$^{+/-}$ heterozygote mice (1 kb + 827 base pair).

11.3. Animal studies

Mice were kept on a standard diet (Kliba, Kaiseraugst, Switzerland) if not stated otherwise. This diet contained 1.05 % calcium and 0.2 % magnesium. In order to induce acute metabolic acidosis in *Ogr1*$^{-/-}$ and wild-type mice (8 animals per group), mice were given 0.28 M NH_4Cl/ 2% sucrose in drinking water for 1 day as described previously (58). Another group of animals was given 2 g NH_4Cl/100 g food for 7 days to induce chronic metabolic acidosis. Alternatively, addition of the carbonic anhydrase inhibitor acetazolamide (54) to mouse chow (20 mg/kg per d) during 7 days was applied in a third group of animals; the control group received standard diet for 7 days.

In order to investigate the contribution of OGR1 in the regulation of renal calcium and magnesium handling, mice were treated with different calcium and/or magnesium diets. For the calcium treatment, a group of animals was given a low calcium diet containing 0.05% calcium, and 0.1% magnesium. Another group of mice was given a high calcium diet containing 2% calcium and 0.1% magnesium (SAFE Scientific Animal Food & Engineering, France). Both groups were treated for 2 and 7 days.

For the magnesium treatment, a group of animals was given a low magnesium diet containing 0.01% magnesium, and 0.76% calcium. Another group of mice was given a high magnesium diet containing 0.6% magnesium and 0.76% calcium (SAFE Scientific Animal Food & Engineering, France). Both groups were treated for 2 and 7 days.

48 hours prior to sacrificing mice were housed in metabolic cages (Tecniplast, Buguggiate, Italy) and had free access to food and drinking water. Daily food and water intake, and body weights were measured, urine was collected under mineral oil and all stool samples were frozen at −20°C until analysis. At the end of experiment, mice were sacrificed and heparinised mixed arterial-venous blood was collected and analyzed immediately for pH, blood gases and electrolytes on a Radiometer ABL 505 (Radiometer, Copenhagen, Denmark) blood gas analyser. Serum was collected and frozen until further analysis. Both kidneys were harvested, rapidly frozen in liquid nitrogen, and stored at -80°C.

The 24 hours collected stool samples (around 900mg) were solubilized in 5ml of 1.2M nitric acid. After 12 hours incubation at 95°C, stool samples were centrifuged at 13'000 rpm for 10 min and the supernatants were saved and diluted with water to obtain a final volume of 10ml. The resulted samples were then frozen at −20°C until analysis.

Urinary pH was measured using a pH microelectrode (691 pH-Meter, Metroholm). Urinary creatinine was measured by the Jaffe method (67). Ammonium in urine was measured by the method of Berthelot (68). Urinary and serum phosphate was measured using a commercial kit (Sigma Diagnostics, Munich, Germany). Urinary electrolytes (Ca^{2+}, Mg^{2+},Na^{+}, K^{+}) were measured by ion chromatography (Metrohm ion chromatograph, Herisau, Switzerland). Serum and stool Ca^{2+} and Mg^{2+} were measured using a commercial kit (BioAssay Systems, Hayward, CA, USA).

11.4. Real-time quantitative PCR

11.4.1. RNA extraction from total kidney

30 mg of frozen kidney tissue (8 kidneys for each condition) were homogenized in RLT-Buffer (Qiagen, Basel, Switzerland) supplemented with ß-mercaptoethanol to a final concentration of 1%. Total RNA was extracted using the RNeasy Mini Kit (Qiagen, Basel, Switzerland) according to the manufacturer's instructions. RNA was bound on columns and treated with DNAse for 15 min at 25°C to reduce genomic DNA contamination. Purity of total eluted RNA was assessed by electrophoresis and the concentration was measured spectroscopically using the ND-1000 spectrophotometer NanoDrop Technologies, (Thermo SCIENTIFIC, Wilmington, USA). Total RNA samples were stored at –80°C.

11.4.2. Reverse transcription

Each RNA sample was diluted to 100 ng/µl and 3 µl used as a template for reverse transcription using the TaqMan Reverse Transcription Kit (Applied Biosystems, Forster City, CA, USA). 300 ng RNA templates were diluted in a 20 µl reaction mix that contained (final concentrations): RT buffer (1x), $MgCl_2$ (5.5 mM), random hexamers (2.5 µM), RNAse inhibitor (0.4 U/ µl), the multiscribe reverse transcriptase enzyme (1.25 U/ µl), deoxyNTP mix (500 µM each) and RNAse free water.

11.4.3. Real-time PCR

Quantitative real-time qRT-PCR was performed on the ABI PRISM 7700 Sequence Detection System (Applied Biosystems, Forster City, CA, USA). Primers for all genes of interest were designed using Primer Express from Applied Biosystems (Table 1). Probes were labelled with the reporter dye FAM at the 5' end and the quencher dye TAMRA at the 3' end (Microsynth, Balgach, Switzerland). Primers were chosen to result in amplicons of 70–150 bp spanning intron–exon boundaries to avoid the effect of potentially contaminating genomic DNA. The specificity of all primers was first tested in a standard PCR and resulted always in a single product of the expected size on 1% agarose gels (data not shown). Real-Time PCR reactions were carried out as previously described (61). The expression of the genes of interest was calculated in relation to hypoxanthine guanine phosphoribosyl transferase (HPRT). Relative expression ratios were calculated as $R=2^{(Ct(HPRT/\beta\text{-actin})-Ct(test\ gene)}$, where Ct represents the cycle number at the threshold 0.06.

Gene	Acc. No.	Primers	Probe
OGR1 (Gpr68)	NM_175493	F: 5'-AGCCACGGCACACAGAAGA-3'	5'-CGCAAGGACCAGATTCAGCGGCT-3'
		R: 5'-ATGACCACGGTGCTGAGCA-3'	
TRPM6	NM_153417	F: 5'- GAGAAGCTCAGGCGGAACC-3'	5'- CAGAAGATACACACTTGCTCAAGACAAGGT-3'
		R: 5'- TCCCATACCCAGAGGATGACA-3'	
TRPM7	NM_021450	F: 5'-CAGCTTTGTTACCGGATTGGTT-3'	5'-ACAGAGAAATGCCATCTGAAGGAGGAACAT-3'
		R: 5'-CCACAGCTGAATAATAGTAATTTGTATCCA-3'	
TRPV5	NM_001007572	F: 5'- CGTTGGTTCTTACGGGTTGAAC-3'	5'TGTTTCTCAGATAGCTGCTCTTGTACTTCCTCTTTGT-3'
		5'- GTTTGGAGAACCACAGAGCCTCTA-3	
CaBP28K	NM_009788	F: 5'- AACTGACAGAGATGGCCAGGTTA -3'	5'ACCAGTGCAGGAAAATTTCCTTCTTAAATTCCA-3'
		5'-TGAACTCTTTCCCACACATTTTGAT -3'	
HPRT	NM_013556	F: 5'-TTATCAGACTGAAGAGCTACTGTAAGATC-3'	5'-TGAGAGATCATCTCCACCAATAACTTTTATGTCCC-3'
		R: 5'-TTACCAGTGTCAATTATATCTTCAACAATC-3'	
GPR4	NM_175668	F: 5'- CCTGGGCACTCATGTTGCT-3'	5'-TGC TAC CGT GGC ATC CTG AGG GC-3'
		R: 5'- GGTGGACACACTGCTCTGCA-3'	

Table 1. Sequences of primers and probes used for quantitative RT real-time PCR.

11.5. Immunohistochemistry

Wild-type and *Ogr1*$^{-/-}$ mice were anaesthetized and perfused through the left ventricle with PBS followed by paraformaldehyde–lysine–periodate (PLP) fixative (69). Kidneys were removed, flushed with fixative solution and postfixed overnight at 4°C by immersion in PLP. Organs were washed three times with PBS and 5 µm cryosections were cut after cryoprotection with 2.3 M sucrose in PBS for at least 12 hrs. Immunostaining was carried out as previously described (70). Briefly, sections were incubated with 1% SDS for 5 min, washed 3 times with PBS and incubated with PBS containing 1% bovine serum albumin for 15 min prior to the primary antibody. The primary antibodies were diluted in PBS (rabbit anti-TRPV5 1:200, mouse anti Calbindin-D28k (1:20'000) and applied at room temperature for 75 min or overnight at 4°C. Sections were then washed twice for 5 min with PBS + 2.7% NaCl and once with PBS, and incubated with the secondary antibodies (Donkey anti-rabbit Alexa 594 and donkey-anti-mouse Alexa 488 (Jackson ImmunoResearch, West Grove, PA, USA) at dilutions of 1: 1000 and 1:400, respectively) for 1 h at room temperature. Sections were again washed twice with PBS + 2.7% NaCl and once with PBS before mounting with VectaMount (Vector Laboratories, Burlingame, CA, USA). Sections were viewed with a Nikon ECLIPSE TE 300/200 inverted microscope or a Leica SP1 UV CLSM confocal microscope. Pictures were processed and assembled using Adobe Photoshop**.**

11.6. Western blot analysis

Mice were anaesthetized with ketamine-xylazine intraperitonally, kidneys removed and rapidly frozen in liquid nitrogen. Kidneys were homogenized in an ice-cold K-HEPES buffer (200 mM mannitol, 80 mM K-HEPES, 41 mM KOH, pH 7.5) with pepstatin, leupeptin, K-EDTA, and phenylmethylsulfonyl fluoride (PMSF) as protease inhibitors. Samples were centrifuged at 1'000 x *g* for 10 min at 4°C and the supernatant was saved. After measurement of the total protein concentration (Bio-Rad, Hercules, CA), 50 µg of proteins were solubilized in Laemmli sample buffer, and SDS-PAGE

was performed on 10% polyacrylamide gels. For immunoblotting, the proteins were transferred electrophoretically to polyvinylidene fluoride membranes (Immobilon-P; Millipore, Bedford, MA). After blocking with 5% milk powder in Tris-buffered saline/0.1% Tween-20 for 60 min, the blots were incubated with the primary antibodies and mouse monoclonal anti-β-actin antibody (42 kDa; Sigma, St. Louis, MO) 1:5,000 either for 2 h at room temperature or overnight at 4°C. The primary antibodies were: rabbit anti TRPV5 (Alomone, Jerusalem, Israel) (1:1000), mouse monoclonal anti Calbindin-D28K (1:20000), guinea pig anti TRPM6 (1:1000) (AbCam, Cambridge, UK).

The membranes were then washed three times, blocked for 1 h, and again incubated for 1 h at room temperature with the secondary goat anti-rabbit or goat anti-mouse or goat anti-guinea pig antibodies (1:5,000) linked to alkaline phosphatase (Promega). The protein signal was detected with the CDP Star chemiluminescence system (Roche Diagnostics, Basel, Switzerland) using the DIANA III-chemiluminescence detection system (Raytest, Straubenhardt, Germany). All images were analyzed using appropriate software (Advanced Image Data Analyser AIDA, Raytest) to calculate the protein of interest/actin ratio.

11.7. Statistical analysis

Results are expressed as mean ± SEM. All data were tested for significance using ANOVA and unpaired student's test where appropriate. Only values with $p < 0.05$ were considered as significant. Levels of significance are indicated in tables and figures.

12. RESULTS

12.1. The H^+-Activated Ovarian Cancer G Protein-Coupled Receptor 1 (OGR1) is responsible for Renal Calcium and Magnesium Loss during Acidosis

12.1.1. Tissue distribution of OGR1 and its expression in mouse kidney

OGR1 mRNA is expressed in most mouse organs (Fig. 6A, B). High levels were found in spleen, lung and testis. Interestingly, OGR1 mRNA was also found with moderate levels in several epithelial structures including kidney and intestine (Fig. 6). Distribution of OGR1 mRNA was detected in various mouse nephron segments such as proximal tubule, thick ascending limb, distal convoluted tubule (major sites of regulated calcium and magnesium absorption), and along the collecting duct.

Similarly, GPR4 mRNA expression was detected in most mouse organs (Fig. 8). High levels were found in spleen, lung, testis, pancreas, and fat tissues. Interestingly, GPR4 mRNA was also found with moderate levels in several epithelial structures including kidney and intestine. Finally, GPR4 mRNA expression in the kidney did not show significant differences between wild-type and *Ogr1*$^{-/-}$ mice (Fig. 9).

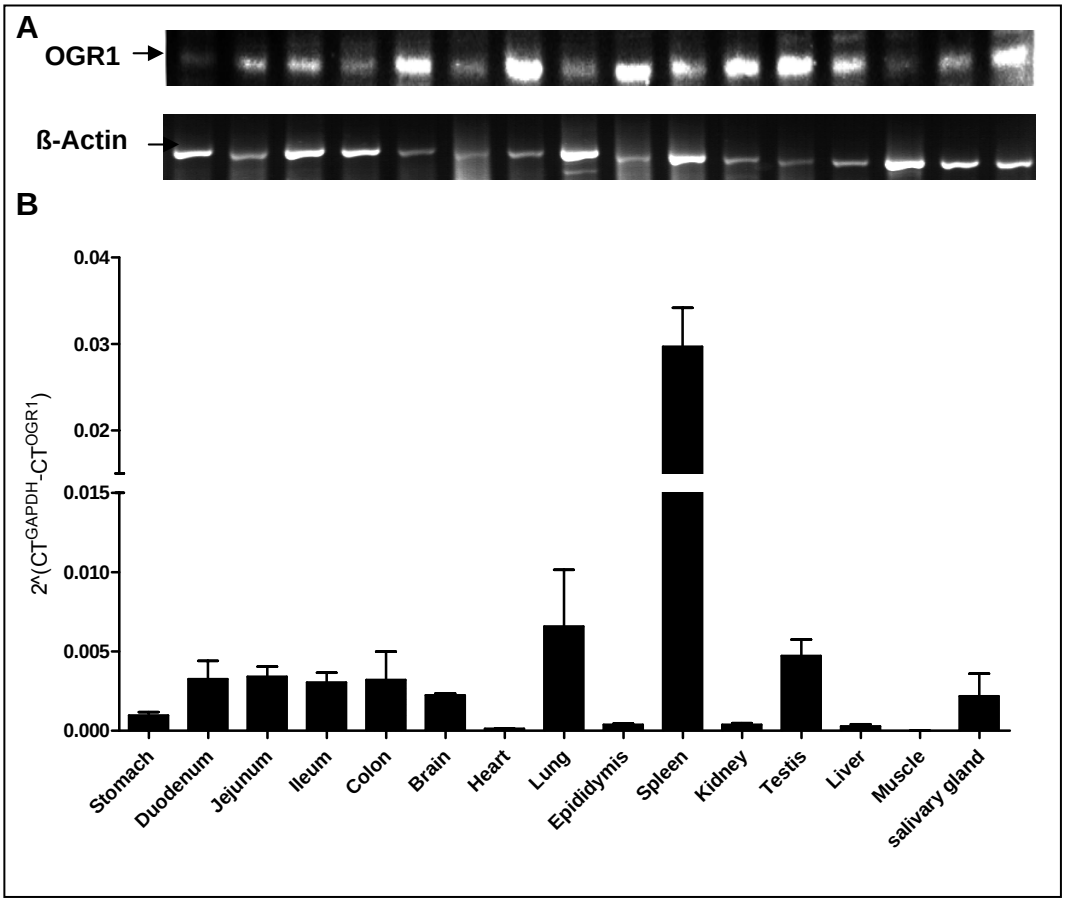

Fig. 6 OGR1 expression in mouse organs. (A) Normal PCR and **(B)** real-time quantitative PCR analysis (n=4 animals) showing the tissue distribution of OGR1 in different mouse organs. **(A)** ß-actin served as control. **(B)** The expression of genes was calculated in relation to Glycerinaldehyd-3-phosphat-Dehydrogenase (GAPDH), and relative expression ratios were calculated as $R=2^{(Ct\ (HPRT)-Ct\ (test\ gene))}$ Data are presented as means ± SEM.

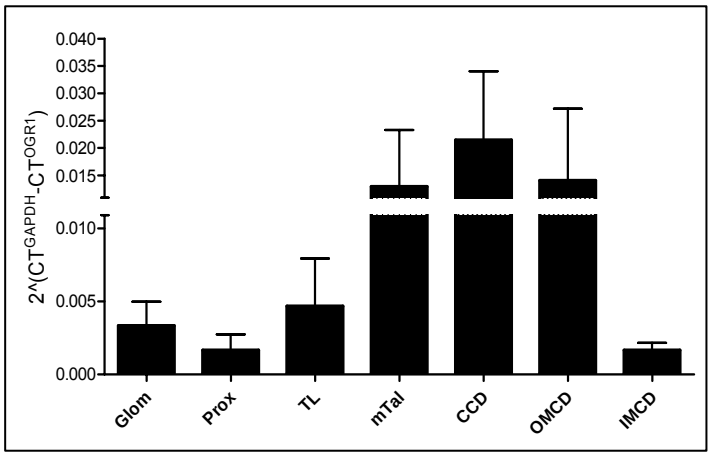

Fig. 7 OGR1 expression in mouse nephron segments. Real-time quantitative PCR (n=4 animals) showing the distribution of OGR1 mRNA in different mouse nephron segments. The expression of genes was calculated in relation to Glycerinaldehyd-3-phosphat-Dehydrogenase (GAPDH), and relative expression ratios were calculated as $R=2^{(Ct\ (HPRT)-Ct\ (test\ gene))}$. Data are presented as means ± SEM.

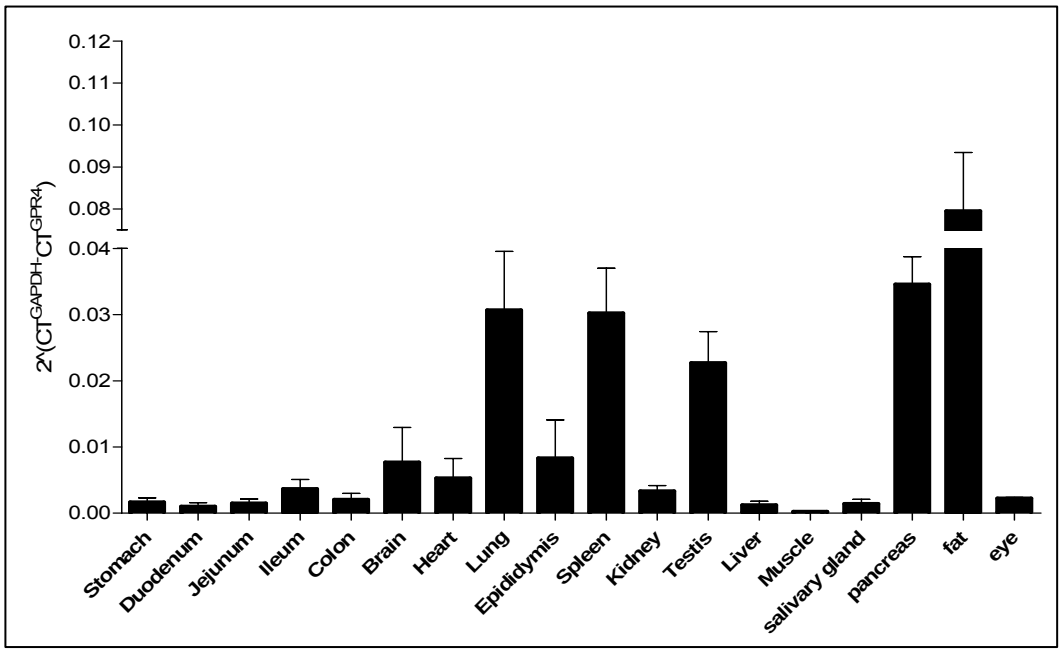

Fig. 8 GPR4 expression in mouse organs: Real-time quantitative PCR analysis (n=4 animals) showing the tissue distribution of GPR4 mRNA in different mouse organs. The expression of genes was calculated in relation to Glycerinaldehyd-3-phosphat-Dehydrogenase (GAPDH), and relative expression ratios were calculated as $R=2^{(Ct\ (HPRT)-Ct\ (test\ gene))}$ .Data are presented as means ± SEM.

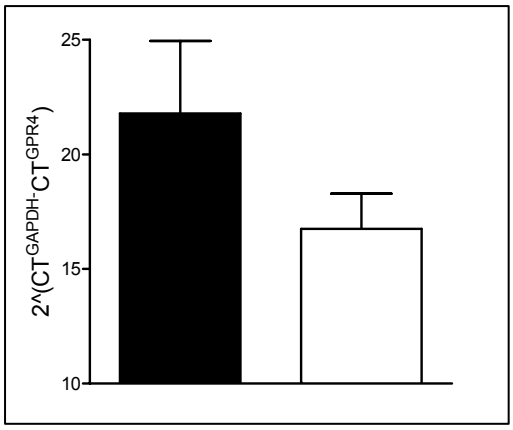

Fig. 9 Renal GPR4 mRNA expression in wild-type (*Ogr1*$^{+/+}$) and OGR1 knockout mice (*Ogr1*$^{-/-}$). Real-time quantitative PCR analysis (n=4 animals) showing GPR4 mRNA expression in wild-type (*Ogr1*$^{+/+}$) and OGR1 knockout mice (*Ogr1*$^{-/-}$). The expression of genes was calculated in relation to Glycerinaldehyd-3-phosphat-Dehydrogenase (GAPDH), and relative expression ratios were calculated as $R=2^{(Ct\ (HPRT)-Ct\ (test\ gene))}$. Data are presented as means ± SEM. * $p < 0.05$.
(■ *Ogr1*$^{+/+}$, □ *Ogr1*$^{-/-}$).

12.1.2. OGR1 is dispensable for systemic acid-base homeostasis

OGR1 is present in nephron segments that play a major role in renal acid excretion. Renal acid excretion is adapted to systemic acid-base status which may be mediated by intra- and extracellular acid sensors (72). Thus, we tested if OGR1 is required for normal acid-base status under basal conditions and during an acid-load. Mice were investigated on normal standard chow in metabolic cages and blood and urine were analyzed. No differences could be detected between *Ogr1*$^{+/+}$ and *Ogr1*$^{-/-}$ mice with the exception of lower urinary magnesium excretion in Ogr1 deficient mice (Table 2).

To induce acute or chronic metabolic acidosis animals were given NH_4Cl in the drinking water for 1 day or in food for 7 days, respectively (58). Despite similar intake of NH_4Cl in wild-type and *Ogr1*$^{-/-}$ mice, OGR1 deficient mice were less acidotic at day 1 but were indistinguishable after 7 days. Urine analysis did not reveal any difference in acid excretion at day 1 or day 7 of NH_4Cl-loading (Table 2). Thus, OGR1 is not required for normal acid-base homeostasis and appears not to be involved in the renal compensatory increase in acid excretion during a systemic acid load.

	Control		1 day NH_4Cl		7 days NH_4Cl	
	***Ogr1*$^{+/+}$**	***Ogr1*$^{-/-}$**	***Ogr1*$^{+/+}$**	***Ogr1*$^{-/-}$**	***Ogr1*$^{+/+}$**	***Ogr1*$^{-/-}$**
Blood						
pH	7.29 ± 0.02	7.28 ± 0.01	7.12 ± 0.04 $^{\#\#\#}$	7.20 ± 0.03 $^{\#}$	7.03 ± 0.05 $^{\#\#\#}$	7.08 ± 0.05
pCO_2 mmHg	45.6 ± 1.5	48.4 ± 1.7	42.5 ± 2.5	49.2 ± 2.6	38.6 ± 3.1	40.2 ± 3.3
$[HCO_3^-]$ mM	21.2 ± 0.7	22.4 ± 0.6	13.7 ± 1.7 $^{\#\#\#}$	18.3 ± 0.7 $^{\#\#\#*}$	10.7 ± 1.4 $^{\#\#\#}$	11.7 ± 0.8 $^{\&\&\&}$
$[Na^+]$ mM	144.5 ± 0.7	144.8 ± 1.0	149.0 ± 0.8 $^{\#\#\#}$	149.5 ± 0.7 $^{\#\#}$	151.2 ± 1.6 $^{\#\#\#}$	150.0 ± 1.2 $^{\#\#}$
$[K^+]$ mM	5.6 ± 0.5	5.8 ± 0.4	8.0 ± 0.3 $^{\#\#}$	7.5 ± 0.2 $^{\#}$	6.8 ± 0.4 $^{\&}$	6.7 ± 0.1 $^{\&\&}$
$[Cl^-]$ mM	112.1 ± 0.5	112.0 ± 0.9	120.0 ± 1.0 $^{\#\#\#}$	118.2 ± 1.2 $^{\#\#\#}$	121.0 ± 1.5 $^{\#\#\#}$	120.8 ± 1.2 $^{\#\#\#}$
Ionized $[Ca^{2+}]$ mM	1.24 ± 0.04	1.26 ± 0.04	1.26 ± 0.02	1.37 ± 0.03 $^{\#**}$	1.35 ± 0.02 $^{\&\&\#}$	1.34 ± 0.03
$[Ca^{2+}]$ mM in serum	2.10 ± 0.17	2.33 ± 1.13	2.38 ± 0.09	2.51 ± 0.06	2.43 ± 0.05	2.26 ± 0.10
$[Mg^{2+}]$ mM in serum	1.02 ± 0.04	1.06 ± 0.04	1.20 ± 0.10	1.30 ± 0.03 $^{\#\#}$	1.20 ± 0.03 $^{\#\#}$	1.15 ± 0.10
Urine						
pH	6.28 ± 0.10	6.65 ± 0.30	5.72 ± 0.05 $^{\#\#\#}$	5.83 ± 0.09 $^{\#}$	5.54 ± 0.03 $^{\&\#\#\#}$	5.94 ± 0.08 $^{\#**}$
Creatinine (mg/dl)	66.7 ± 6.4	62.0 ± 5.0	88.9 ± 10.7	57.0 ± 3.7	44.2 ± 3.3	52.56 ± 14.3
NH_3/NH_4^+/ (mM)/crea (mg/dl)	0.75 ± 0.23	1.4 ± 0.40	2.91 ± 0.52 $^{\#\#}$	3.97 ± 0.54 $^{\#\#}$	8.82 ± 1.04 $^{\#\#\#\&\&\&}$	7.98 ± 1.52 $^{\#\#\#\&}$

Na^+(mM)/crea (mg/dl)	1.9 ± 0.1	1.6 ± 0.1	2.4 ± 0.1 ##	2.9 ± 0.1 ###*	4.0 ± 0.6 ##&	3.9 ± 0.7 ##
K^+(mM)/crea (mg/dl)	6.0 ± 0.2	5.6 ± 0.2	6.2 ± 0.3	8.2 ± 0.4 **###	8.5 ± 0.8 &&	6.0 ± 0.2
Ca^{2+}(mM)/crea (mg/dl)	0.04 ± 0.003	0.03 ± 0.004	0.03 ± 0.004	0.04 ± 0.003	0.12 ± 0.010###&&&	0.05 ± 0.010 **
Mg^{2+}(mM)/crea (mg/dl)	0.56 ± 0.03	0.37 ± 0.07 *	0.47 ± 0.03	0.36 ± 0.07	0.86 ± 0.09 ##&&	0.48 ± 0.10 **
Phosphate(mg/dl)/crea (mg/dl)	0.3 ± 0.03	0.3 ± 0.02	0.4 ± 0.03	0.3 ± 0.01 *	0.5 ± 0.08 #	0.3 ± 0.05
Osmolality (mOsm/kg H_2O)	2949 ± 315	2344 ± 182.2	3825 ± 471	2687 ± 176 *	2602 ± 260	2837 ± 164
Urine volume (ml)/ BW (g)	0.05 ± 0.005	0.05 ± 0.006	0.04 ± 0.004	0.06 ± 0.003**	0.06 ± 0.008 &	0.06 ± 0.006
Weight change %	1.6 ± 0.5	1.7 ± 0.4	2.3 ± 0.3	2.6 ± 0.6	2.6 ± 0.9	1.8 ± 0.6

Table 2. Control and NH_4Cl groups: Summary of blood and urine analysis for. (n=8 animals per group) Control group: animals that received standard diet; acidosis group: animals that received 0.28M NH_4Cl in the drinking water for 1 day; or 2g NH_4Cl/100g food for 7 days.

Urinary excretion was normalized against creatinine (crea). BW: body weight.

* Significantly different between *Ogr1*$^{+/+}$ and *Ogr1*$^{-/-}$ for the same treatment, * $p \leq 0.05$, ** $p \leq 0.01$, *** $p \leq 0.001$

Significantly different between control group and treated group for the same genotype, # $p \leq 0.05$, ## $p \leq 0.01$, ### $p \leq 0.001$

& significantly different between treated groups 1 day versus 7 days NH_4Cl for the same genotype, & $p \leq 0.05$, && $p \leq 0.01$, &&& $p \leq 0.001$

12.1.3. OGR1 is responsible for renal Ca^{2+} and Mg^{2+} loss during chronic metabolic acidosis

NH_4Cl-induced metabolic acidosis enhanced urine Ca^{2+} and Mg^{2+} excretion in wild-type mice, similar to what has been described previously (55; 54). Surprisingly, urinary total Ca^{2+} and Mg^{2+} excretion as well as the corrected values for creatinine did not increase in *Ogr1*$^{-/-}$ mice (Fig. 10A,B), whereas all other urinary parameters were similar between wild-type and *Ogr1*$^{-/-}$ mice (Table 2) indicating a specific difference. Serum calcium and magnesium concentrations were not different between *Ogr1*$^{+/+}$ and *Ogr1*$^{-/-}$ under all conditions (Fig. 11A, B). Also food intake and calculated intestinal Ca^{2+} and Mg^{2+} (the difference between the amount of Ca^{2+} and Mg^{2+} ingested over 24 hrs and the amount of Ca^{2+} and Mg^{2+} detected in 24 hrs stool collections) were similar in both genotypes (Fig. 12) strongly suggesting an alteration on the level of the kidney. Hence, the proton-activated receptor OGR1 appears to be involved in the renal Ca^{2+} and Mg^{2+} loss during chronic metabolic acidosis.

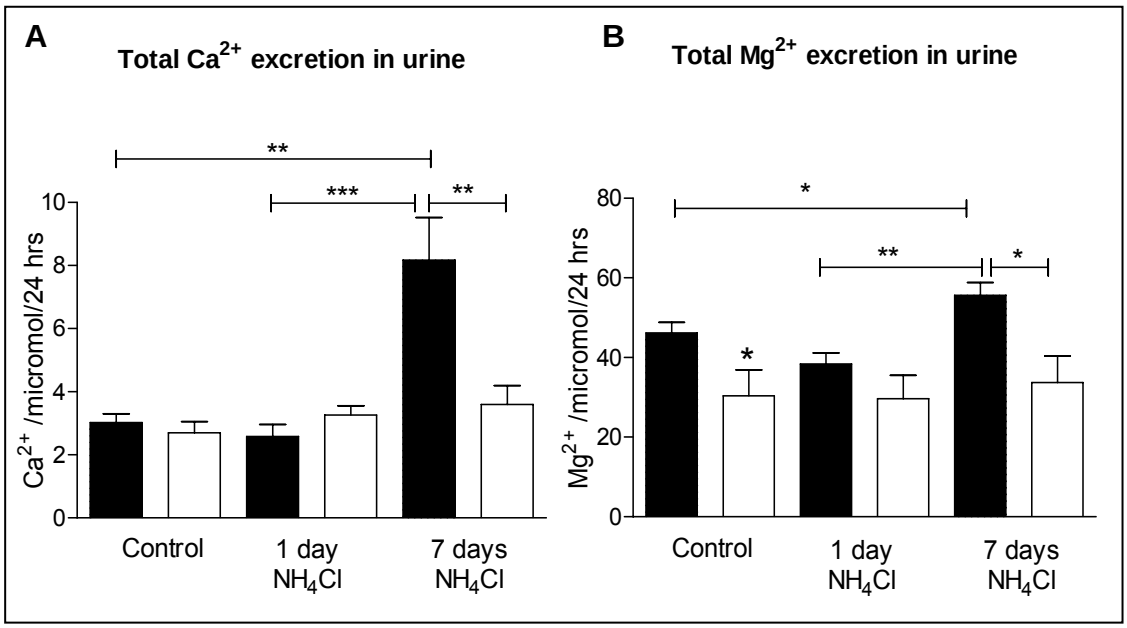

Fig 10. Urinary Ca^{2+} and Mg^{2+} excretion during metabolic acidosis in wild-type (*Ogr1*$^{+/+}$) and OGR1 knockout mice (*Ogr1*$^{-/-}$). (n=8 animals per group) Acute and chronic metabolic acidosis were induced by NH_4Cl-loading and resulted after 7 days in massive renal Ca^{2+} **(A)** and Mg^{2+} **(B)** excretion which was absent from *Ogr1*$^{-/-}$ mice. Control group: animals that received standard diet; acidosis group: animals that received 0.28M NH_4Cl in the drinking water for 1 day; or 2g NH_4Cl/100g food for 7 days. (■ *Ogr1*$^{+/+}$, □*Ogr1*$^{-/-}$*).*
Data are presented as means ± SEM. * $p < 0.05$, ** $p < 0.01$, *** $p < 0.001$.

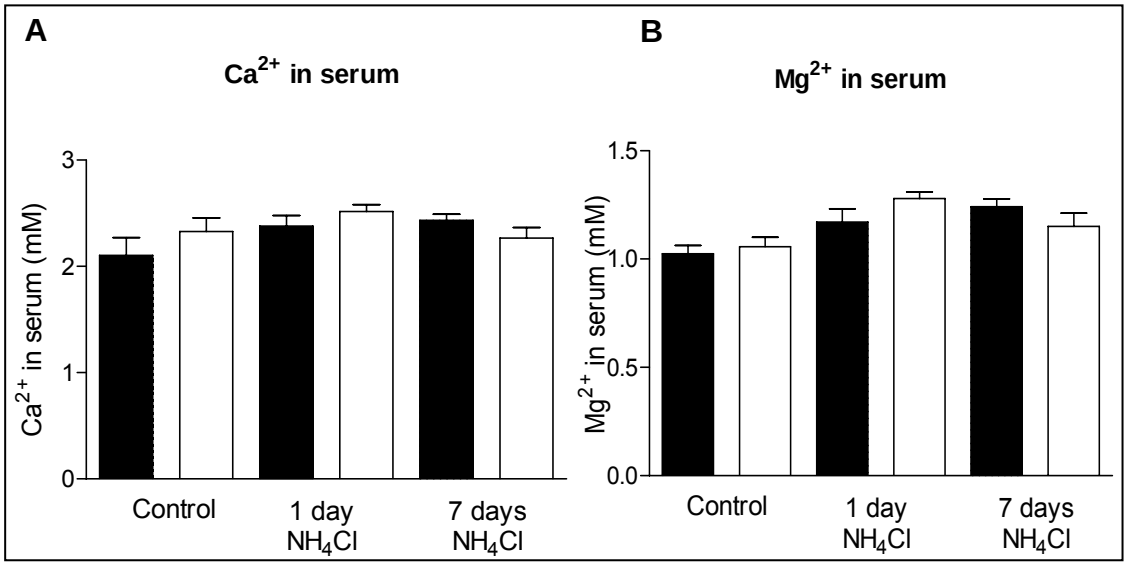

Fig 11. Serum Ca^{2+} and Mg^{2+} concentration during metabolic acidosis in wild-type (*Ogr1*$^{+/+}$) and OGR1 knockout mice (*Ogr1*$^{-/-}$). (n=8 animals per group). Serum total calcium **(A)** and magnesium **(B)** levels were not affected by NH_4Cl-treatment and comparable in wild-type and OGR1 deficient mice. Control group: animals that received standard diet; acidosis group: animals that received 0.28M NH_4Cl in the drinking water for 1 day; or 2g NH_4Cl/100g food for 7 days.

(■ *Ogr1*$^{+/+}$,□ *Ogr1*$^{-/-}$).

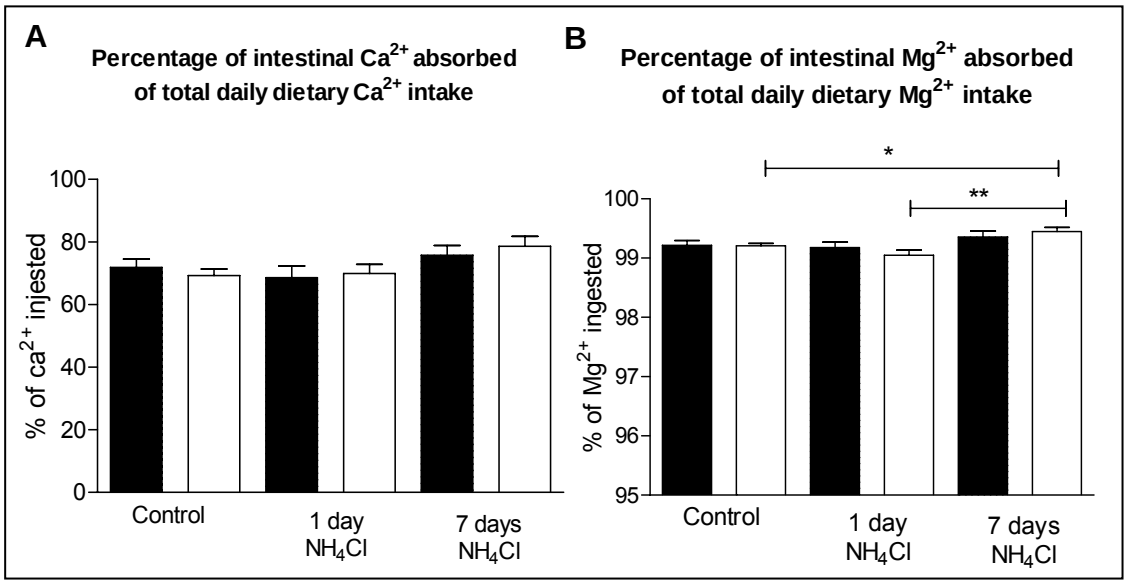

Fig 12. Intestinal absorption of Ca^{2+} and Mg^{2+} during metabolic acidosis in wild-type (*Ogr1*$^{+/+}$) and OGR1 knockout mice (*Ogr1*$^{-/-}$). Intestinal calcium **(A)** and magnesium **(B)** absorption were not affected by NH_4Cl-treatment and comparable in wild-type and OGR1 deficient mice. Control group: animals that received standard diet; acidosis group: animals that received 0.28M NH_4Cl in the drinking water for 1 day; or 2g NH_4Cl/100g food for 7 days.

(■ *Ogr1*$^{+/+}$, □ *Ogr1*$^{-/-}$).

12.1.4. OGR1 does not affect total bone development (data produced by Jürg Gasser at Novartis in Basel)

NH_4Cl-treatment did not affect the in vitro reabsorptive activity of osteoclasts from *Ogr1*$^{+/+}$ and *Ogr1*$^{-/-}$ male and female mice (Fig. 12.1A; B). In addition, bone mineral density, cortical thickness and cancellous bone mineral density of wild-type (*Ogr1*$^{+/+}$) and OGR1 knockout (*Ogr1*$^{-/-}$) male and female mice were similar during metabolic acidosis (Fig. 12.2), suggesting that OGR1 is not responsible for bone resorption during chronic metabolic acidosis.

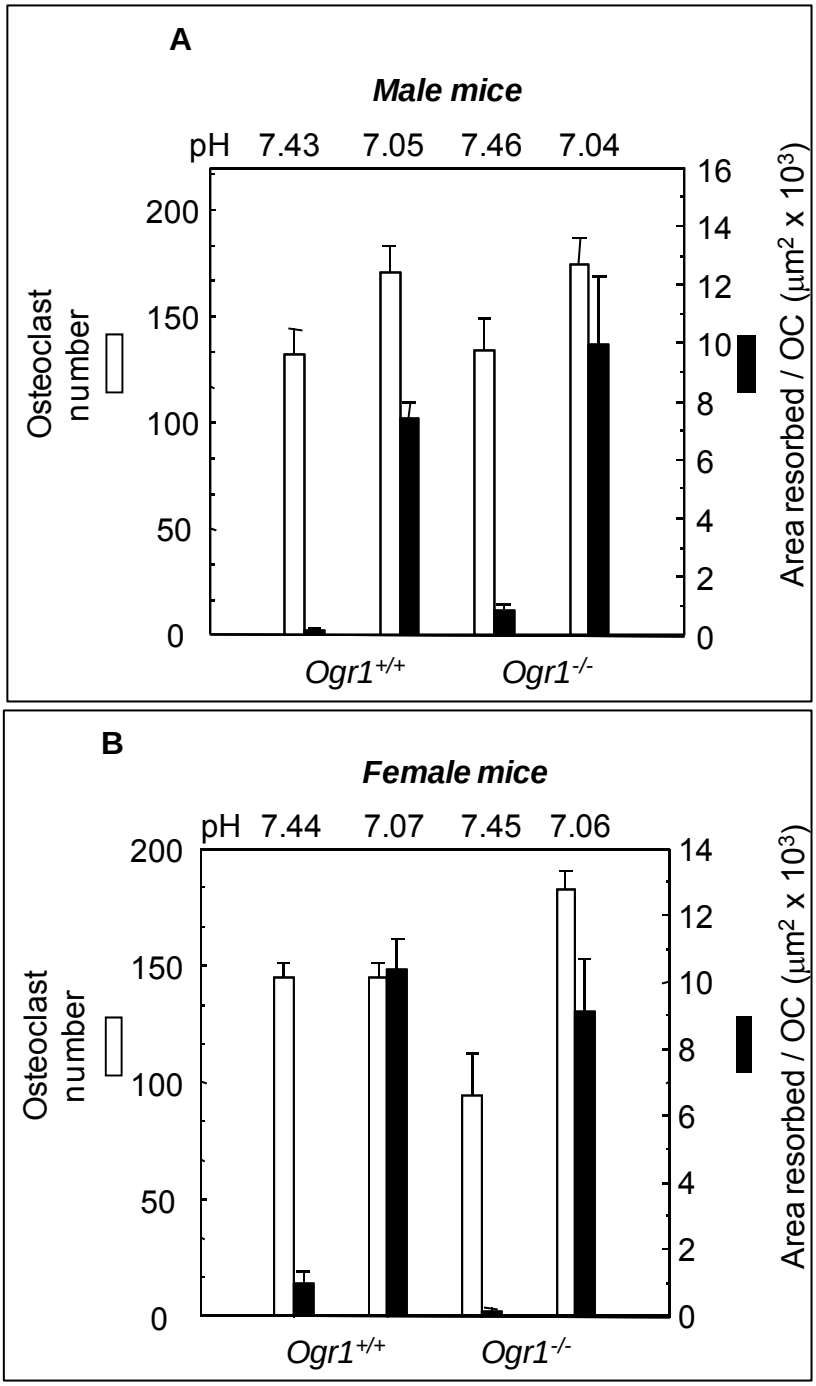

Fig 12.1. In vitro reabsorptive activity of osteoclasts from wild-type (*Ogr1*$^{+/+}$) and OGR1 knockout (*Ogr1*$^{-/-}$) mice during acidosis. (A) Male mice, (B) female mice. The in vitro reabsorptive activity of osteoclasts was not affected by NH_4Cl-treatment and comparable in wild-type and OGR1 deficient mice.

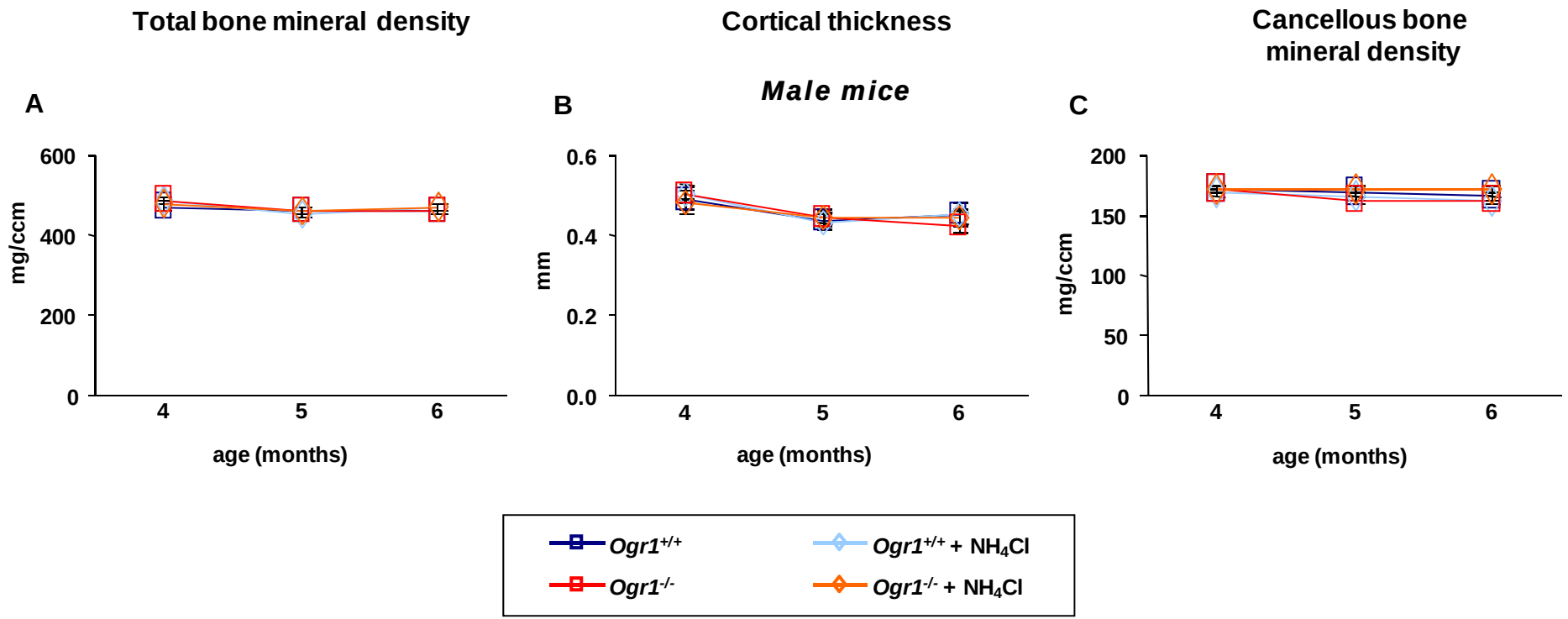

Fig 12.2. (A)Total bone mineral density, (B) cortical thickness and (C) cancellous bone mineral density of wild-type (*Ogr1*$^{+/+}$) and OGR1 knockout (*Ogr1*$^{-/-}$) male mice during metabolic acidosis. Total bone development was not affected by NH_4Cl-treatment and comparable in wild-type and OGR1 deficient mice. Control group: animals that received standard diet; acidosis group: animals that received NH_4Cl for 8 weeks.

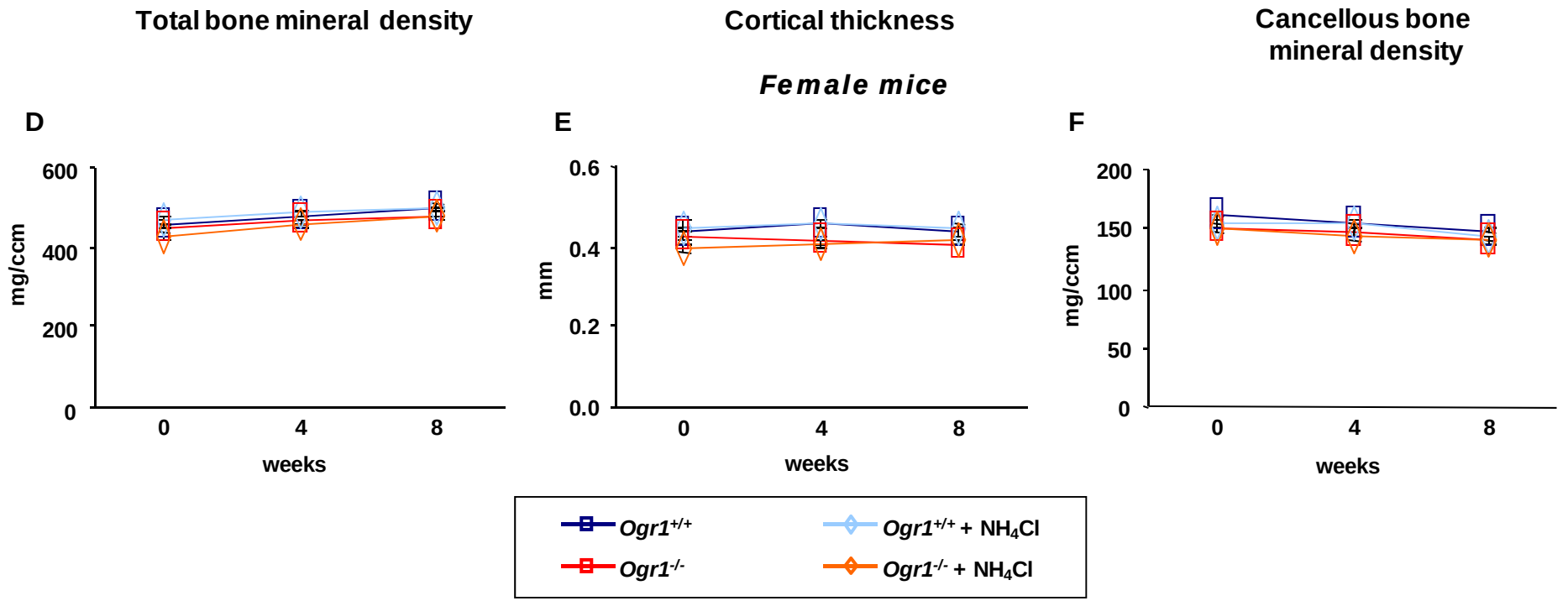

Fig 12.2. (A)Total bone mineral density, (B) cortical thickness and (C) cancellous bone mineral density of wild-type (*Ogr1*$^{+/+}$) and OGR1 knockout (*Ogr1*$^{-/-}$) female mice during metabolic acidosis. Total bone development was not affected by NH_4Cl-treatment and comparable in wild-type and OGR1 deficient mice. Control group: animals that received standard diet; acidosis group: animals that received NH_4Cl for 8 weeks.

12.1.5. OGR1 induces TRPV5 internalization during metabolic acidosis

Quantitative RT-PCR demonstrated that metabolic acidosis did not affect mRNA abundance of the TRPV5 Ca^{2+}-channel. Calbindin D28k mRNA expression increased after 2 days NH_4Cl-loading as demonstrated previously (55). Moreover, chronic metabolic acidosis was associated with elevated mRNA expression of the TRPM6 Mg^{2+} channel whereas TRPM7 mRNA remained unaffected. However, no differences were detected between *Ogr1*$^{+/+}$ and *Ogr1*$^{-/-}$ (Fig. 13). Furthermore, immunoblotting for TRPV5, calbindin D28k, and TRPM6 under basal conditions or after 7 days of NH_4Cl demonstrated comparable expression levels of these proteins in kidney (Fig. 14 and 15).

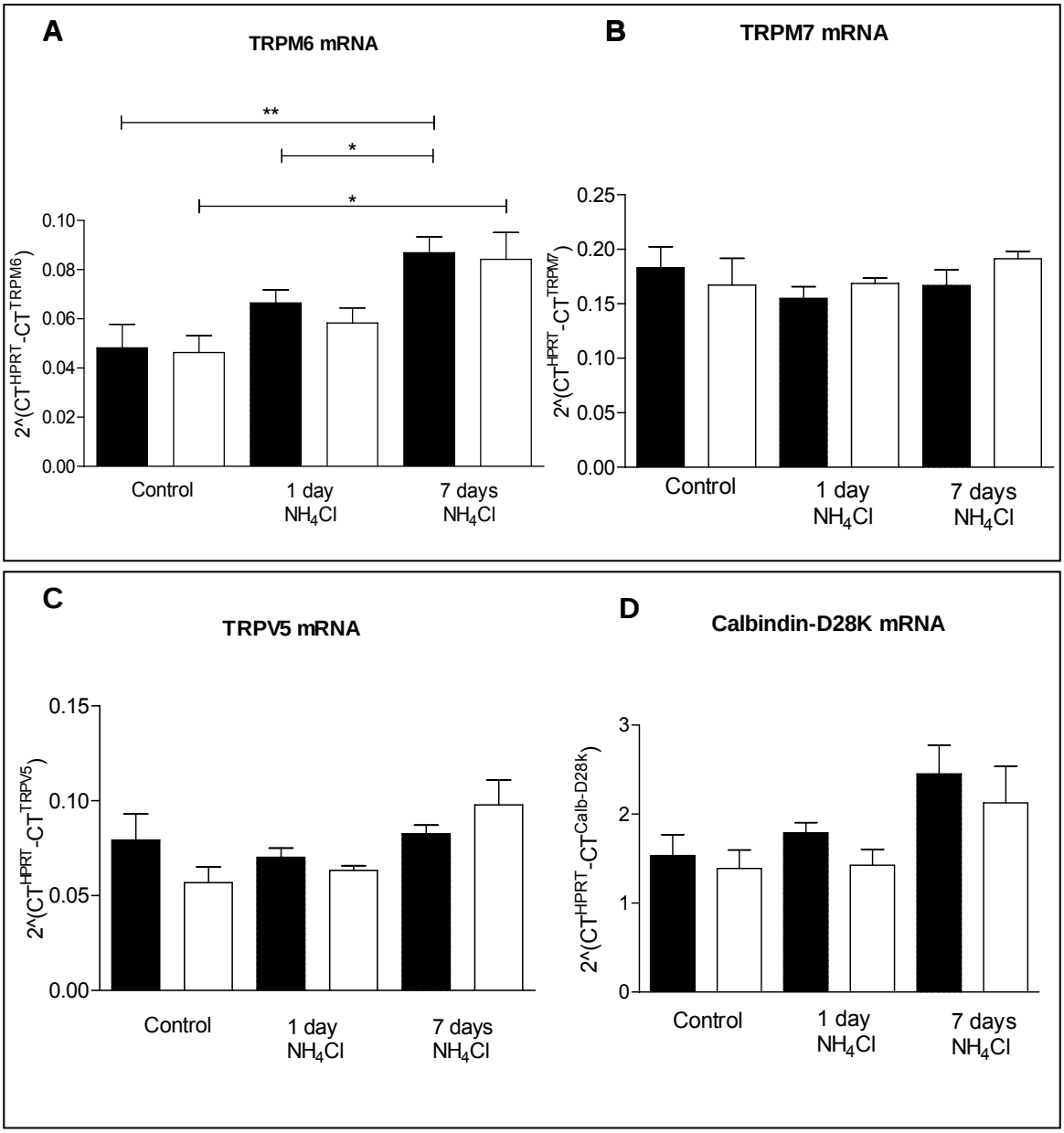

Fig 13. Effect of acute and chronic metabolic acidosis on renal mRNA expression of Ca^{2+} and Mg^{2+} transport proteins in (*Ogr1*$^{+/+}$) and (*Ogr1*$^{-/-}$) mice.

Renal mRNA expression levels of the epithelial Mg^{2+} channels TRPM6 and TRPM7 **(A and B,** respectively) and the epithelial Ca^{2+} channel TRPV5 and the cytosolic Ca^{2+}-binding protein calbindin-D_{28K} ($CaBP_{28K}$) **(C and D,** respectively**)** were determined during acute and chronic metabolic acidosis by real-time quantitative PCR analysis (n=8 animals per group), The expression of genes was calculated in relation to hypoxanthine guanine phosphoribosyl transferase (HPRT), and relative expression ratios were calculated as $R=2^{(Ct(HPRT)-Ct(test\ gene)}$; Control group: animals that received standard diet; acidosis group: animals that received 0.28M NH_4Cl in the drinking water for 1 day; or 2g NH_4Cl/100g food for 7 days. Data are presented as means ± SEM. * $p < 0.05$, ** $p < 0.01$, *** $p < 0.001$.

(■*Ogr1*$^{+/+}$, □ *Ogr1*$^{-/-}$).

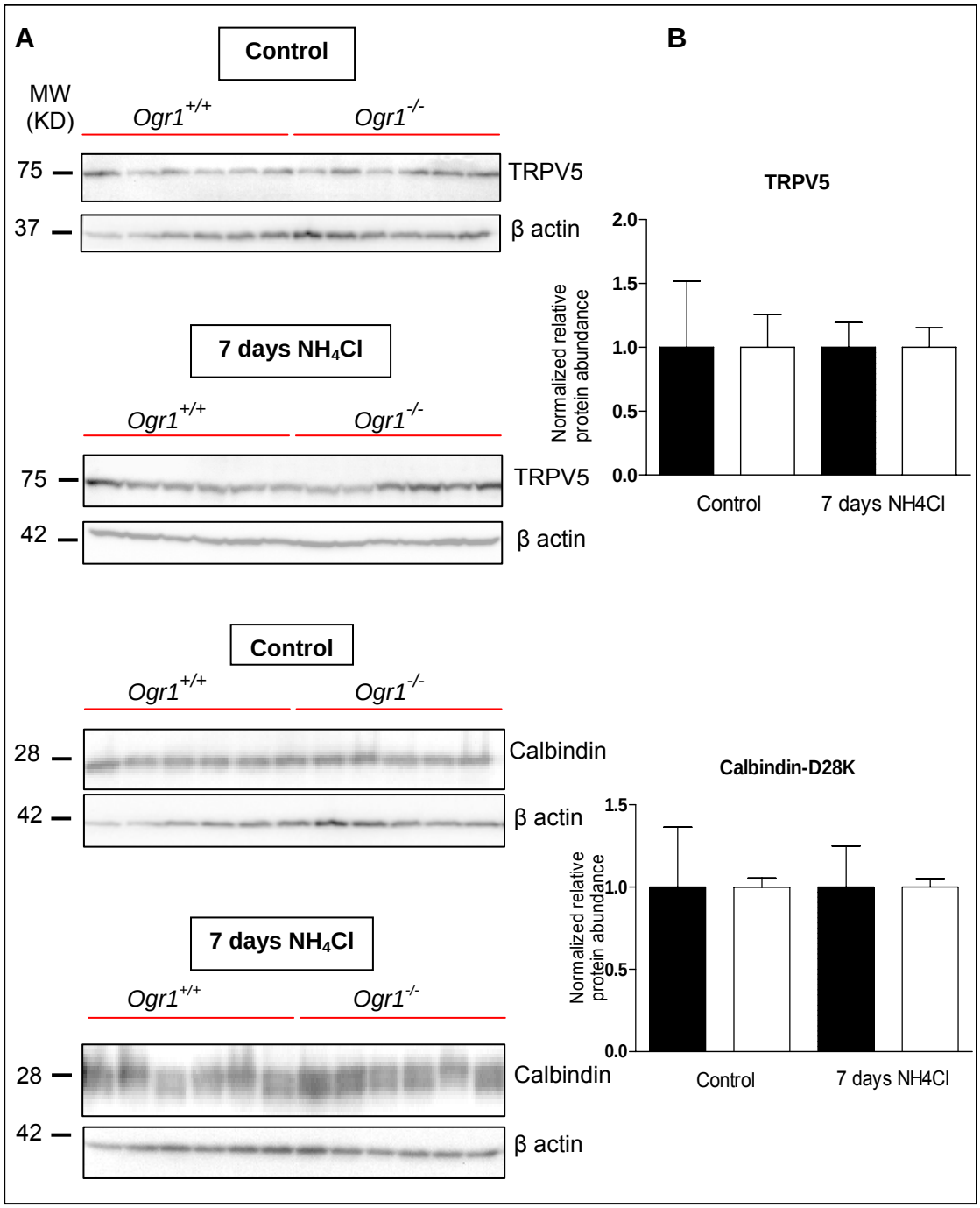

Fig 14. Effect of chronic metabolic acidosis on renal protein abundance of Ca^{2+} transport proteins in (*Ogr1*$^{+/+}$) and (*Ogr1*$^{-/-}$) mice.

Renal protein expression levels of the epithelial Ca^{2+} channel TRPV5 and the cytosolic calbindin-D_{28K} were determined during chronic metabolic acidosis by western blotting analysis **(A)**. Bar graphs summarizing data from immunoblotting **(B);** (n=6 animals per group), All data were normalized against β-actin. Control group: animals that received standard diet; acidosis group: animals that received 2g NH_4Cl/100g food for 7 days. Data are presented as means ± SEM. * $p < 0.05$, ** $p < 0.01$, *** $p < 0.001$.

(■ *Ogr1*$^{+/+}$, □ *Ogr1*$^{-/-}$).

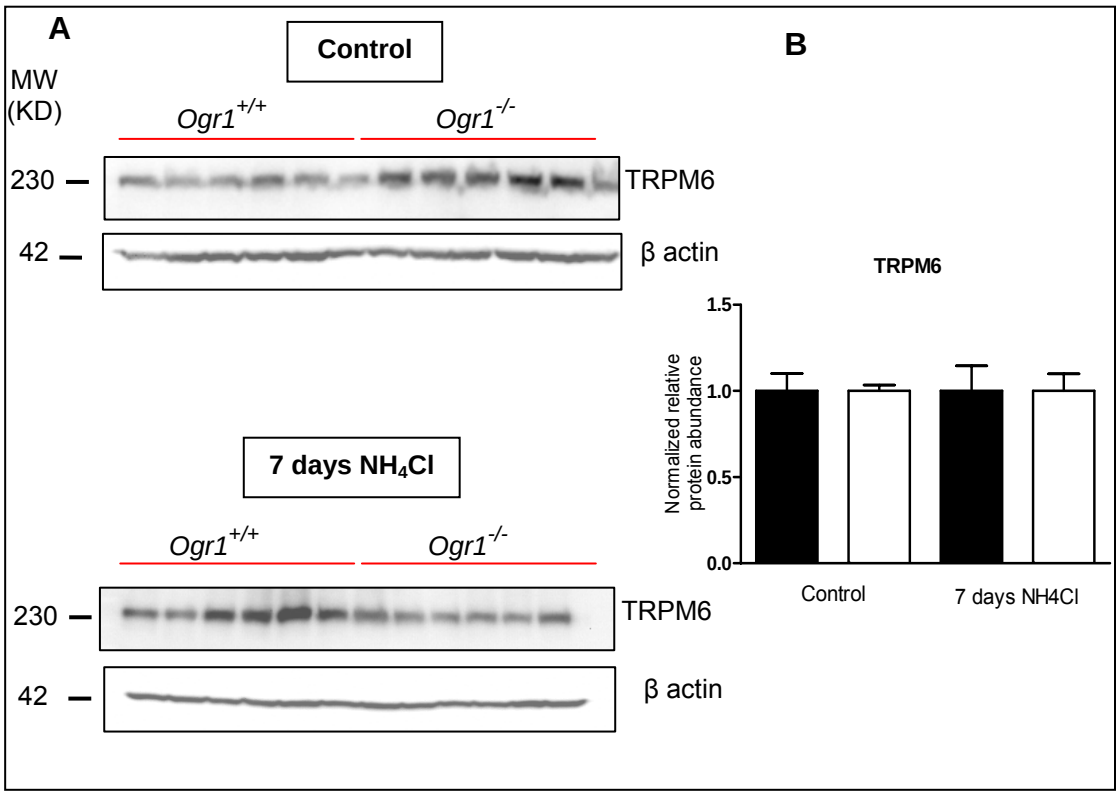

Fig 15. Effect of chronic metabolic acidosis on renal protein abundance of the Mg^{2+} transporting channel TRPM6 in $OGR1^{+/+}$ and $OGR1^{-/-}$ mice. Renal protein expression levels of the epithelial Mg^{2+} channel TRPM6 was determined during chronic metabolic acidosis by western blotting analysis **(A)**. Bar graphs summarizing data from immunoblotting **(B)**; (n=6 animals per group), All data were normalized against β-actin. Control group: animals that received standard diet; acidosis group: animals that received 2g NH_4Cl/100g food for 7 days.

Data are presented as means ± SEM. * $p < 0.05$, ** $p < 0.01$, *** $p < 0.001$.
(■ *Ogr1*$^{+/+}$ □*Ogr1*$^{-/-}$).

TRPV5 channels can be internalized in a regulated manner (83; 85). We therefore tested if changes in subcellular distribution could contribute to the absence of hypercalciuria in *Ogr1*$^{-/-}$ mice. Kidneys from wild-type and *Ogr1* deficient mice under basal conditions and after 7 days of NH_4Cl-induced metabolic acidosis were stained with antibodies against TRPV5 and calbindin D28k (Fig. 16A and B). TRPV5 and calbindin D28k related staining was detected only in the distal convoluted tubule and connecting segments as described previously (71). TRPV5 staining was predominantely located at the apical membrane in both wild-type and *Ogr1*$^{-/-}$ mouse kidneys under basal conditions consistent with similar urinary calcium excretion (Fig. 16A). However, in kidneys from wild-type mice with 7 days of NH_4Cl treatment, TRPV5 staining was almost absent from the luminal membrane and detected mostly intracellularly (Fig 16B). In contrast, in *Ogr1*$^{-/-}$ kidneys, NH_4Cl for 7 days did not redistribute TRPV5 staining which remained mainly on the luminal membrane (Fig 16B). Thus, absence of OGR1 prevents internalization of TRPV5 during chronic metabolic acidosis.

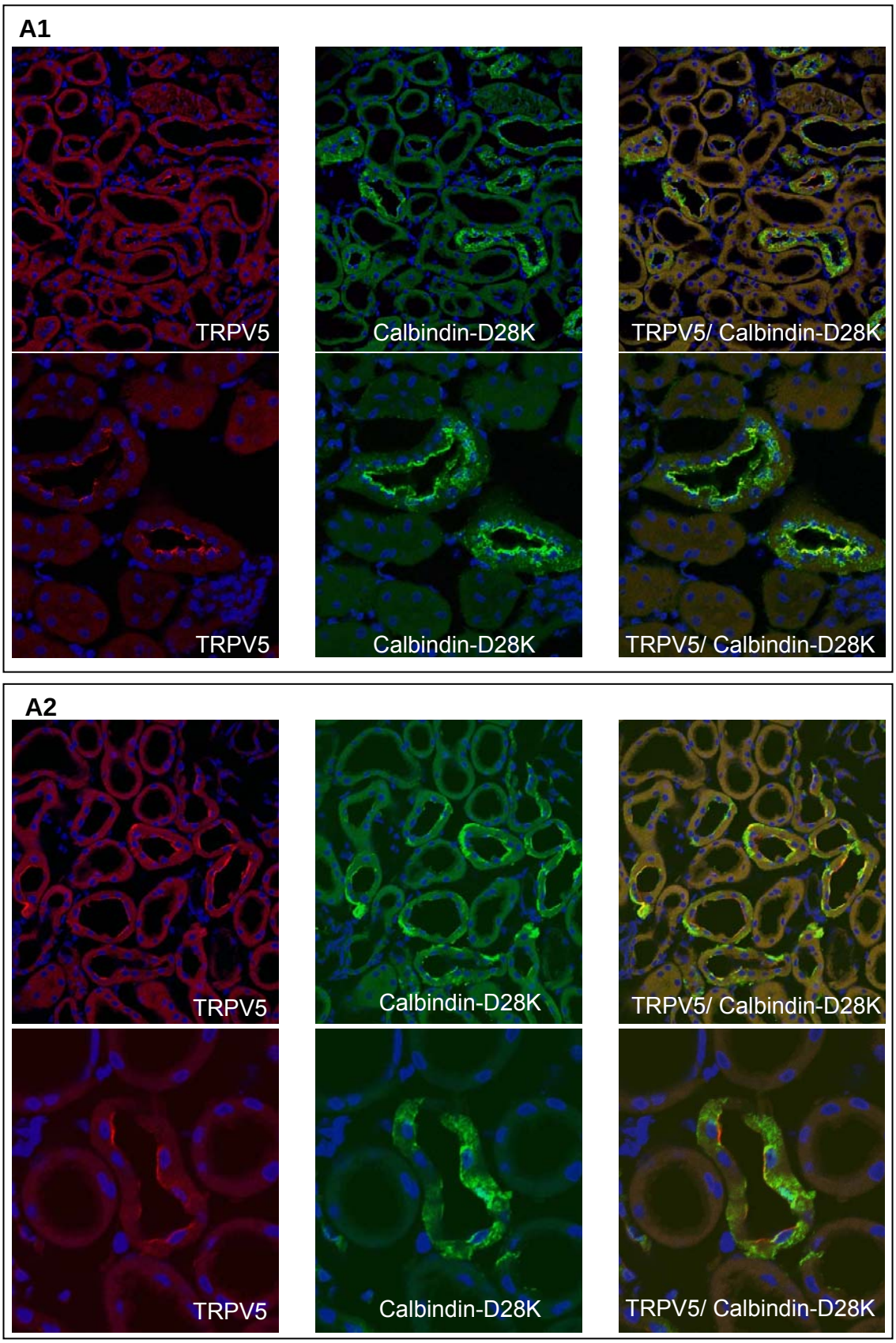

Fig 16A. Effects of chronic metabolic acidosis on the cellular localization of the epithelial Ca^{2+} channel TRPV5 in *Ogr1*$^{+/+}$ and *Ogr1*$^{-/-}$ mice. Immunohistochemical imaging of TRPV5 and calbindin-D_{28K} staining in kidney cortex of control group, (n=4 animals per group), **(A1)** *Ogr1*$^{+/+}$, (**A2**) *Ogr1*$^{-/-}$. TRPV5 (red), calbindin-D_{28K} (green) Control group: animals that received standard diet.

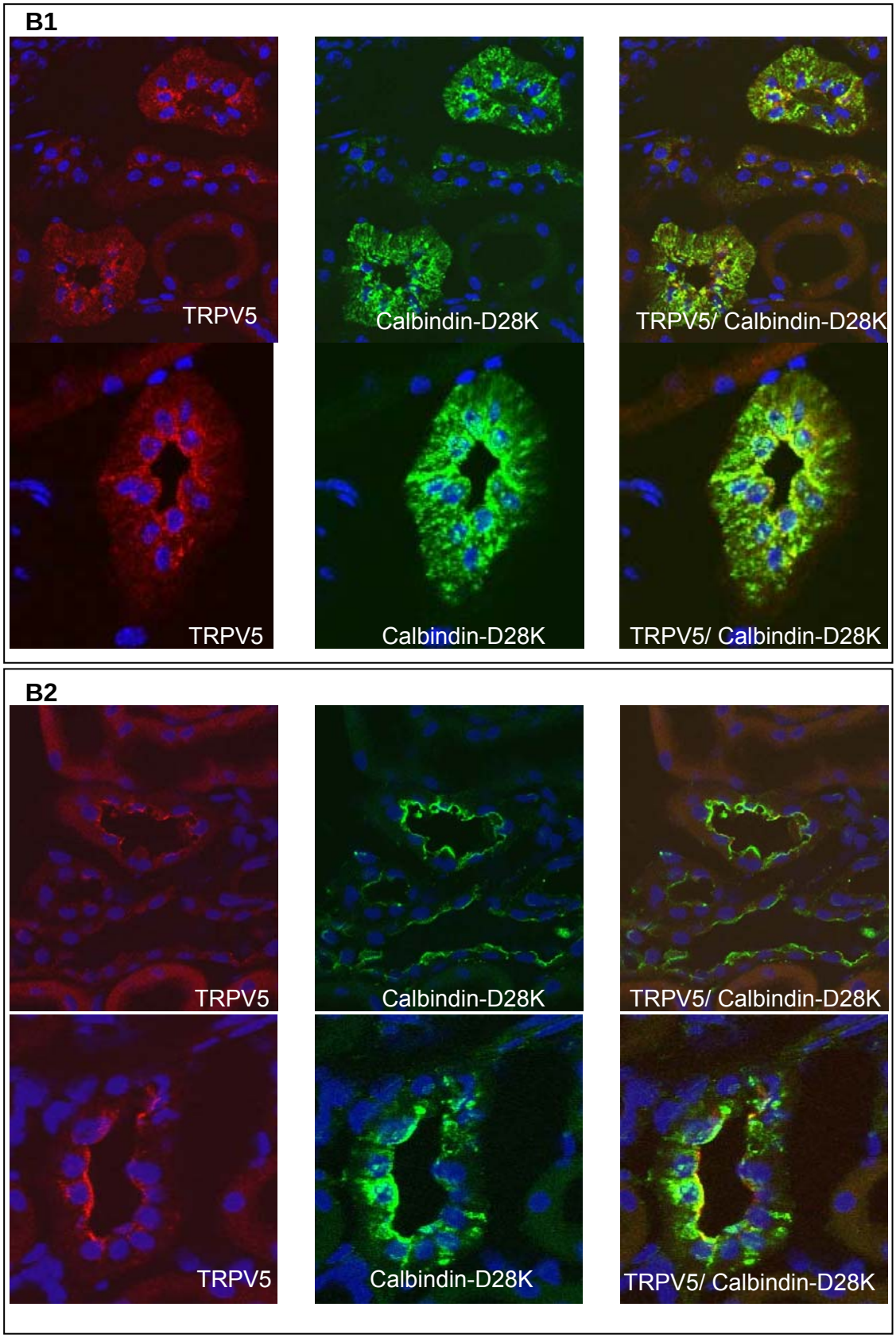

Fig 16B. Effects of chronic metabolic acidosis on the renal localization of the epithelial Ca^{2+} channel TRPV5 in *Ogr1*$^{+/+}$ and *Ogr1*$^{-/-}$ mice. Immunohistochemical imaging of TRPV5 and calbindin-D_{28K} staining in kidney cortex of 7 days NH_4Cl treated group; (n=4 animals per group) **(B1)** *Ogr1*$^{+/+}$, (**B2**) *Ogr1*$^{-/-}$, TRPV5 (red), calbindin-D_{28K} (green) Control group: animals that received standard diet; acidosis group: animals that received 2g NH_4Cl/100g food for 7 days.

12.1.6. Acetazolamide-induced metabolic acidosis does not alter urinary Ca^{2+} and Mg^{2+} excretion in knockout mice ($Ogr1^{-/-}$)

In an alternative model of metabolic acidosis, acidosis was induced in mice treated with the carbonic anhydrase inhibitor acetazolamide. Acetazolamide causes metabolic acidosis by inducing urinary bicarbonate wasting due to inhibition of proximal tubular bicarbonate reabsorption (73; 74). This type of metabolic acidosis is thus associated with high urinary pH and high net anion excretion and may therefore allow distinguishing between the effects of urinary and systemic pH (75).

Acetazolamide caused alkaline urinary pH, as expected (Table 3). In addition, urinary total and fractional Ca^{2+} and Mg^{2+} excretion were similar between wild-type and *Ogr1*$^{-/-}$ mice during acetazolamide treatment (Fig. 17A; B), also serum Ca^{2+} and Mg^{2+} concentrations (Fig. 18A; 18B), and all other urinary parameters (Table. 3) did not show significant differences between genotypes. Hence, inhibition of carbonic anhydrase does not alter urinary Ca^{2+} and Mg^{2+} excretion in knockout mice (*Ogr1*$^{-/-}$), whereas NH_4Cl-induced metabolic acidosis results in the exact opposite effects. Thus, luminal pH in the DCT/CNT seems to be important in the long-term hypercalciuric effect of chronic metabolic acidosis.

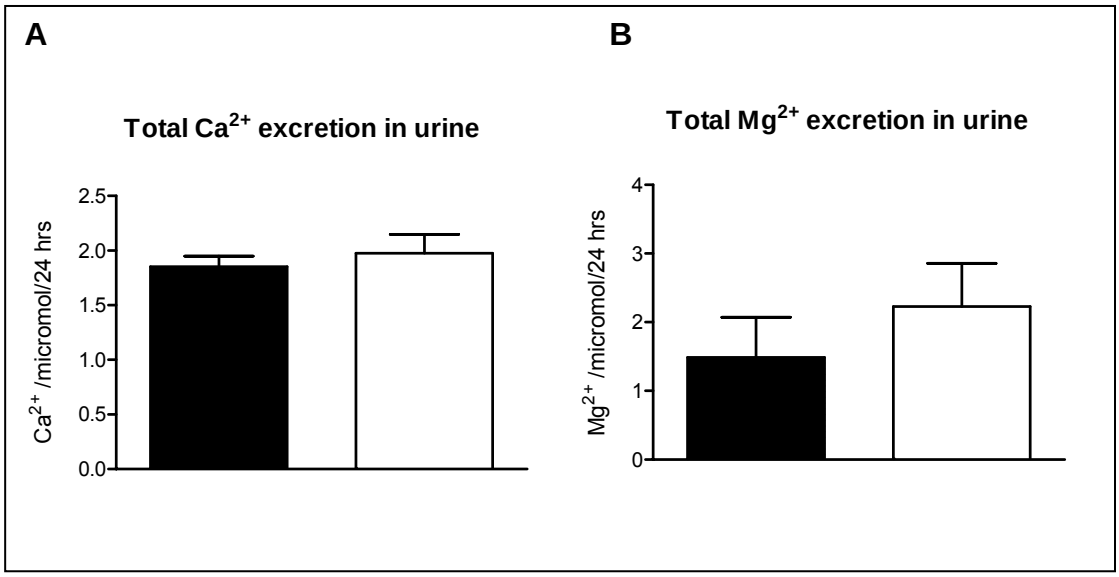

Fig. 17. Effect of acetazolamide-induced metabolic acidosis on urinary Ca^{2+} and Mg^{2+} excretion in wild-type (*Ogr1*$^{+/+}$) and OGR1 knockout mice (*Ogr1*$^{-/-}$). (n=8 animals per group) Mice were given the carbonic anhydrase inhibitor acetazolamide in food (20 mg/kg per d) for 7 days, which caused metabolic acidosis; Urinary Ca^{2+} **(A)** and Mg^{2+} **(B)** excretion were similar between wild-type and *Ogr1*$^{-/-}$ mice. Data are presented as means ± SEM, * $p < 0.05$. (■*Ogr1*$^{+/+}$, □*Ogr1*$^{-/-}$).

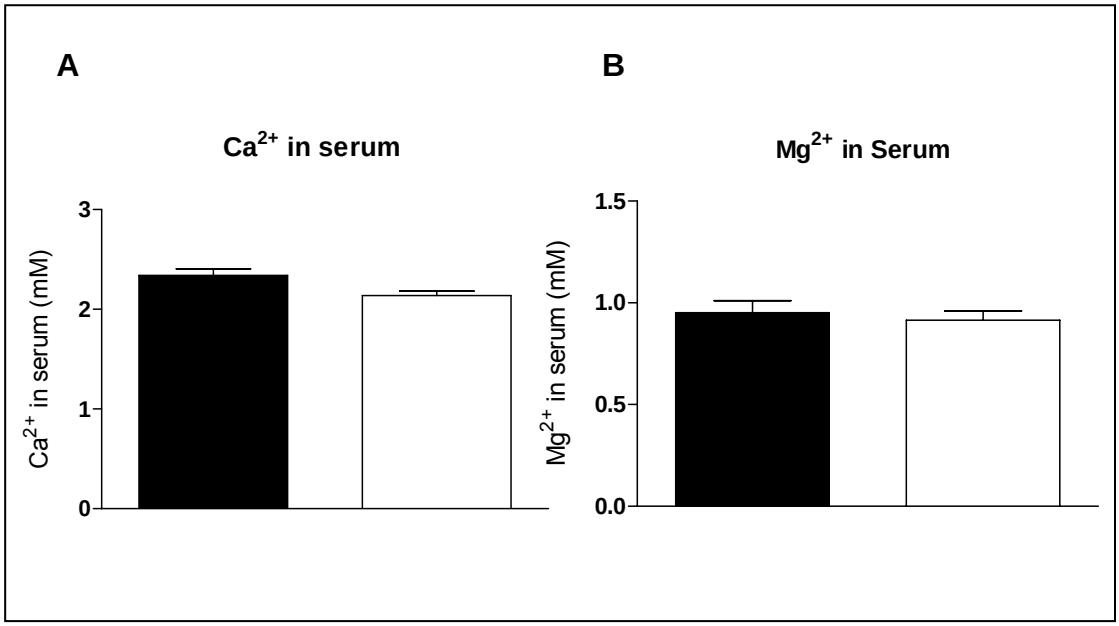

Fig. 18. Effect of acetazolamide-induced metabolic acidosis on serum Ca^{2+} and Mg^{2+} levels in wild-type (*Ogr1*$^{+/+}$) and OGR1 knockout mice (*Ogr1*$^{-/-}$). (n=8 animals per group) Mice were given the carbonic anhydrase inhibitor acetazolamide in food (20 mg/kg per d) for 7 days, which caused metabolic acidosis; Serum Ca^{2+} **(A)** and Mg^{2+} **(B)** levels were similar between wild-type and *Ogr1*$^{-/-}$ mice. Data are presented as means ± SEM * $p < 0.05$. (■*Ogr1*$^{+/+}$, □*Ogr1*$^{-/-}$).

	Acetazolamide group	
	***Ogr1*$^{+/+}$**	***Ogr1*$^{-/-}$**
Blood		
$[Ca^{2+}]$ mM in serum	2.34 ± 0.06	2.14 ± 0.04
$[Mg^{2+}]$ mM in serum	0.95 ± 0.06	0.91 ± 0.05
Urine		
pH	8.00 ± 0.08	7.83 ± 0.27
Creatinine (mg/dl)	27.1 ± 1.1	43.4 ± 5.4 *
NH_3/NH_4^+/ (mM)/crea (mg/dl)	2.0 ± 0.3	0.9 ± 0.1 **
Na^+(mM)/crea (mg/dl)	3.3 ± 0.3	2.7 ± 0.4
K^+(mM)/crea (mg/dl)	7.6 ± 0.3	6.9 ± 0.7
Ca^{2+}(mM)/crea (mg/dl)	0.031 ± 0.002	0.039 ± 0.002 *
Mg^{2+}(mM)/crea (mg/dl)	0.024 ± 0.009	0.042 ± 0.012
Phosphate(mg/dl)/crea(mg/dl)	2.2 ± 0.2	1.7 ± 0.3
Urine volume (ml)/ BW (g)	0.08 ± 0.01	0.05 ± 0.01 **
Weight change %	3.0 ± 0.9	1.2 ± 0.5

Table 3. Acetazolamide group: blood and urine analysis. (n=8 animals per group) Mice were given the carbonic anhydrase inhibitor acetazolamide in food (20 mg/kg per d) for 7 days,

Urinary excretion was normalized against creatinine (crea). BW: body weight.

* Significantly different between *Ogr1*$^{+/+}$ and *Ogr1*$^{-/-}$, * $p \leq 0.05$, ** $p \leq 0.01$.

12.1.7. Acetazolamide-induced metabolic acidosis does not alter renal mRNA and protein expression of Ca^{2+} and Mg^{2+} transport proteins in knockout mice ($Ogr1^{-/-}$)

During acetazolamide-induced metabolic acidosis, quantitative RT-PCR did not show differences between *Ogr1*$^{+/+}$ and *Ogr1*$^{-/-}$ in renal mRNA expression levels of the epithelial Ca^{2+} channel TRPV5 and the cytosolic Ca^{2+}-binding protein calbindin-D_{28K} ($CaBP_{28K}$) and the epithelial Mg^{2+} channels TRPM6 and TRPM7 (Fig. 19). Furthermore, immunoblotting for TRPV5, calbindin D28k, and TRPM6 after 7 days of acetazolamide demonstrated comparable expression levels of these proteins in kidney (Fig. 20).

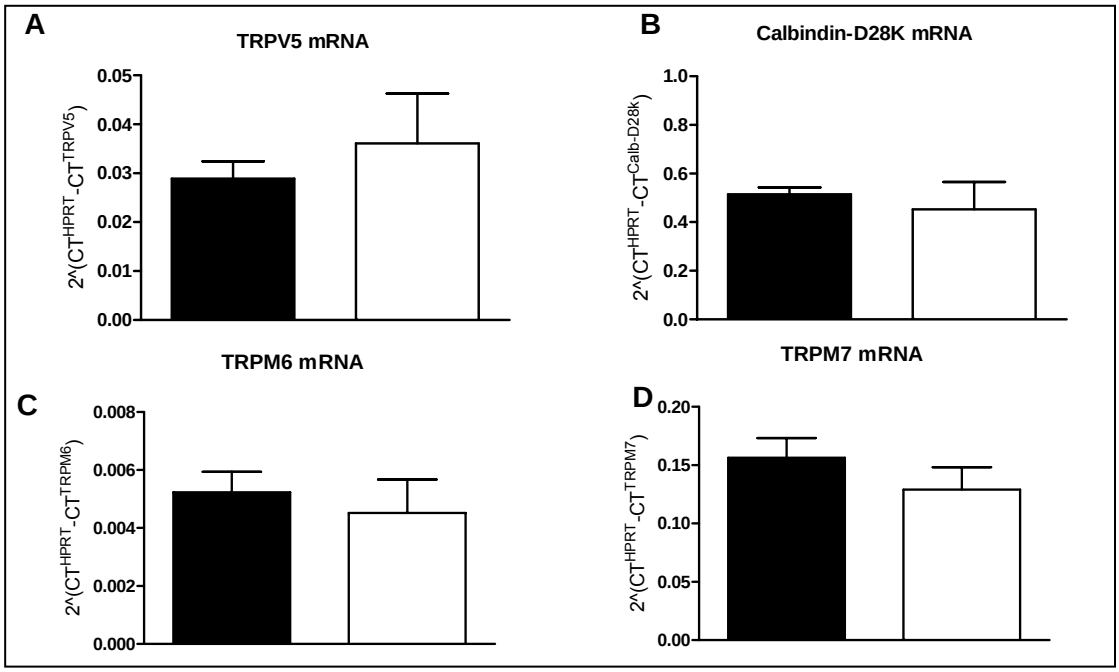

Fig 19. Effect of acetazolamide-induced metabolic acidosis on renal mRNA expression of Ca^{2+} and Mg^{2+} transport proteins in (*Ogr1*$^{+/+}$) and (*Ogr1*$^{-/-}$) mice. (n=6 animals per group) Renal mRNA expression levels of the epithelial Ca^{2+} channel TRPV5 and the cytosolic Ca^{2+}-binding protein calbindin-D_{28K} ($CaBP_{28K}$) **(A and B,** respectively**)** and the epithelial Mg^{2+} channels TRPM6 and TRPM7 **(C and D,** respectively**)** were determined during chronic metabolic acidosis by real-time quantitative PCR analysis (n=8 animals per group), The expression of genes was calculated in relation to hypoxanthine guanine phosphoribosyl transferase (HPRT), and relative expression ratios were calculated as $R=2^{(Ct(HPRT)-Ct(test\ gene)}$. Mice were given the carbonic anhydrase inhibitor acetazolamide in food (20 mg/kg per d) for 7 days, Data are presented as means ± SEM.
(■*Ogr1*$^{+/+}$, □*Ogr1*$^{-/-}$).

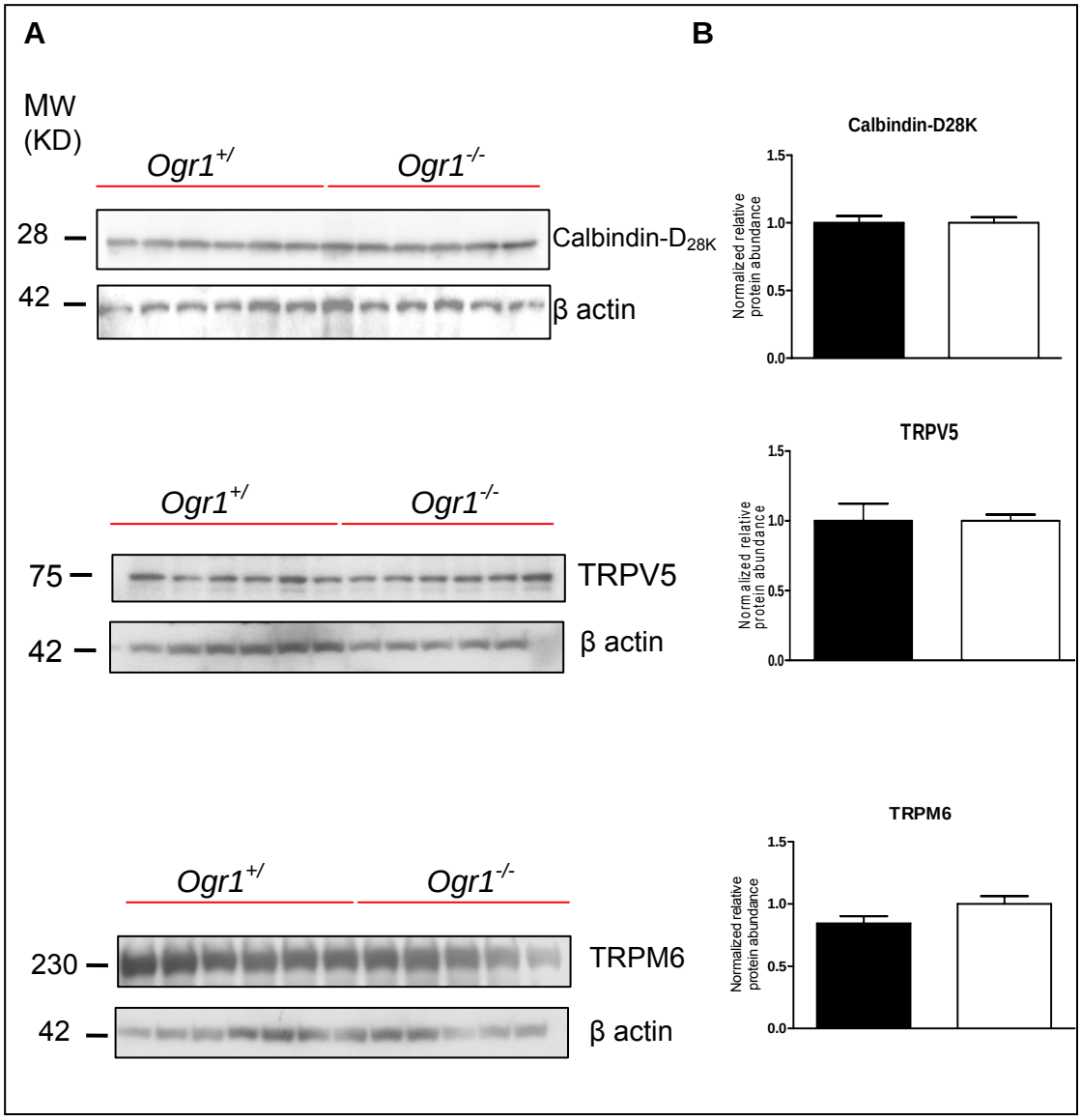

Fig 20. Effect of acetazolamide-induced metabolic acidosis on renal protein abundance of Ca^{2+} transport proteins in (*Ogr1*$^{+/+}$) and (*Ogr1*$^{-/-}$) mice.

Renal protein expression levels of the epithelial Ca^{2+} channel TRPV5, the cytosolic calbindin-D_{28K}, and the epithelial Mg^{2+} channel TRPM6 were determined during chronic metabolic acidosis by western blotting analysis **(A)**. Bar graphs summarizing data from immunoblotting **(B);** (n=6 animals per group), All data were normalized against β-actin. Mice were given the carbonic anhydrase inhibitor acetazolamide in food (20 mg/kg per d) for 7 days. Data are presented as means ± SEM. * $p < 0.05$.

(■*Ogr1*$^{+/+}$, □*Ogr1*$^{-/-}$).

12.2. Role of the H^+-Activated Ovarian Cancer G Protein-Coupled Receptor 1 (OGR1) in Renal Calcium and Magnesium handling

The expression of the proton activated receptor OGR1 as described earlier in the text, was detected in the kidney in most nephron segments including the thick ascending limb and distal tubule, major sides of regulated calcium and magnesium reabsorption (37; 38; 50; 51; 52). Under normal conditions, analysis of different urinary electrolytes in the *Ogr1*$^{-/-}$ mice did not show any changes compared to the wild-type animals (table 4). However, urinary magnesium excretion was reduced, and a tendency to a lower urinary calcium excretion was observed (Fig. 21, Table 4). Thus we tested if OGR1 contributes to the regulation of renal calcium and magnesium handling using different calcium and magnesium diets.

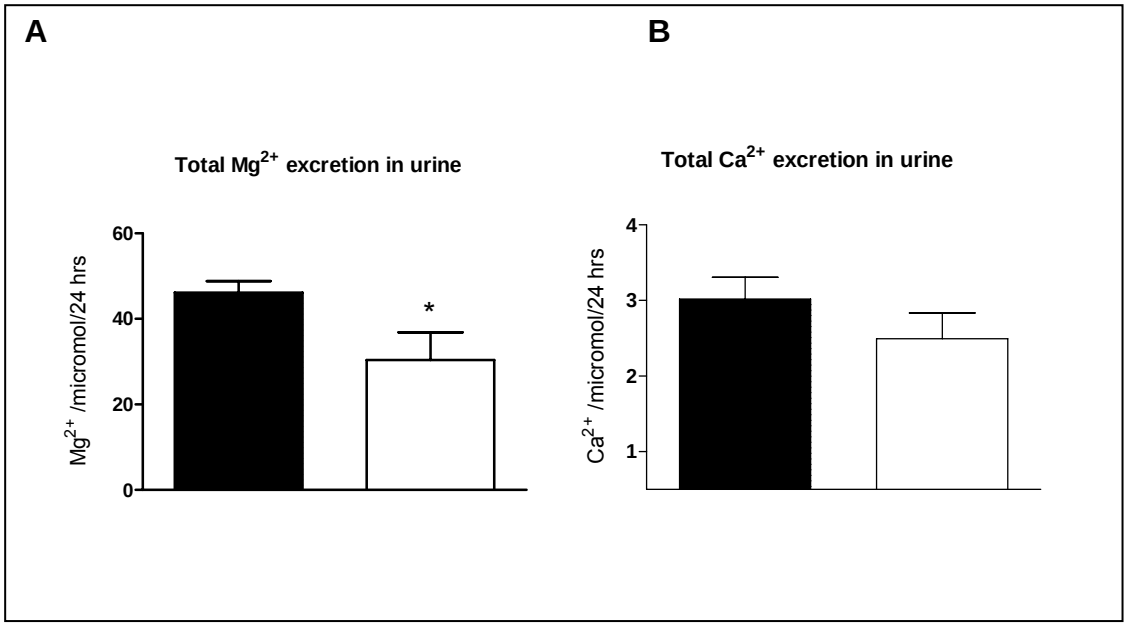

Fig 21. Urinary Ca^{2+} and Mg^{2+} excretion in wild-type (*Ogr1*$^{+/+}$) and OGR1 knockout mice (*Ogr1*$^{-/-}$). (n=8 animals per group) Mice were investigated on normal standard chow in metabolic cages and urine analyzed. *Ogr1* deficient mice showed lower urinary magnesium excretion **(A)**, However; no significant differences could be detected for calcium excretion between *Ogr1*$^{+/+}$ and *Ogr1*$^{-/-}$ mice **(B)**.

Data are presented as means ± SEM. * $p < 0.05$.

(■*Ogr1*$^{+/+}$, □*Ogr1*$^{-/-}$).

	Control group	
	***Ogr1*$^{+/+}$**	***Ogr1*$^{-/-}$**
Serum		
[Ca^{2+}] mM	2.10 ± 0.16	2.30 ± 0.12
[Mg^{2+}] mM	1.02 ± 0.04	1.06 ± 0.04
Urine		
pH	6.28 ± 0.14	6.65 ± 0.26
Creatinine (mg/dl)	55.8 ± 8.4	58.2 ± 8.3
Na^+(mM)/crea (mg/dl)	2.1 ± 0.5	2.5 ± 0.6
K^+(mM)/crea (mg/dl)	6.0 ± 1.1	6.7 ± 0.6
Ca^{2+}(mM)/crea (mg/dl)	0.042 ± 0.003	0.031 ± 0.004
Mg^{2+}(mM)/crea (mg/dl)	0.51 ± 0.14	0.34 ± 0.10 *
Phosphate(mg/dl)/crea(mg/dl)	0.33 ± 0.03	0.29 ± 0.02
Osmolality (mOsm/kg H_2O)	2518 ± 525	3050 ± 509
Urine volume (ml)/ BW (g)	0.04 ± 0.01	0.04 ± 0.06
Weight change %	1.4 ± 1.3	0.3 ± 1.1

Table 4. Control group: Summary of blood and urine analysis. (n=8 animals per group)
Mice were investigated in normal standard chow in metabolic cages and urine and blood analyzed.
Urinary excretion was normalized against creatinine (crea). BW: body weight.
* Significantly different between *Ogr1*$^{+/+}$ and *Ogr1*$^{-/-}$, * $p \leq 0.05$, ** $p \leq 0.01$, *** $p \leq 0.001$

12.2.1. OGR1 and regulation of Ca^{2+} and Mg^{2+} handling by dietary intake of Ca^{2+}

12.2.1.1. OGR1 may be involved in the renal regulation of Mg^{2+} and Ca^{2+} handling by dietary intake of Ca^{2+}

Ogr1$^{-/-}$ mice showed an altered renal excretion of Mg^{2+} after 2 and 7 days high Ca^{2+} diet (Fig. 22A; Table 5) and after 7 days low Ca^{2+} diet (Fig. 22B; Table 6). Serum Mg^{2+} concentrations were not different between *Ogr1*$^{+/+}$ and *Ogr1*$^{-/-}$ in all conditions (Fig. 24; Tables 5; 6) except after 7 days high Ca^{2+} treatment where the Mg^{2+} level in serum was higher in the *Ogr1*$^{-/-}$ compared to the wild-type mice. These results suggest possible alterations of Mg^{2+} handling on the kidney level.

In addition, *Ogr1*$^{-/-}$ mice showed an altered renal excretion of Ca^{2+} after 2 and 7 days high Ca^{2+} diet (Fig. 23A; Table 5), However, urinary Ca^{2+} excretion levels were not different between *Ogr1*$^{+/+}$ and *Ogr1*$^{-/-}$ when animals were treated with a low calcium diet (Fig. 23B) in all conditions, serum Ca^{2+} concentrations were not different between *Ogr1*$^{+/+}$ and *Ogr1*$^{-/-}$ (Fig. 25; Table 5; 6). These data suggest that OGR1 could be involved in the control of renal Ca^{2+} handling.

It is important to note that after 2 days high Ca^{2+} diet changes in urinary Ca^{2+} and Mg^{2+} excretion were parallel, however, after 7 days high Ca^{2+} diet the differences between Ogr1$^{+/+}$ and Ogr1$^{-/-}$ mice in the urinary Ca^{2+} and Mg^{2+} excretion were opposite (Fig 22A; 23A). In addition, after 7 days low Ca^{2+} diet, urinary Mg^{2+} level in Ogr1$^{-/-}$ was significantly higher compared to the Ogr1$^{+/+}$ while no changes were detected in the urinary Ca^{2+} excretion (Fig. 22B; 23B).

Taken together, these preliminary results suggest that the proton-activated receptor OGR1 may be involved in the renal regulation of Mg^{2+} and Ca^{2+} handling by dietary intake of Ca^{2+}.

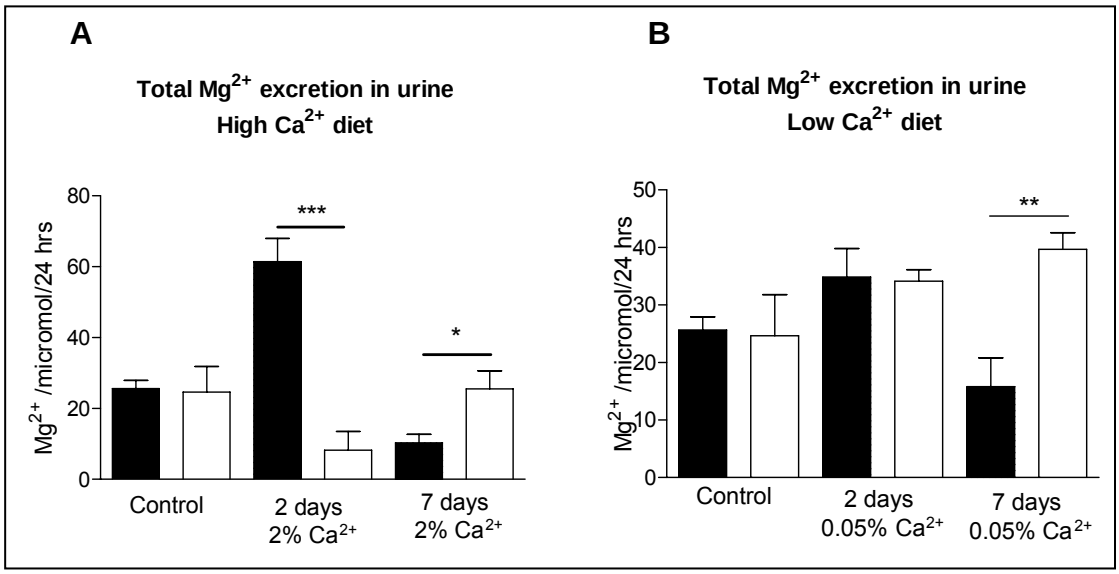

Fig 22. Urinary Mg^{2+} excretion during high (2 %) or low (0.05 %) calcium diets in wild-type (*Ogr1*$^{+/+}$) and OGR1 knockout mice (*Ogr1*$^{-/-}$). (n=8 animals per group) Mice were given either a high calcium diet (2% Ca^{2+}) **(A)** or a low calcium diet (0.05% Ca^{2+}) **(B)** for 2 or 7 days, respectively. *Ogr1*$^{-/-}$ mice showed altered Mg^{2+} excretion in these conditions. Control group: animals that received standard diet. Data are presented as means ± SEM. * $p < 0.05$, ** $p < 0.01$, *** $p < 0.001$.

(■*Ogr1*$^{+/+}$, □*Ogr1*$^{-/-}$).

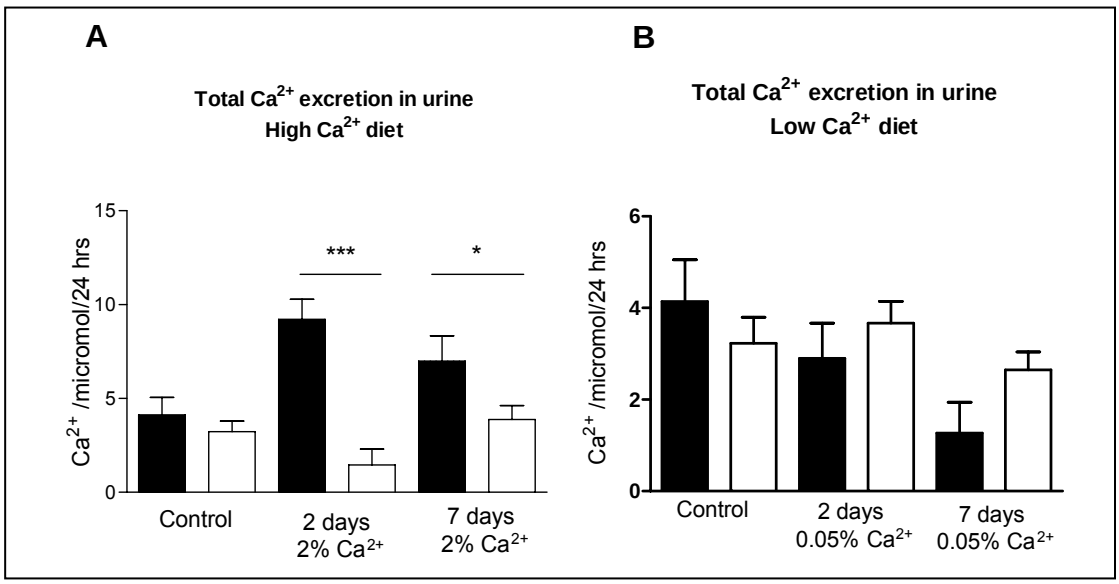

Fig 23. Urinary Ca^{2+} excretion during high and low calcium diets in wild-type (*Ogr1*$^{+/+}$) and OGR1 knockout mice (*Ogr1*$^{-/-}$). (n=8 animals per group) Mice were given either a high calcium diet (2% Ca^{2+}) **(A)** or a low calcium diet (0.05% Ca^{2+}) **(B)** for 2 or 7 days, respectively. Control group: animals that received standard diet.

Data are presented as means ± SEM. * $p < 0.05$, ** $p < 0.01$, *** $p < 0.001$.

(■*Ogr1*$^{++}$, □*Ogr1*$^{-/-}$).

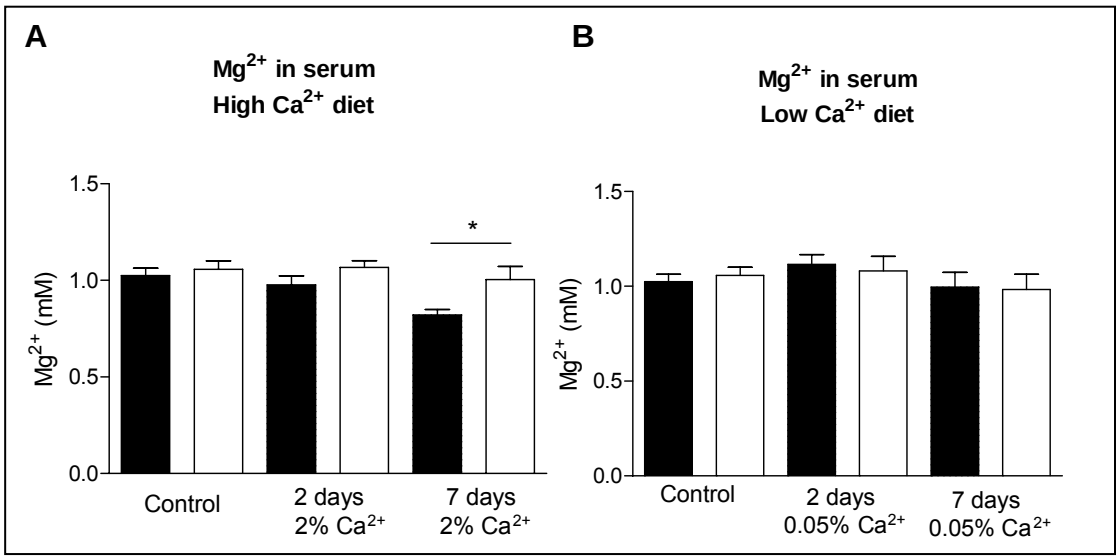

Fig 24. Serum Mg^{2+} concentration during high and/or low calcium diets in wild-type (*Ogr1*$^{+/+}$) and OGR1 knockout mice (*Ogr1*$^{-/-}$). (n=8 animals per group) Mice were given either a high calcium diet (2% Ca^{2+}) **(A)** or a low calcium diet (0.05% Ca^{2+}) **(B)** for 2 and 7 days, respectively. Serum magnesium levels were not affected by low and high calcium diets and are comparable in wild-type and OGR1 deficient mice. Control group: animals that received standard diet.

Data are presented as means ± SEM. * $p < 0.05$.

(■*Ogr1*$^{+/+}$, □*Ogr1*$^{-/-}$).

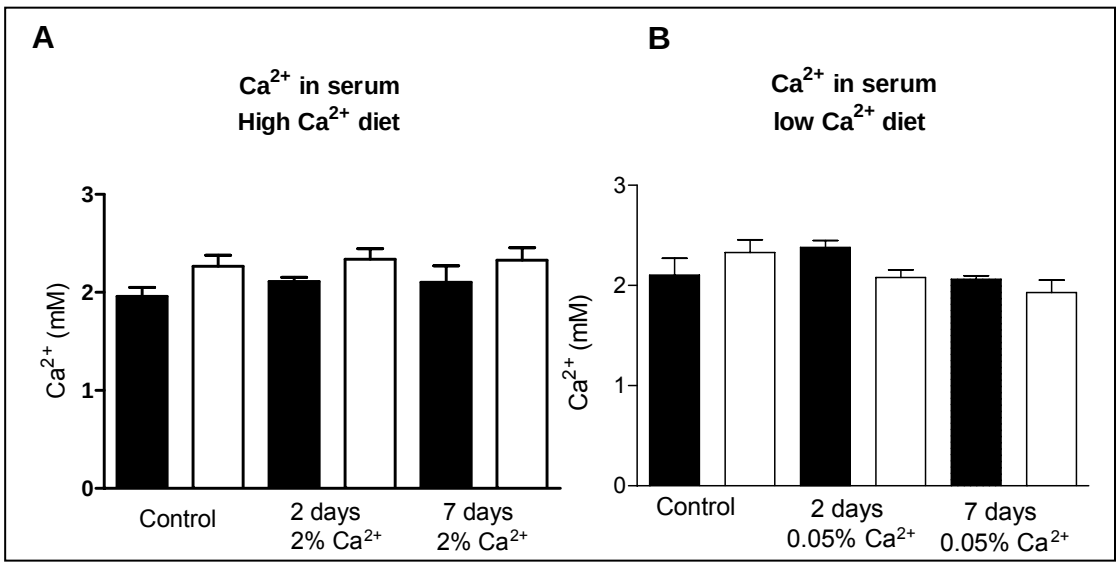

Fig 25. Serum total Ca^{2+} concentration during high and low calcium diets in wild-type (*Ogr1*$^{+/+}$) and OGR1 knockout mice (*Ogr1*$^{-/-}$). (n=8 animals per group) Mice were given either a high calcium diet (2% Ca^{2+}) **(A)** or a low calcium diet (0.05% Ca^{2+}) **(B)** for 2 and 7 days, respectively. Serum total calcium levels were not affected by low and high calcium diets and are comparable in wild-type and OGR1 deficient mice. Control group: animals that received standard diet. Data are presented as means ± SEM. * $p < 0.05$.

(■*Ogr1*$^{++}$, □*Ogr1*$^{-/-}$).

	2 days 2% Ca^{2+}		7 days 2% Ca^{2+}	
	Ogr1$^{+/+}$	*Ogr1*$^{-/-}$	*Ogr1*$^{+/+}$	*Ogr1*$^{-/-}$
Serum				
$[Ca^{2+}]$ mM	1.96 ± 0.10	2.30 ± 0.1	2.11 ± 0.04	2.34 ± 0.1
$[Mg^{2+}]$ mM	0.98 ± 0.04	1.06 ± 0.03	0.82 ± 0.03	1.00 ± 0.07 *
Urine				
pH	7.77 ± 0.41 ##	7.50 ± 0.25 #	7.53 ± 0.16 ###	7.53 ± 0.17 #
Creatinine (mg/dl)	45.1 ± 2.8	57.6 ± 8.4	35.5 ±9.3	32.6 ± 4.0 #
Na^{+}(mM)/crea (mg/dl)	9.4 ± 1.4 ###	9.8 ± 1.0 ###	15.3 ± 1.3 ###	11.4 ±2.0 ##
K^{+}(mM)/crea (mg/dl)	2.8 ± 0.4 ###	2.8 ± 0.4	5.4 ± 0.4	4.1 ± 0.8 #
Ca^{2+}(mM)/crea (mg/dl)	0.05 ± 0.01	0.04 ± 0.01	0.14 ± 0.02	0.05 ± 0.01 **
Mg^{2+}(mM)/crea (mg/dl)	0.38 ± 0.05	0.23 ± 0.06	0.18 ± 0.04 #	0.5 ± 0.1 *
Phosphate(mg/dl)/crea(mg/dl)	0.20 ± 0.03 #	0.34 ± 0.08	0.65 ± 0.10 #	0.70 ± 0.20 #
Osmolality (mOsm/kg H_2O)	1028 ± 135 #	2006 ± 316 *	1953 ± 298	2062 ± 222
Urine volume (ml)/ BW (g)	0.11 ± 0.02	0.02 ± 0.01 *	0.07 ± 0.01	0.07 ± 0.01
Weight change %	2.0 ± 0.7	1.7 ± 0.4	0.8 ± 0.7	1.7 ± 1.0

Table 5. High calcium group: Summary of Blood and urine analysis. (n=8 animals per group) High calcium group: animals that received high calcium diet (2% Ca^{2+}) for 2 and 7 days. Urinary excretion was normalized against creatinine (crea). BW: body weight.

* Significantly different between *Ogr1*$^{+/+}$ and *Ogr1*$^{-/-}$ for the same treatment, * $p \leq 0.05$, ** $p \leq 0.01$, *** $p \leq 0.001$

Significantly different between control group (Table 4) and treated group for the same genotype, # $p \leq 0.05$, ## $p \leq 0.01$, ### $p \leq 0.001$

	2 days 0.05% Ca^{2+}		7 days 0.05% Ca^{2+}	
	***Ogr1*$^{+/+}$**	***Ogr1*$^{-/-}$**	***Ogr1*$^{+/+}$**	***Ogr1*$^{-/-}$**
Serum				
$[Ca^{2+}]$ mM	2.40 ± 0.07	2.08 ± 0.07 *	2.06 ± 0.03	2.00 ± 0.12 #
$[Mg^{2+}]$ mM	1.12 ± 0.05	1.10 ± 0.08	1.00 ± 0.08	1.00 ± 0.10
Urine				
pH	5.87 ± 0.17	5.82 ± 0.12 #	5.84 ± 0.04 #	5.86 ± 0.03 #
Creatinine (mg/dl)	41.6 ± 6.0	37.6 ± 5.3	24.5 ± 5.3 ##	18.7 ± 1.3 ##
Na^{+}(mM)/crea (mg/dl)	16.0 ± 2.3 ###	9.4 ± 0.7 ###*	16.5 ± 1.9 ###	17.5 ± 0.6 ###
K^{+}(mM)/crea (mg/dl)	4.7 ± 0.2	3.2 ± 0.3 ###**	5.5 ± 0.7	6.5 ± 0.3
Ca^{2+}(mM)/crea (mg/dl)	0.06 ± 0.02	0.04 ± 0.01	0.07 ± 0.01	0.05 ± 0.01
Mg^{2+}(mM)/crea (mg/dl)	0.60 ± 0.005	0.41 ± 0.03 *	0.41 ± 0.10	0.72 ± 0.07 #*
Phosphate(mg/dl)/crea(mg/dl)	2.36 ± 0.44 ###	1.88± 0.24 ###	5.18 ± 0.6 ###	6.00 ± 0.41 ###
Osmolality (mOsm/kg H_2O)	3451 ± 345	1954 ± 241**	1731 ± 224	1852 ± 162 #
Urine volume (ml)/ BW (g)	0.07 ± 0.01 #	0.1 ± 0.01 ###	0.06 ± 0.02	0.1 ± 0.01 ###
Weight change %	0.94 ± 0.2	0.97 ± 0.6	1.3 ± 1.4	2.8 ± 0.5

Table 6. Low calcium group: Summary of Blood and urine analysis. (n=8 animals per group) Low calcium group: animals that received low calcium diet (0.05% Ca^{2+}) for 2 and 7 days. Urinary excretion was normalized against creatinine (crea). BW,: body weight.

* Significantly different between *Ogr1*$^{+/+}$ and *Ogr1*$^{-/-}$ for the same treatment, * $p \leq 0.05$, ** $p \leq 0.01$, *** $p \leq 0.001$

Significantly different between control group (Table 4) and treated group for the same genotype, # $p \leq 0.05$, ## $p \leq 0.01$, ### $p \leq 0.001$

12.2.1.2 OGR1 may be involved in the renal regulation of the epithelial Mg^{2+} channel TRPM6 by dietary intake of Ca^{2+}

Quantitative RT-PCR demonstrated that loss of OGR1 affects TRPM6 mRNA expression in the kidney in response to 2 and 7 days low and high Ca^{2+} diets (Fig. 26). After 2 and 7 days high Ca^{2+} diet changes in TRPM6 mRNA expression were parallel to the urinary magnesium excretion in the kidney (Fig. 26; 22). However, after 2 days low Ca^{2+} diet, TRPM6 mRNA levels in $Ogr1^{-/-}$ were significantly higher compared to the $Ogr1^{+/+}$ while no changes were detected in the urinary magnesium excretion (Fig. 26; 22).

Importantly, TRPM7 and Paracellin (Claudin 16) mRNA levels remained unaffected after low and high Ca^{2+} dietary intake (Fig. 27 A and B) indicating a selective difference.

In the intestine, no differences between *$Ogr1^{+/+}$* and *$Ogr1^{-/-}$* mice were detected in TRPM6 and TRPM7 mRNA expression after 2 days high and low Ca^{2+} diet (Fig. 28). Thus, our preliminary data suggest that OGR1 may be involved in the renal regulation of the epithelial magnesium channel TRPM6 expression by dietary Ca^{2+} intake.

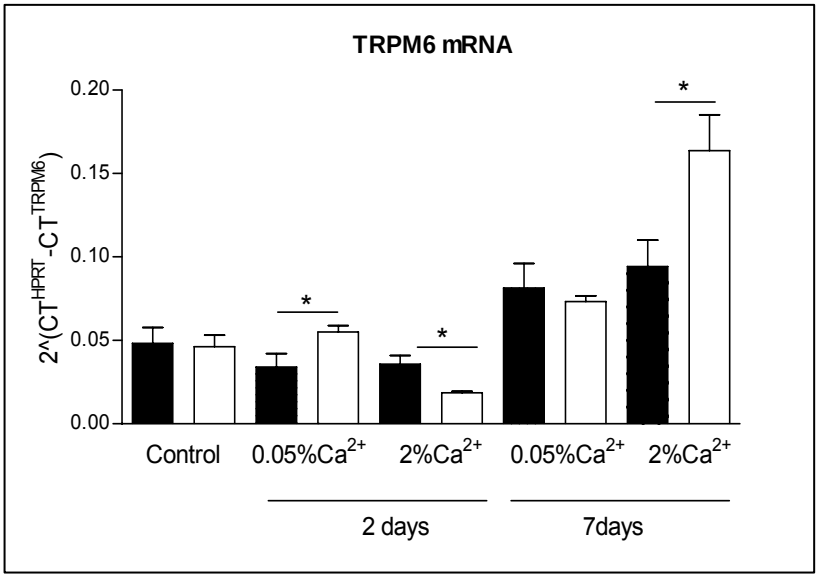

Fig 26. Effect of high and low calcium diets on renal mRNA expression of the epithelial Mg^{2+} channels TRPM6 in (*Ogr1*$^{+/+}$) and (*Ogr1*$^{-/-}$) mice.

Renal mRNA expression levels of the epithelial Mg^{2+} channels TRPM6 were determined in control, low calcium and high calcium groups by real-time quantitative PCR analysis (n=8 animals per group), The expression of genes was calculated in relation to hypoxanthine guanine phosphoribosyl transferase (HPRT), and relative expression ratios were calculated as $R=2^{(Ct(HPRT)-Ct(test\ gene)}$; Control group: animals that received standard diet; Low calcium group: animals that received low calcium diet (0.05% Ca^{2+}) for 2 and 7 days. High calcium group: animals that received high calcium diet (2% Ca^{2+}) for 2 and 7 days. Data are presented as means ± SEM. * $p < 0.05$

(■*Ogr1*$^{+/+}$, □*Ogr1*$^{-/-}$).

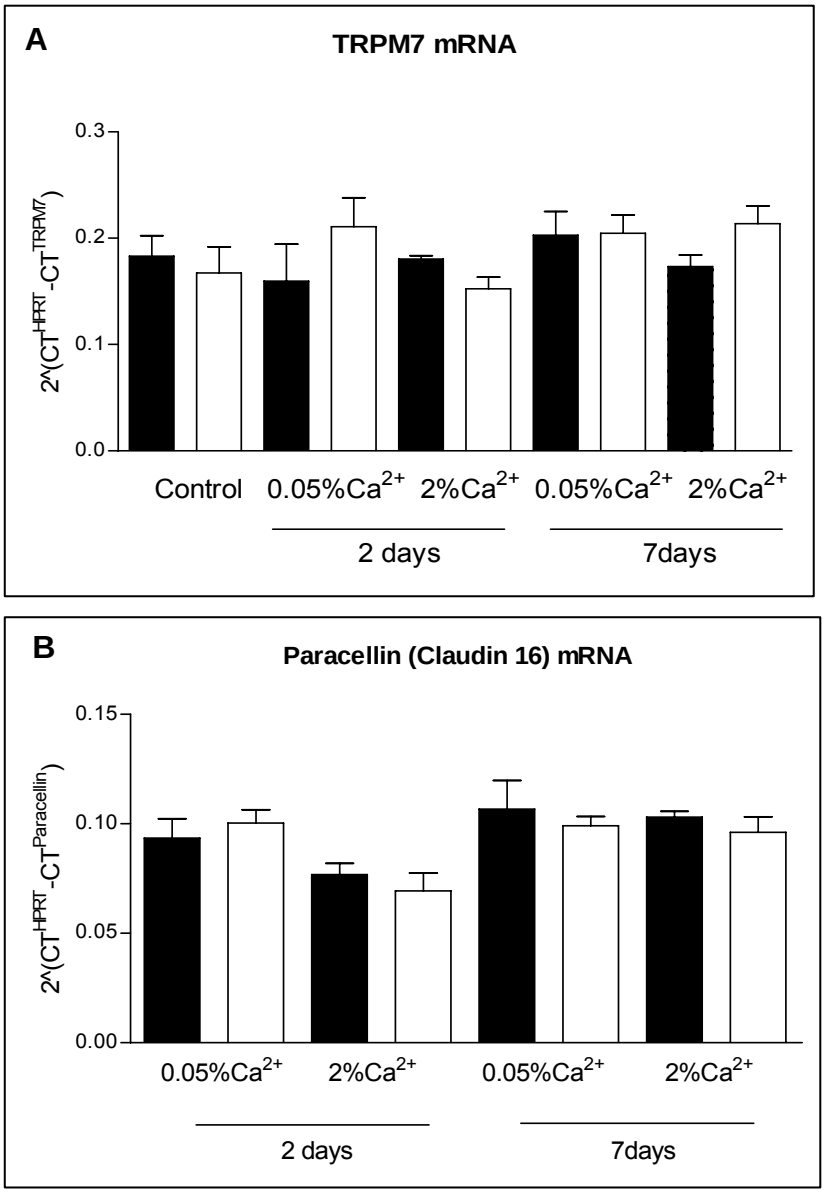

Fig 27. Effect of high and low calcium diets on renal mRNA expression of Mg^{2+} transport proteins in (*Ogr1*$^{+/+}$) and (*Ogr1*$^{-/-}$) mice.

Renal mRNA expression levels of the epithelial Mg^{2+} channel TRPM7 **(A)** and Paracellin (Claudin 16) **(B)** were determined in control, low calcium and high calcium groups by real-time quantitative PCR analysis (n=8 animals per group), The expression of genes was calculated in relation to hypoxanthine guanine phosphoribosyl transferase (HPRT), and relative expression ratios were calculated as $R=2^{(Ct(HPRT)-Ct(test\ gene)}$; Control group: animals that received standard diet; Low calcium group: animals that received low calcium diet (0.05% Ca^{2+}) for 2 and 7 days. High calcium group: animals that received high calcium diet (2% Ca^{2+}) for 2 and 7 days. Data are presented as means ± SEM. * $p < 0.05$.

(■*Ogr1*$^{+/+}$, □*Ogr1*$^{-/-}$).

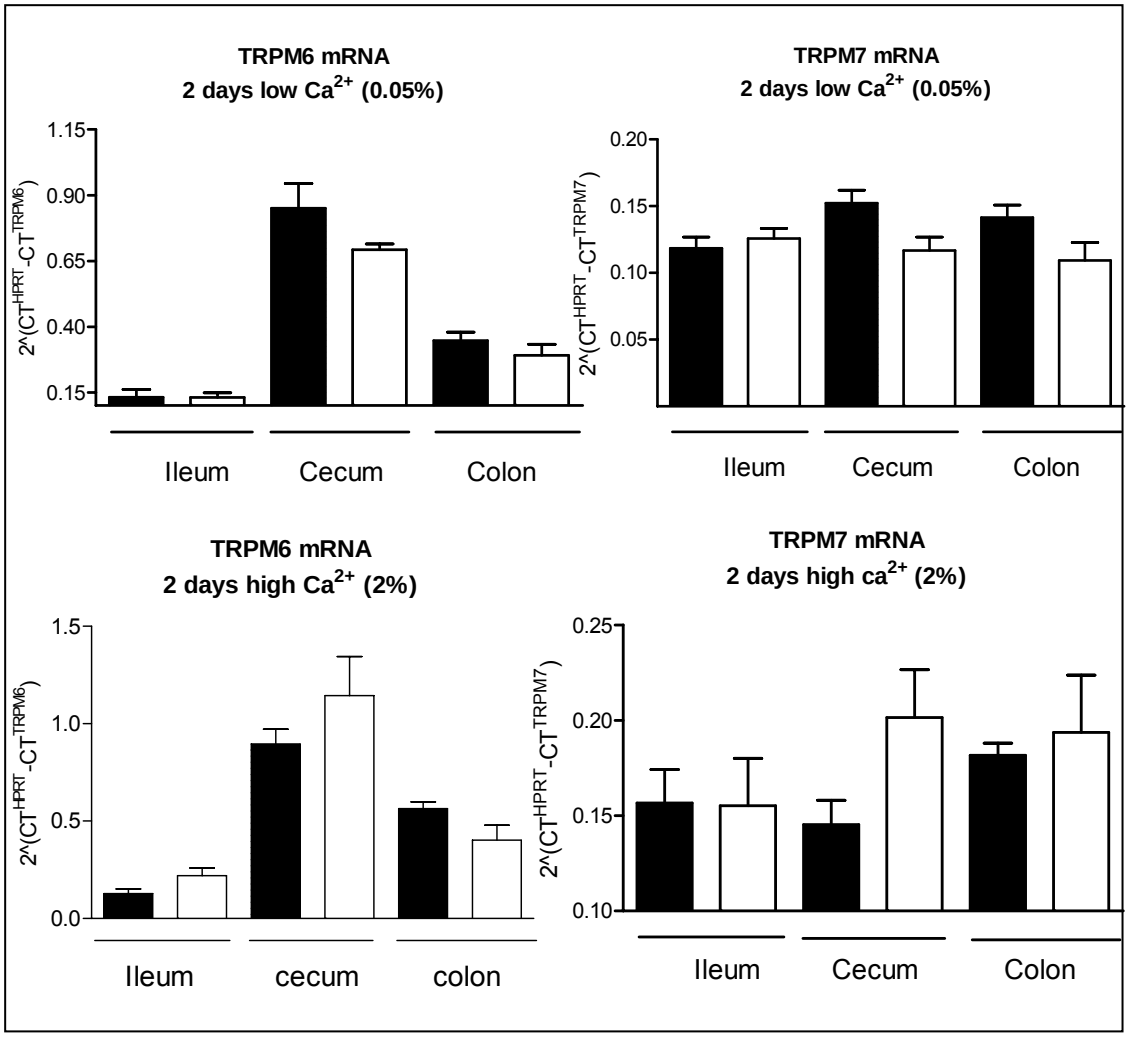

Fig. 28 Effect of low and high calcium diets on intestinal mRNA expression of Mg^{2+} transport proteins in (*Ogr1*$^{+/+}$) and (*Ogr1*$^{-/-}$) mice.

Renal mRNA expression levels of the epithelial Mg^{2+} channels TRPM6 and TRPM7 were determined in 2 days low and high calcium groups by real-time quantitative PCR analysis (n=8 animals per group), The expression of genes was calculated in relation to hypoxanthine guanine phosphoribosyl transferase (HPRT), and relative expression ratios were calculated as $R=2^{(Ct(HPRT)-Ct(test\ gene)}$; Control group: animals that received standard diet; Low calcium group: animals that received low calcium diet (0.05% Ca^{2+}) for 2 and 7 days. High calcium group: animals that received high calcium diet (2% Ca^{2+}) for 2 and 7 days. Data are presented as means ± SEM. * $p < 0.05$.

(■*Ogr1*$^{+\,+}$, □*Ogr1*$^{-/-}$).

12.2.2. OGR1 and regulation of Ca^{2+} and Mg^{2+} handling by dietary intake of Mg^{2+}

12.2.2.1 OGR1 may be involved in the renal regulation of Ca^{2+} and Mg^{2+} handling by dietary intake of Mg^{2+}

Ogr1$^{-/-}$ mice showed an altered renal excretion of Mg^{2+} after 7 days high Mg^{2+} diet (Fig. 29A; Table 7) but not after low Mg^{2+} treatment (Fig. 24B; Table 8). Additionaly, urinary Ca^{2+} excretion levels were not different between *Ogr1*$^{+/+}$ and *Ogr1*$^{-/-}$ when animals were treated with both high and low Mg^{2+} diets (Fig. 30; tables 7 and 8).

After 7 days high Mg^{2+} diet, serum Ca^{2+} and Mg^{2+} concentrations showed higher levels in the *Ogr1*$^{-/-}$ compared to the *Ogr1*$^{+/+}$ (Fig. 31A; 32A), however no significant changes in the serum Ca^{2+} and Mg^{2+} concentrations were observed after 2 days high Mg^{2+} diet (Fig. 31A; 32A) or 2 and 7 days low Mg^{2+} diet (Fig. 31B; 32B).

These preliminary data suggest that OGR1 could be involved in the control of renal Ca^{2+} and Mg^{2+} handling by dietary intake of Mg^{2+}.

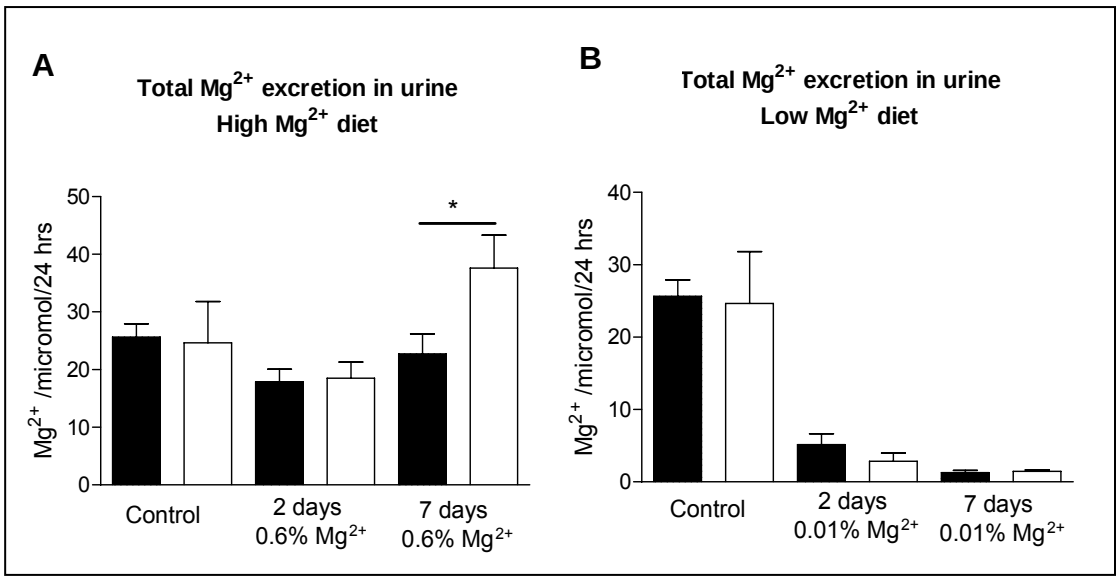

Fig 29. Urinary Mg^{2+} excretion during high and low magnesium diets in wild-type (*Ogr1*$^{+/+}$) and OGR1 knockout mice (*Ogr1*$^{-/-}$). (n=8 animals per group) Mice were given either a high magnesium diet (0.6% Mg^{2+}) **(A)** or a low magnesium diet (0.01% Mg^{2+}) **(B)** for 2 and 7 days, respectively. *Ogr1*$^{-/-}$ mice showed altered Mg^{2+} excretion only after 7 days high magnesium diet. Control group: animals that received standard diet.

Data are presented as means ± SEM. * $p < 0.05$.

(■*Ogr1*$^{+/+}$, □*Ogr1*$^{-/-}$).

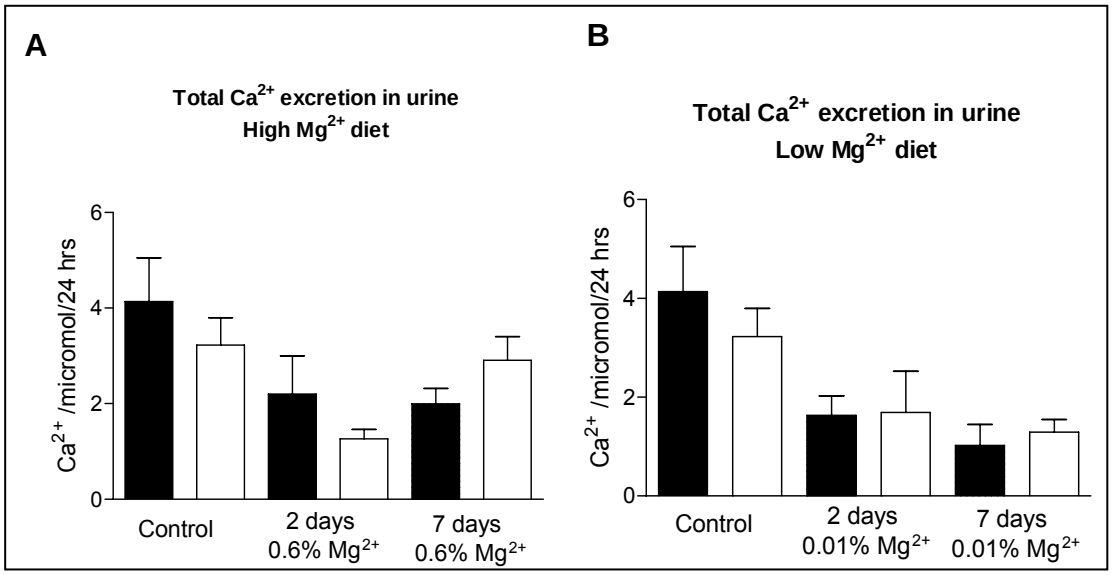

Fig 30. Urinary Ca^{2+} excretion during high and low Magnesium diets in wild-type (*Ogr1*$^{+/+}$) and OGR1 knockout mice (*Ogr1*$^{-/-}$). (n=8 animals per group) Mice were given either a high magnesium diet (0.6% Mg^{2+}) **(A)** or a low magnesium diet (0.01% Mg^{2+}) **(B)** for 2 and 7 days, respectively. Control group: animals that received standard diet.

Data are presented as means ± SEM. * $p < 0.05$.

(■*Ogr1*$^{++}$, □*Ogr1*$^{-/-}$).

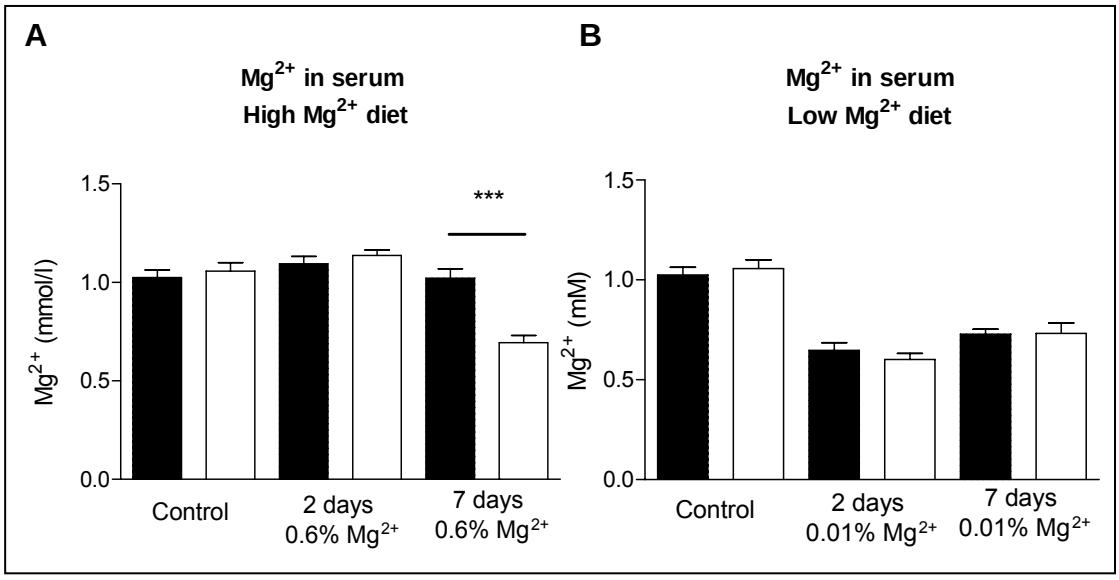

Fig 31. Serum Mg^{2+} concentration during high and low magnesium diets in wild-type (*Ogr1*$^{+/+}$) and OGR1 knockout mice (*Ogr1*$^{-/-}$). (n=8 animals per group) Mice were given either a high magnesium diet (0.6% Mg^{2+}) **(A)** or a low calcium diet (0.01% Mg^{2+}) **(B)** for 2 and 7 days, respectively. Control group: animals that received standard diet.

Data are presented as means ± SEM. * $p < 0.05$.

(■*Ogr1*$^{+/+}$, □*Ogr1*$^{-/-}$).

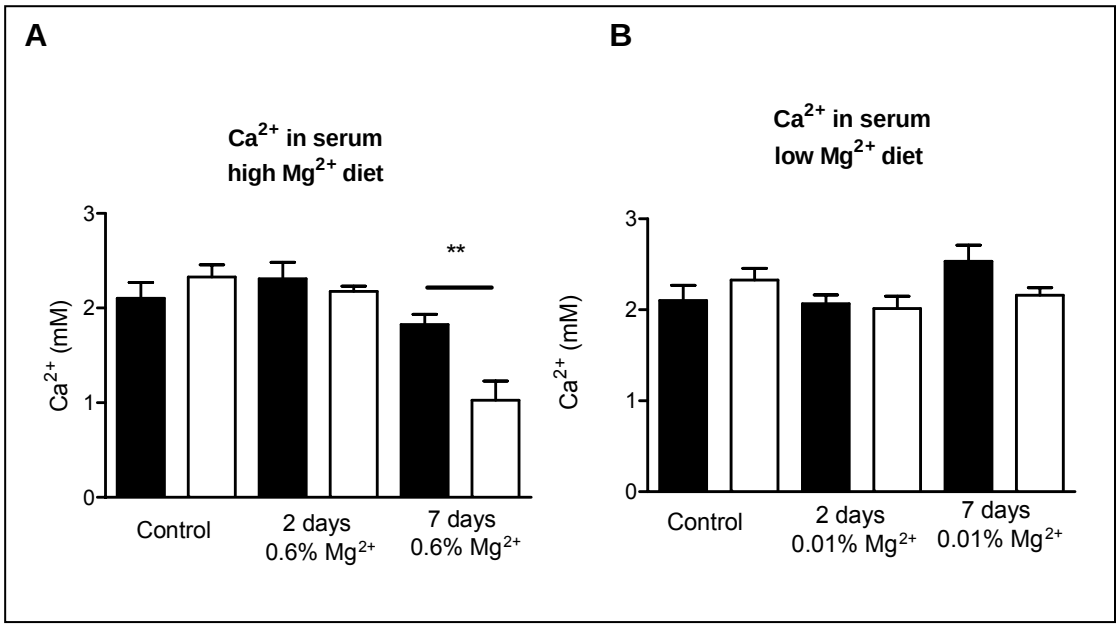

Fig 32. Serum total Ca^{2+} concentration during high and low magnesium diets in wild-type (*Ogr1*$^{+/+}$) and OGR1 knockout mice (*Ogr1*$^{-/-}$). (n=8 animals per group) Mice were given either a high magnesium diet (0.6% Mg^{2+}) **(A)** or a low calcium diet (0.01% Mg^{2+}) **(B)** for 2 and 7 days, respectively. Control group: animals that received standard diet.

Data are presented as means ± SEM. * $p < 0.05$.

(■*Ogr1*$^{+/+}$, □*Ogr1*$^{-/-}$).

	2 days 0.6% Mg^{2+}		7 days 0.6% Mg^{2+}	
	***Ogr1*$^{+/+}$**	***Ogr1*$^{-/-}$**	***Ogr1*$^{+/+}$**	***Ogr1*$^{-/-}$**
Serum				
$[Ca^{2+}]$ mM	2.31 ± 0.17	2.17 ± 0.05	1.83 ± 0.11 $^{\#}$	1.03 ± 0.20 **
$[Mg^{2+}]$ mM	1.10 ± 0.04	1.14 ± 0.03	1.02 ± 0.05	0.70 ± 0.03 $^{\#\#\#}$ ***
Urine				
pH	6.80 ± 0.23	7.40 ± 0.13 $^{\#}$	7.09 ± 0.14 $^{\#\#}$	6.83 ± 0.12
Creatinine (mg/dl)	127.2 ± 23.34	133.1± 21.38 $^{\#}$	16.17 ± 3.56 $^{\#\#\#}$	33.55 ± 4.07 **$^{\#}$
Na^{+}(mM)/crea (mg/dl)	3.58 ± 0.56	4.13 ± 0.24 $^{\#}$	25.37 ± 2.19 $^{\#\#\#}$	12.69 ±1.03 $^{\#\#\#}$ ***
K^{+}(mM)/crea (mg/dl)	1.65 ±0.14 $^{\#\#\#}$	1.74 ±0.13 $^{\#\#\#}$	8.04 ± 0.86	4.63 ± 0.48 $^{\#}$**
Ca^{2+}(mM)/crea (mg/dl)	0.02 ±0.005 $^{\#\#}$	0.01 ± 0.001 $^{\#}$	0.1 ± 0.012	0.054 ± 0.012 *
Mg^{2+}(mM)/crea (mg/dl)	0.18 ± 0.03 $^{\#\#}$	0.16 ± 0.02 $^{\#}$	1.16 ± 0.12 $^{\#\#}$	0.62 ± 0.1 **
Phosphate(mg/dl)/crea(mg/dl)	0.18 ± 0.01 $^{\#\#}$	0.10±0.02 $^{\#\#\#}$**	1.00 ± 0.08 $^{\#\#\#}$	0.56 ± 0.14 *
Urine volume (ml)/ BW (g)	0.043 ± 0.01	0.04 ± 0.01	0.06 ± 0.006	0.1 ± 0.01 $^{\#\#}$
Weight change %	3.64 ± 0.63	2.54 ± 0.59	2.83 ± 0.32	2.33 ± 0.60

Table 7. High magnesium group: Summary of Blood and urine analysis. (n=8 animals per group) High magnesium group: animals that received high magnesium diet (0.6% Mg^{2+}) for 2 and 7 days. Urinary excretion was normalized against creatinine (crea). BW: body weight.

* Significantly different between *Ogr1*$^{+/+}$ and *Ogr1*$^{-/-}$ for the same treatment, * $p \leq 0.05$, ** $p \leq 0.01$, *** $p \leq 0.001$

$^{\#}$ Significantly different between control group (Table 4) and treated group for the same genotype, $^{\#}$ $p \leq 0.05$, $^{\#\#}$ $p \leq 0.01$, $^{\#\#\#}$ $p \leq 0.001$

	2 days 0.01% Mg^{2+}		7 days 0.01% Mg^{2+}	
	***Ogr1*$^{+/+}$**	***Ogr1*$^{-/-}$**	***Ogr1*$^{+/+}$**	***Ogr1*$^{-/-}$**
Serum				
$[Ca^{2+}]$ mM	2.06 ± 0.09	2.01 ± 0.13	2.53 ± 0.18 $^{\&}$	2.16 ± 0.08
$[Mg^{2+}]$ mM	0.65 ± 0.04 $^{\#\#\#}$	0.60 ± 0.03 $^{\#\#\#}$	0.73 ± 0.02 $^{\#\#\#}$	0.73 ± 0.05 $^{\&\ \#\#\#}$
Urine				
pH	6.55 ± 0.1	6.24 ± 0.05	6.07 ± 0.03	6.1 ± 0.02
Creatinine (mg/dl)	40.72 ± 7.7	53.85 ± 12.9	33.06 ± 2.8 $^{\#\#}$	17.4 ± 4.19 $^{\#\#\#}$ **
Na^{+}(mM)/crea (mg/dl)	12.75±1.24 $^{\#\#\#}$	10.26 ±1.47 $^{\#\#}$	12.26 ± 1.14 $^{\#\#\#}$	24.78 ±2.99$^{\#\#\#}$ **
K^{+}(mM)/crea (mg/dl)	4.94 ± 0.4	3.34 ± 0.4 $^{\#\#\#\ *}$	4.56 ± 0.43	8.96 ± 0.88 ***
Ca^{2+}(mM)/crea (mg/dl)	0.03 ± 0.01$^{\#}$	0.03 ± 0.01	0.03 ± 0.01$^{\#}$	0.04 ± 0.01
Mg^{2+}(mM)/crea (mg/dl)	0.08 ± 0.01 $^{\#\#}$	0.07 ± 0.01 $^{\#\#}$	0.025 ± 0.01 $^{\#\#\#}$	0.04 ±0.01 $^{\#\#}$
Phosphate(mg/dl)/crea(mg/dl)	1.37 ± 0.12 $^{\#\#\#}$	1.02 ± 0.21 $^{\#\#}$	1.52 ± 0.10 $^{\#\#}$	3.28 ± 0.63$^{\#\#\#\ *}$
Urine volume (ml)/ BW (g)	0.062 ± 0.01	0.03 ± 0.01	0.07 ± 0.01 $^{\#}$	0.1 ± 0.01 $^{\#\#}$
Weight change %	5.36 ± 0.7 $^{\#}$	4.45 ± 0.7 $^{\#}$	1.28 ± 0.2	1.0 ± 0.7

Table 8. Low magnesium group: Summary of blood and urine analysis. . (n=8 animals per group) Low magnesium group: animals that received low magnesium diet (0.01% Mg^{2+}) for 2 and 7 days. Urinary excretion was normalized against creatinine (crea). BW: body weight.

* Significantly different between *Ogr1*$^{+/+}$ and *Ogr1*$^{-/-}$ for the same treatment, * $p \leq 0.05$, ** $p \leq 0.01$, *** $p \leq 0.001$

$^{\#}$ Significantly different between control group (Table 4) and treated group for the same genotype, $^{\#}$ $p \leq 0.05$, $^{\#\#}$ $p \leq 0.01$, $^{\#\#\#}$ $p \leq 0.001$

13. DISCUSSION

13.1. Role of OGR1 in systemic and renal acid-base homeostasis

Systemic acid-base homeostasis is mainly characterized by a constant pH of around 7.40 and a bicarbonate concentration of 25 mM in blood and most extracellular fluids. Both blood pH and bicarbonate concentration are regulated by different organs including kidney, lungs, intestine, skeletal muscle and bone, and may be altered by many factors such as physical activity, dietary intake, metabolism and diseases (106; 107). The kidney plays a major role in controlling systemic acid-base homeostasis and thus needs to respond to systemic and local changes in pH and bicarbonate levels. Several regulatory factors have been implicated into the control of renal acid-base handling such as the renin-angiotensin-aldosterone system or endothelin, in addition, local pH sensing mechanisms have been observed (107), however their molecular identity and regulation have remained elusive to date.

Recently, *Ludwig et al.* reported that the novel G-protein coupled receptor OGR1 acts as a proton sensing receptor, and that its activation by extracellular protons leads to IP_3 production and transient intracellular calcium release (5). In the present project, we demonstrated in agreement with previous studies (Xu Y 1996, Zhu K 2001), that OGR1 mRNA is expressed in various tissues including epithelial structures such as kidney and small and large intestine, where are expressed the major acid-base transporters. In the kidney we detected OGR1 expression in different nephron segments, importantly; the distal convoluted tubule and the collecting duct.

Interestingly, using stably OGR1-transfected cells we demonstrated in a different project that did not contribute to this work (N Mohebbi, C Benabbas, CA Wagner unpublished results) that OGR1 affects in a pH-dependent manner the activity of two important proton transporters in the kidney: NHE3, a major Na^+/H^+ exchanger in the proximal tubule (109), and vacuolar H^+-ATPases which are expressed in the proximal tubule and the type A intercalated cells of the collecting duct (110). Therefore, we aimed in the present study to evaluate the potential role of OGR1 in the regulation of acid-

base transport and homeostasis *in vivo* using the OGR1 deficient mouse model.

Under control conditions, no differences in systemic acid-base parameters in blood or urine could be detected. Importantly, both wild-type and *Ogr1*$^{-/-}$ mice that received NH_4Cl developed chronic metabolic acidosis characterized by a decrease in blood pH, a reduced serum HCO_3^- concentration, and a low urine pH with similar ammonium excretion, as was described in previous studies from our laboratory for other mouse models (75; 61).

However, in contrast to our expectations, during NH_4Cl induced chronic metabolic acidosis, no impairment of acid-base handling was seen in the *Ogr1*$^{-/-}$ mice indicating that OGR1 is dispensable for normal acid-base status and adaptation to an acute or chronic acid-load.

These results could be explained by the presence of other extracellular proton sensing receptors or pH-sensitive regulatory processes as well as by different mechanisms which may have a compensatory effect. Indeed, the presence of other regulatory factors *in vivo* (*Ogr1*$^{-/-}$ mouse model) could compensate for loss of OGR1 activity. The G-protein coupled receptor GPR4 is expressed in various tissues including epithelial structures such as kidney and intestine, major sides of regulated acid-base transport. In the kidney, GPR4 mRNA expression was detected in different nephron segments importantly in the collecting duct along with OGR1 (A Velic, C Benabbas, CA Wagner unpublished results). However, we did not find changes in GPR4 mRNA expression in OGR1 deficient mice. Moreover, mice deficient for OGR1 and GPR4 do not show more exacerbated metabolic acidosis compared to their wild-type or single KO mice indicating that OGR1 and GPR4 do not compensate for each other (Velic, Wagner, unpublished results).

Furthermore, the soluble adenylyl cyclase (sAC) has been described as an intracellular pH sensor that is expressed in different tissues including epididymis, testis and kidney (119; 120; 121; 122). In the kidney the sAC is mainly expressed in the thick ascending limb, the distal tubule and the collecting duct. The sAC is activated by a rise in intracellular calcium and bicarbonate ions, and its stimulation leads to intracellular elevation of cAMP concentrations (120; 123). Recently, *Paunescu et al.* (2008) showed that in

the kidney, the sAC is highly expressed in type A and B intercalated cells, and its localization partially overlaps with the V-ATPases (124). They therefore suggested that the sAC regulated cAMP signaling may constitute a general sensing mechanism for regulating V-ATPase mediated proton transport in the kidney (124). These findings are consistent with the hypothesis that the sAC could be a part of the pH sensing mechanism compensating the absence of OGR1.

Furthermore, in a kidney proximal tubule epithelial cell line, Pyk2 activation by intracellular acidification was shown to be required for acid activation of NHE3 and c-Src kinase (125). In addition, other studies suggested that intracellular acidosis in the proximal tubule cells is sensed by Pyk2 kinase which then activates c-Src. In a parallel pathway, acid activates ERK1/2 resulting in increased c-fos/c-jun abundance. Together with c-fos/c-jun, Pyk2/c-Src increases transcription factors leading to the increased NHE3 activity in the proximal tubule. We therefore speculate that Pyk2/c-Src pathway may be involved in the pH sensing mechanism compensating the absence of OGR1 activity (128).

Clearly, further work is needed to elucidate the role of OGR1 in the acid base regulation and to understand the exact mechanism of local pH sensing in the kidney.

13.2. Role of OGR1 in renal calcium and magnesium excretion during metabolic acidosis

It is well known that acid-base status affects renal handling of calcium and magnesium (35; 50; 54; 55). Different studies, including micropuncture experiments, demonstrated that disturbances in systemic acid-base balance specifically influenced Ca^{2+} and Mg^{2+} reabsorption in the DCT and CNT (103; 111) major sides of OGR1 mRNA localization. In our study, we show that chronic metabolic acidosis that was induced by NH_4Cl loading enhanced urine Ca^{2+} and Mg^{2+} excretion in wild-type mice. These results are in line with what has been described in previous studies (55; 54), however, the elevated urinary Ca^{2+} and Mg^{2+} excretion during acid load was not detected in *Ogr1*$^{-/-}$ mice, suggesting a participation of OGR1 in renal Ca^{2+} and Mg^{2+} handling.

Therefore, our study provided the first evidence for a pH-dependent role of OGR1 in the renal Ca^{2+} and Mg^{2+} loss during chronic metabolic acidosis.

In addition, our findings clearly demonstrated that during chronic metabolic acidosis OGR1 is not involved in the regulation of transcriptional and translational levels of the epithelial Mg^{2+} channel TRPM6 that plays an important role in the active Mg^{2+} reabsorption (77; 78), the epithelial Ca^{2+} channel TRPV5 and the cytosolic calcium binding protein calbindin-D_{28K}. Both proteins are involved in the active Ca^{2+} reabsorption in the DCT and CNT (35).

Our study also demonstrated that in wild-type mice, chronic metabolic acidosis is responsible for the elevation of renal TRPM6 mRNA expression, but does not influence its protein level. However, the renal protein as well as mRNA levels of TRPV5 and calbindin-D_{28K} were not influenced by these disturbances of acid-base balance. In contrast to our findings, Nijenhuis *et al*. reported that chronic metabolic acidosis is associated with decreased renal expression of TRPV5 calbindin-D_{28K} and TRPM6 leading to the development of hypercalciuria and hypomagnesemia in mice (54). In this study, however, protein abundance was estimated from the intensity of immunohistochemical staining, a method that is rather error-prone and not very quantitative.

Other observations clearly pointed out that extracellular acidification in vitro results in decreased TRPV5 channel activity at the apical cell membrane, as well as in a rapid retrieval of TRPV5 from the apical membrane, Lambers *et al 2007* (83) demonstrated that the exposure of TRPV5-expressing cells to an alkaline extracellular environment (pH 8.0) caused rapid recruitment of TRPV5-containing vesicles to the cell surface and a consequent increase in TRPV5 activity (83). In the reciprocal experiment, acidic extracellular milieu (pH 6.5) induced the internalization of TRPV5-containing vesicles from the plasma membrane, resulting in a reduced channel activity (83). These data are compatible with our results which demonstrate for the first time in vivo that direct sensing of acid-base status at the membrane by OGR1 may participate in the regulation mechanism of the apically localized epithelial Ca^{2+} channel TRPV5 and lead to its internalization inducing hypercalciuria during chronic metabolic acidosis.

Indeed, TRPV5 can be controlled by trafficking of the protein to and from the plasma membrane. S100A10 was recently identified as a binding

partner of TRPV5 (84). S100A10 is predominantly present as a heterotetrameric complex with annexin-2, which has been implicated in many cellular processes, including endocytosis and exocytosis (85). An important regulatory role has been proposed for the S100A10–annexin-2 heteromer in TRPV5 functioning (84). The binding of annexin-2 to TRPV5 through S100A10 was shown to facilitate the translocation of TRPV5 toward the plasma membrane (85). S100A10 activity is regulated by intracellular calcium and stimulated by rises in intracellular calcium. The small GTPase Rab11a has also been identified as a novel TRPV5- associated protein (86). Rab11a is one of the key regulatory proteins that control the recycling of endosomes (87; 89).

On the other hand, experiments in transfected cell lines suggested that stimulation of OGR1 results in activation of phospholipase C via pertussis toxin sensitive G-proteins and a rise in intracellular Ca^{2+} concentrations (5). Also increased phosphorylation of ERK1/2 MAPK kinases upon overexpression of OGR1 was described (19).

Therefore, our data suggest that the OGR1 signaling cascade may converge with the TRPV5 regulation pathway leading to the control of the protein trafficking to and from the plasma membrane, but future studies will have to elucidate the exact mechanism of this regulation.

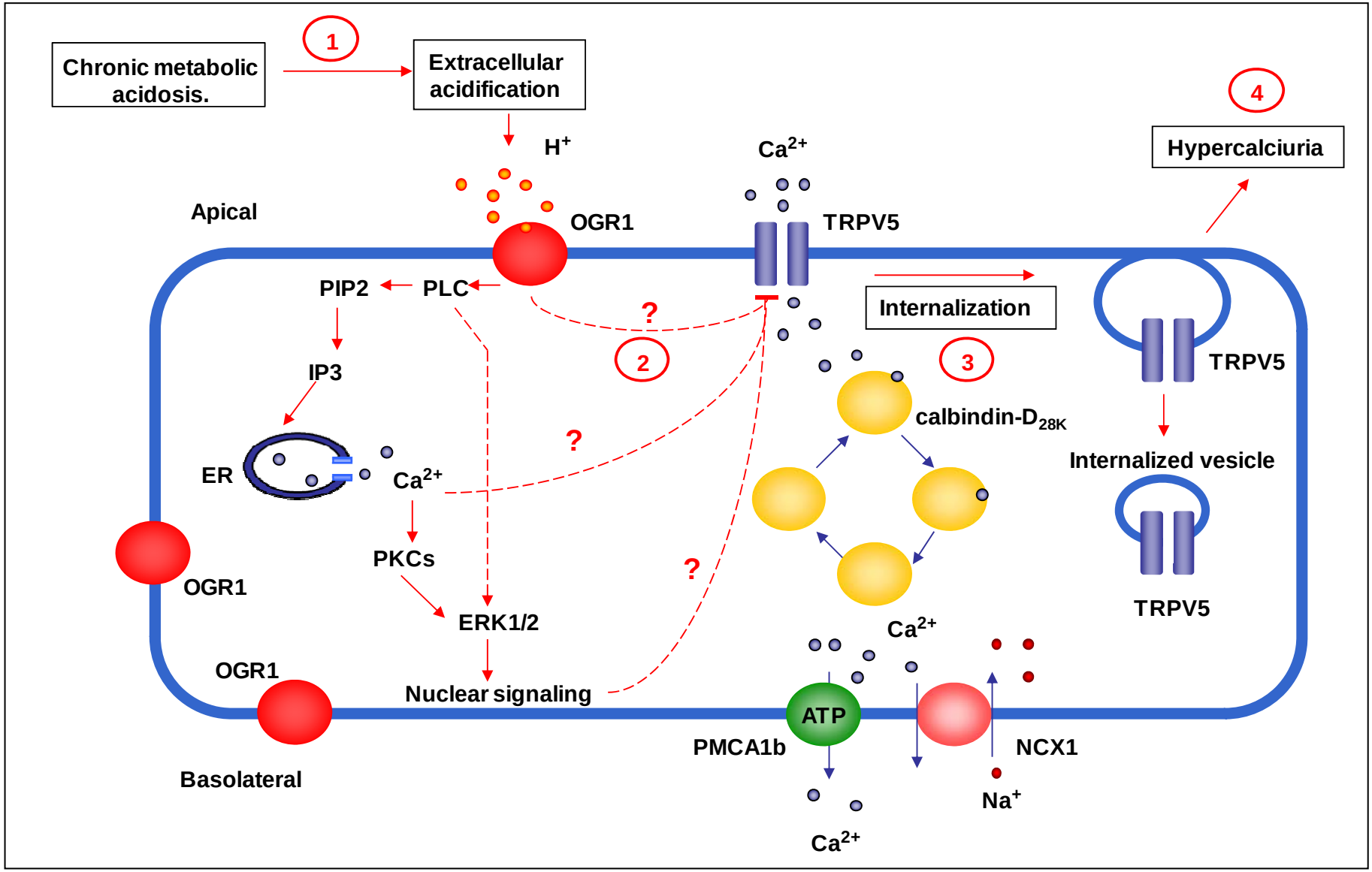

Fig 33. Putative pathways of OGR1-TRPV5 regulation during chronic metabolic acidosis

In our study, acetazolamide treated mice demonstrated that in mild systemic metabolic acidosis in the presence of an alkaline urine, no difference between wild-type and OGR1 deficient mice could be detected. Thus, these results may indicate that either OGR1 is localized to the luminal membrane and senses urinary pH or that another pH –sensitive mechanism is sensing luminal pH and overrides OGR1 dependent signals from the basolateral membrane. Unfortunately, OGR1 subcellular localization has not been determined to date due to the lack of specific antibodies (Mohebbi, Wagner, unpublished results). The localization of OGR1 on the luminal membrane would be difficult to reconcile with its pH-dependent activation which shows half-maximal activation around pH 7.3 and full activity at pH 6.8. Urinary pH in the DCT and CNT is physiologically in the range of pH 6.6- pH 7.0 and would lead to the tonic activation of OGR1.

Regarding our results concerning the regulatory mechanism of the epithelial Ca^{2+} channel TRPV5, we can hypothesize that OGR1 may also participate in the regulation of the apically localized epithelial Mg^{2+} channel TRPM6 and leads to its internalization inducing hypomagnesemia during chronic metabolic acidosis. In line with our hypothesis, previous studies demonstrated that TRPM6 can be controlled by trafficking of the protein to and from the plasma membrane. Very recently, *Thébault et al.* (118) showed that the epidermal growth factor EGF stimulates TRPM6 trafficking from the cytosol to the plasma membrane leading to its increased expression (118). Therefore, future studies will have to elucidate the exact mechanism by which OGR1 may regulate the renal TRPM6 expression during chronic metabolic acidosis.

13.3. OGR1 and its role in bone

It is well known that chronic metabolic acidosis increases urinary calcium excretion (35), hypercalciuria in these states may contribute to loss of calcium from bone resulting in the development of metabolic bone disease, such as osteopenia and osteoporosis (56). The proton sensing receptor OGR1 was reported to be expressed and functional in both osteoblasts and

osteoclasts (5; 26). A recent study suggested that OGR1 is an osteoblast proton sensor and showed that this receptor is involved in acid induced bone resorption (27). Similarly, OGR1 was shown to be strongly up-regulated during osteoclastogenesis (25) and that in osteoclasts, its activation with extracellular protons results in intracellular calcium rise and bone resorption (26).

Therefore, we aimed in a collaborative project with Novartis to evaluate the potential role of OGR1 in the proton sensing mechanism of bone cells using the OGR1 deficient mouse model. During NH_4Cl induced chronic metabolic acidosis for 8 weeks bone morphology, total bone mineral density, in *Ogr1*$^{+/+}$ and *Ogr1*$^{-/-}$ mice were similar. Moreover, the in vitro absorptive activity of osteoclasts insolated from wild-type and OGR1 deficient mice showed almost identical proliferation and reabsorptive capacities, in stark contrast to previous reports suggesting that OGR1 was criticial for osteoclast activation and activity (25; 26). Thus, our results strongly indicate that OGR1 is not responsible for bone resorption during chronic metabolic acidosis. Bone resorption releases calcium and the hypercalcuria during chronic metabolic acidosis has been ascribed mainly to the release of calcium from bone (128). However, the fact that mice lacking the renal TRPV5 channel do not increase renal calcium excretion during metabolic acidosis may indicate that the major mechansim of hypercalcuria is actually the down-regulation of TRPV5 in the kidney (54).

Thus our study suggests strongly that OGR1 is responsible for renal calcium loss due to the internalization of the renal epithelial Ca^{2+} channel TRPV5, and that its role in osteoclasts, that have been described in previously published data (25; 26; 27), is not sufficient to affect total bone development.

Indeed, in line with our findings, *Hui Li et al.* (2009) recently reported OGR1 to be involved in osteoclastogenesis; however its role was not strong enough to affect overall bone development and density (126).

13.4. OGR1 as a regulator of renal calcium and magnesium homeostasis and adaptation ?

Previous studies in animal and cell models showed that Ca^{2+} and Mg^{2+} homeostasis is regulated by the dietary intake of Ca^{2+} and Mg^{2+}. Indeed

TRPV5 channel, NCX1, and calbindin-D_{28K} expression have been shown to be tightly regulated by the dietary intake of Ca^{2+} (49; 107). Similarly, the epithelial Mg^{2+} channel TRPM6 mRNA expression has been described to be regulated by dietary Mg^{2+} (105). Using different Ca^{2+} and Mg^{2+} diets, we demonstrated that OGR1 may participate in the renal regulation of Mg^{2+} and Ca^{2+} reabsorption by the dietary intake of Ca^{2+} and Mg^{2+}. Our preliminary findings suggested that OGR1 may have a role in the regulation of the epithelial Mg^{2+} channel TRPM6 expression. Preliminary data also showed that OGR1 may be involved in the regulation of Ca^{2+} reabsorption by the dietary intake of Ca^{2+} and Mg^{2+}. Collectively, our findings suggest that OGR1 may play a role in the regulation of renal Ca^{2+} and Mg^{2+} handling.

Different mechanisms have been described to regulate total body Ca^{2+} and Mg^{2+} balance. Indeed, the Ca^{2+}-sensing receptor (CaSR) plays crucial role in the molecular mechanism through which parathyroid cells are able to detect small changes in the blood Ca^{2+} and Mg^{2+} concentrations and control parathyroid hormone PTH secretion (100; 113). This hormone in turn is directly involved in the regulation of Ca^{2+} and Mg^{2+} homeostasis.

In the kidney, the CaSR controls Ca^{2+} and Mg^{2+} reabsorption and regulates water and other electrolytes transepithelial movements (35). Indeed, increases in plasma Ca^{2+} and Mg^{2+} levels are sensed by the CaSR which permits the reabsorbed Ca^{2+} to decease Ca^{2+} and Mg^{2+} reabsorption by a negative feedback onto the cell preventing hypercalcemia (114). Recently *van Abel et al.* (115) demonstrated that the NPS R-467 (calcimimetic compound that activates CaSRs) reduced PTH and Ca^{2+} serum levels, and downregulates mRNA expression and protein levels of proteins involved in the active calcium reabsorption in the kidney (115). In addition experiments in DCT cells model showed that the vitamin D induced magnesium influx is blocked by high concentrations of extracellular calcium and this effect was inhibited by transfection with antisense CaSR oligodeoxynucleotides (116) suggesting a role of the CaSR in the regulation of Mg^{2+} transport in the DCT.

Regarding our findings showing the calcium dependent role of OGR1 in the renal Ca^{2+} and Mg^{2+} handling regulation, we can hypothesize that the CaSR may be a part of this unknown mechanism. However our data are not

sufficient to define if OGR1 acts as agonist or antagonist to the CaSR. Experiments using specific blockers of the CaSR in *Ogr1*$^{-/-}$ mice are needed to elucidate the potential interaction between these two receptors and more studies are important to determine the exact intracellular pathway that may combine the effect of the CaSR and OGR1 on the renal calcium and magnesium handling.

The PTH hormone plays also a crucial role in the regulation Ca^{2+} and Mg^{2+} balance, this hormone is secreted in the systemic circulation in response to low blood Ca^{2+} and Mg^{2+} concentrations, and acts directly on kidney and bone, where it activates the PTH hormone receptor. In the kidney PTH hormone receptor stimulates Ca^{2+} reabsorption in the DCT and CNT by increasing the renal expression of TRPV5, calbindin-D_{28K}, and NCX1 (102; 40, 41), and enhances Mg^{2+} transport in the DCT by an unknown mechanism (112; 50). The level of PTH is unknown in OGR1 deficient mice. However, the fact that phosphate homeostasis and urinary excretion is normal, suggests rather normal PTH and vitamin D_3 levels.

Vitamin D_3 (1,25-$(OH)_2$ Vitamin D_3) is also involved in the Ca^{2+} and Mg^{2+} homeostasis regulation (40; 42; 43; 44; 49; 50). In the kidney, v1,25-$(OH)_2$ vitamin D_3 increases active Mg^{2+} transport in the DCT (50; 112) and enhances active Ca^{2+} reabsorption by increasing TRPV5, calbindin-D_{28K}, and NCX1 mRNA expressions (49). According to our results, we can speculate that the role of OGR1 in the regulation of renal Ca^{2+} and Mg^{2+} handling may converge with the mechanisms of PTH and vitamin D_3 action in the kidney in response to changes in serum Ca^{2+} and Mg^{2+} concentrations. More studies are therefore essential to elucidate the role of PTH and vitamin D_3 in the regulation mechanism of Ca^{2+} and Mg^{2+} homeostasis by OGR1. However, OGR1 itself is not sensitive to extracellular Ca^{2+} and Mg^{2+} concentrations, since variation of these divalent does not alter the pH-depdendent stimulation of IP_3 formation in OGR1 transfected cell lines (Ludwig, Seuwen, Novartis Biomedical Reserach Institutes, unpublished results).

In summary, our findings demonstrate in contrast to our expectations that there is no obvious role for OGR1 in maintaining or controlling systemic acid-base status and renal acid excretion. We suggest that OGR1 may be a part of the mechanism involved in the renal regulation of Ca^{2+} and Mg^{2+} balance by acting on Ca^{2+} and Mg^{2+} transport proteins. Therefore, we OGR1 might be a novel target for the treatment of diseases related to Mg^{2+} and Ca^{2+} handling in the DCT such as isolated dominant hypomagnesemia IDH (93; 94), Gitelman's syndrome (91; 91) and renal osteodystrophy (127).

Finally, the relation between OGR1 and the active Ca^{2+} and Mg^{2+} reabsorption in the DCT needs further investigation. Hypomagnesemia is frequently accompanied by inappropriate renal Ca^{2+} wasting (95), this is the case of patients with hypomagnesemia with secondary hypocalcemia HSH (95), the molecular explanation of this phenomenon however remains obscure.

14. PUBLICATIONS THAT DID NOT CONTRIBUTE TO THIS THESIS

14.1. The Proton-Activating G Protein Coupled Receptor OGR1 Acutely Regulates Epithelial Proton Transport Proteins

(Draft manuscript)

Nilufar Mohebbi[1,2], **Chahira Benabbas[1,2]**, Soline Bourgeois[1,2], Ana Velic[1,2], Marie-Gabrielle Ludwig[3], Klaus Seuwen[3], Carsten A Wagner[1,2]

1 Institute of Physiology, University of Zürich, Switzerland
2 Centre for Integrative Human Physiology, University of Zürich, Switzerland
3 Novartis Institute of biomedical research, Basel, Switzerland

Corresponding author:
Carsten A. Wagner
Institute of Physiology and Zurich Center for
Integrative Human Physiology (ZIHP)
University of Zurich
Winterthurerstrasse 190
CH-8057 Zurich
Switzerland
Phone: +41-44-63 50659
Fax: +41-44-63 56814
E-Mail: Wagnerca@access.uzh.ch

The proton-activating G protein coupled receptor OGR1 acutely regulates epithelial proton transport proteins

Nilufar Mohebbi, Chahira Benabbas, Soline Bourgeois, Ana Velic, Marie-Gabrielle Ludwig, Klaus Seuwen, Carsten A Wagner

Institute of Physiology and Zurich Center for Integrative Human Physiology (ZIHP), University of Zurich, Switzerland

Corresponding author:
Carsten A. Wagner
Institute of Physiology and Zurich Center for
Integrative Human Physiology (ZIHP)
University of Zurich
Winterthurerstrasse 190
CH-8057 Zurich
Switzerland
Phone: +41-44-63 50659
Fax: +41-44-63 56814
E-Mail: Wagnerca@access.uzh.ch

ABSTRACT

The ovarian cancer G protein coupled receptor 1 (OGR1) is activated by extracellular protons in the pH range between pH 7.8 and pH 6.8 leading to the formation of inositol-tris-phosphate and intracellular calcium transients (1). The downstream targets and the physiological role in native tissues, however, have not been investigated to date. Here we show that OGR1 modulates sodium/proton exchanger (NHE) and H^+-ATPase activity in the renal HEK293B cell line as well as in renal tubule cell fragments from mouse kidney. HEK293B cells were stably transfected with active OGR1 and a mutant lacking 5 histidine residues (H5Phe-OGR1) involved in the activation of the receptor. Switching extracellular pH from 8 to pH 7.1 stimulated NHE and H^+-ATPase activity in OGR1 transfected cells but not in H5Phe-OGR1 transfected cells. Moreover, the stimulatory effect was reduced by $ZnCl_2$ and $CuCl_2$ that have been shown to inhibit OGR1 activation. The stimulatory effect of OGR1 on NHE activity was blocked by chelerythrine whereas the ERK1/2 inhibitor PD 098059 had only a partially inhibitory effect. OGR1 activation caused also transient increases in intracellular calcium in transfected HEK293B cells. Surprisingly, surface biotinylation revealed that activation of OGR1 caused a decrease in NHE3 abundance. Furthermore, we isolated proximal tubules and outer medullary collecting ducts from kidneys of wildtype and OGR1 deificent mice and measured the effect of extracellular pH on NHE and H^+-ATPase activity. In both nephron segments, the absence of OGR1 affected the pH-dependent activity of these proton extruding transport proteins. However, we did not detect OGR1

dependent increases in intracellular calcium in the proximal tubule, whereas the absence of OGR1 reduced intracellular calcium at pH 7.1 in the outer medullary collecting duct cells.

In summary, this is the first evidence that OGR1 modulates the activity of two major plasma membrane proton transport systems, NHE and H^+-ATPase, in a manner dependent on extracellular pH suggesting that OGR1 may be involved in the regulation of plasma membrane transport proteins and intra- and/or extracellular pH. These effects may help explaining the role of OGR1 in native tissues and its overexpression in cancer cell lines.

INTRODUCTION

Protons in the extracellular compartments are produced by metabolism and excreted by cells using various pathways including transporters or vesicle-mediated release (2-7). These protons challenge systemic acid-base balance and need to be buffered in order to avoid acidification of extracellular compartments. More recently, protons have attracted also attention as signalling molecules that may be involved in rapid transmission of signals. In the nematode C. elegans protons may act as neurotransmitters inducing contraction of certain muscles (8,9). Here, two genes encoding for cation channels, *pbo-5* and *pbo-6*, are part of the proton-sensing and signal transducing complex (8). In mammals, a number of proton-activated channels or receptors have been identified, including the proton-activated ASIC-channels (10), proton-sensitive TRP-channels (11), or the Calcium-sensing receptor modulated by extracellular pH (12-14). However, these receptors or channels are activated or modulated by proton concentrations that may occur in specialized compartments where pH may reach values in the range between pH 5 and pH 6.5.

In contrast, a recently emerged small subfamily of G protein-coupled receptors is activated in the physiologic range prevailing in many extracellular compartments with half-maximal activation (EC50) around pH 7.2 – 7.4 (15). This subfamily is comprised of three members, OGR1 (ovarian cancer G protein-coupled receptor 1; GPR68), GPR4 (G protein-coupled receptor 4), and TDAG8 (T cell death-associated gene 8; GPR65) (15,16). Ludwig et al. have shown in stably transfected cells and various cell lines that OGR1 acts as a proton-

activated receptor stimulating inositol-trisphosphate (IP_3) formation, release of intracellular calcium transients and activation of the mitogen-activated protein kinase/extracellular signal-regulated (ERK) kinase cascade. However, the downstream targets of OGR1 have remained elusive and very little is known about its physiological role (15,16). In fact, the recent generation of OGR1 deficient mice has not shed new light on the physiological role of this receptor since no clear phenotype was reported (17).

Systemic acid base homeostasis is tightly regulated by the lung and the kidneys mediating the daily renal acid excretion of approximately 70 mmoles of acid from a typical Western diet. Additionally, the kidneys compensate perfectly for variations of daily intake of acid equivalents or metabolic acid-base production by adapting acid-base excretion with great precision. Thus, an elaborate system of regulated acid-base transporters is inevitable to perform this task. Among these transporters, NHE3, the major Na^+/H^+ antiporter isoform in the renal proximal tubule and vacuolar-type H^+-ATPases (H^+-ATPases) on the plasma membrane of proximal tubules and the acid-secretory intercalated cells of the collecting duct provide for the majority of proton secretion by the kidney (18-22).

Both transport proteins, NHE3 and H^+-ATPases, are tightly regulated by a variety of hormones and conditions among them systemic acid-base and electrolyte status, and different hormones, most notably aldosterone and angiotensin II (20-27).

NHE3 activity is not directly regulated by protons but by a signaling pathway including pH-sensing signaling molecules (28,29). Recently, Tsuganezawa et al. have shown that the acid-sensing pathway in the kidney involves activation of the proto-oncogene c-Src and ERK as well as c-fos, c-jun, junB, and egr-1 expression (29). Here, a member of the focal adhesion kinase (FAK) family, Pyk2 (proline-rich tyrosine kinase 2), plays a crucial role in acid activation of c-Src and NHE3 in cultured opossum kidney (OKP) proximal tubule cells (30). Pyk2 is activated by phosphorylation in response to various stimuli requiring intracellular calcium release (31,32). Pyk2 phosphorylation itself may be pH-sensitive and present the pH-sensor. Alternatively, a membrane-bound receptor sensing extracellular pH may affect Pyk2 activation thereby coupling extracellular pH and activity of renal acid-base transport.

In this study, we demonstrate that OGR1 is involved in the acute regulation of proton extruding transporters, namely NHE3 and H^+-ATPase, in response to changes of extracellular pH in cultured renal cells. This activation requires a cluster of histidine residues in the extracellular domains of the receptor and PKC activity. Additionally, using wild type and OGR1 deficient mice, we show that OGR1 modulates the pH-sensitive response of NHE3 and H^+-ATPase activity in isolated proximal tubules and outer medullary collecting ducts (OMCDs).

MATERIALS AND METHODS

Animal model

Ogr1$^{-/-}$ mice were born at the expected mendelian ratio, showed no obvious gross anatomical abnormalities, postnatal survival, growth, body weight, and fertility was undistinguishable from wildtype and heterozygous litters. Histological analysis of various tissues including kidney did not show any abnormalities (data not shown).

Isolation of proximal tubule and OMCD

Proximal tubule and OMCD were isolated from wild type or *Ogr1*$^{-/-}$ mouse kidneys and transferred onto glass coverslips as described previously (23,33).

Cell culture and cell preparations

HEK293 cells and HEK293 cells stably transfected either with the human wildtype OGR1 construct or an OGR1 mutant lacking 5 histidine residues placed on top of helices I, IV and VII, and in extracellular loops 1 and 2 (H17, H20, H84, H169 and H269, substituted by phenylalanine: H5Phe) were described previously (15). All cells were maintained in Dulbecco's modified Eagle's medium/Ham's F-12 medium (1:1) supplemented with 10% fetal calf serum in a humidified atmosphere of 5% CO_2, 95% air at 37 °C. Stable cell populations expressing the OGR1 receptor were isolated following selection with antibiotic G418 (400 µg/ml). For all pH and Ca^{2+} experiments, cells were passaged, disseminated onto coverslips and grown to subconfluency for 48 hours. The final medium exchange

was performed 24 hours before the experiments were started. Medium pH was maintained at pH 7.4.

Intracellular pH and Ca^{2+} measurements

For pH_i measurements, either individual slides coated with cells or coverslips precoated with the cell adhesive Cell-Tak (BD Biosciences, Bedford, MA, USA) containing selected tubules were transferred to a perfusion chamber (≈ 3-5ml/min flow rate). The temperature of the chamber was maintained at 37°C by an electronic feedback circuit. The control bath solution was initially a HEPES-buffered Ringer solution (125 mM NaCl/ 5 mM KCl/ 1 mM $CaCl_2$/ 1.2 mM $MgSO_4$/ 2 mM NaH_2PO_4/ 32.2 mM HEPES/ 5 mM Glucose). Cell coated slides or single tubule fragments were loaded with the acetoxymethyl ester of the pH-sensitive dye BCECF (10 µM, Molecular Probes, Oregon, USA) for 10 min or the Ca^{2+}-sensitive dye FURA-2 (10 µg/ml, Molecular Probes, Oregon, USA) for 20 min and washed to remove all non-deesterified dye. Loading of cells and tubule fragments was performed in control solution at pH 8 to reduce OGR1 receptor activity.

pH_i was measured microfluorometrically by exciting the dye with a spot of light alternately at 490 and 440 nm while monitoring the emission at 532 nm with a video-imaging system (34,35). Intracellular acidification was induced using the NH_4Cl (20 mM) prepulse technique for 5 min and then washed into a Na^+-free solution (36). To measure H^+-ATPase activity, bicarbonate-free solutions were used and Na^+ was replaced by *N*-methyl-D-glucamine (NMDG). Sodium-proton-exchanger (NHE) activity was calculated from the slope of the initial rapid

intracellular alkalinization after readdition of Na^+. Each experiment was calibrated for pH_i using the nigericin/high K^+ method (37) and the obtained ratios were converted to pH_i. Na^+-independent pH_i recovery rates in response to an acid load were calculated in nontransfected and stably transfected cells with OGR1 or the OGR1 mutant H5Phe as well as in proximal tubules and outer medullary collecting ducts (OMCDs) from wild type and *Ogr1*$^{-/-}$ mice. Na^+-dependent pH_i recovery was measured in proximal tubules and OMCDs in the pH_i range of 6.55–6.85. The pH_i range chosen represented the average values found in the respective tubule segment. Data are shown as changes in pH_i (ΔpH_i) per minute.

Ca^{2+} measurements on mouse nephron segments were performed on hand dissected proximal tubules and outer medullary collecting ducts. In brief, mice were anesthetized with xylazine/ketamine i.p.. Both kidneys were cooled in situ with ice-cold control solution (130.7 mM NaCl, 5 mM KCl, 2 mM NaH_2PO_4, 1.2 mM $MgSO_4$, 10.5 Glucose, 2 mM Glutamine, 1 mM $CaCl_2$, 32.5 mM HEPES, pH 7.4) for one minute and then removed and cut into thin coronal slices for tubule dissection. Proximal straight tubules (S3 segments) and outer medullary collecting ducts (OMCD) were dissected, respectively, from the cortex medullary rays and the medulla at 4°C in control solution and the isolated nephron segment was transferred to the bath chamber. To measure intracellular calcium FURA-2 was excited with light of 340/380 nm wavelengths. After loading with FURA-2 nephron segments were first superfused with HEPES buffer at pH 8 and subsequently with HEPES buffer at pH 6.8. ATP at a concentration of 1 mM was used as control before starting the calibration using ionomycin at a final

concentration of 1 µM. $[Ca^{2+}]_i$ was calculated from the ratio of fluorescence at excitations of 340/380 nm using the following equation as described previously: $Ca_i^{2+} = [(R - R_{min})/(R_{max} - R)] \times (F_{min}/F_{max}) \times K_d$, where R is the measured ratio of emitted light, R_{min}, R_{max} and F_{max} are the fluorescence values at 380 nm with 1 mM Ca^{2+} bath solution, F_{min} is the fluorescence at 380 nm with 0 mM Ca^{2+} bath solution, and the dissociation constant (*K*d) = 225 nM for fura-2-calcium binding (38).

Chemicals were added to the perfusion solutions from stock solutions at the given concentrations for each experimental protocol. All chemicals were of highest purity and were purchased from Sigma if not annotated else wise.

HEK cell lysate preparation (membrane fraction) and immunoblotting

Cultures of HEK293 and OGR1-transfected cells were grown to confluency and washed 2x with PBS. Cells were lysed in a resuspension buffer (200 mM Mannitol, 80 mM HEPES, 41 mM KOH, pH 7.5) and protease inhibitor mixture (1:1000, Roche Diagnostics, Indianapolis, IN, USA) by sonication, and centrifuged at 3000 rpm at 4°C for 10min. The supernatant was removed for a subsequent ultracentrifugation step at 41000 rpm at 4°C for 1 hour. The resulting pellets were resuspended in 200– 300 µl resuspension buffer and the protein concentrations were determined (BioRad D_c Protein Assay, Bio-Rad, Hercules, CA, USA). 75 µg of crude membrane protein was solubilized in Laemmli sample buffer, and SDS-PAGE was performed on 10% polyacrylamide gel. Proteins

were transferred electrophoretically from gel to a polyvinylidene difluoride membrane (Immobilon-P, Millipore, MA, USA). After blocking with 5% milk powder in Tris-buffered saline containing 0.1% Tween 20 for 60 min, the blots were incubated with the mouse monoclonal anti-c-myc primary antibody (Invitrogen, Oregon, USA) (1:5000) overnight at 4°C. After washing and subsequent blocking, blots were incubated with the secondary antibody (anti-mouse Ig, horseradish peroxidase conjugated, GE Healthcare UK limited, United Kingdom) 1:10000 for 1 h at room temperature. Antibody binding was detected with the Immobilon Western Chemiluminescent horse radish peroxidase substrate (Millipore, Billerica, MA, USA), using the DIANA III-chemiluminescence detection system (Raytest, Straubenhardt, Germany). All images were analyzed using appropriate software (Advanced Image Data Analyzer, Raytest, Germany).

Biotinylation of Cell-Surface Membrane Proteins

The renal cell lines HEK293-OGR1 and HEK293-OGR1-H5Phe grown to confluency in 10-cm plates were incubated for 20 minutes prior to experiments in HEPES buffered, bicarbonate free solutions at pH 8 or pH 7.1 in order to inactivate or activate OGR1, respectively. After washing with PBS, 0.1 $CaCl_2$ mM, 1 $MgCl_2$ mM, cell surface-expressed proteins were biotinylated for 1 hr with 2 mg/ml sulfo-LC-NHS-Biotin [sulfo-Succinimidyl-6-(biotinamido)hexanoate; Pierce, Rockford, IL, USA] in buffer (150 mM NaCl ,10 mM triethanolamine , 2 mM $CaCl_2$, pH 7.4, 4 C°). After incubation with 100 mM glycine, cells were lysed in RIPA buffer (150 mM NaCl/ 5 mM EDTA/ 50 mM Tris/ 1% Triton X-100/ 0.5%

Na-deoxycholate/0.1% SDS/5 µg/ml leupeptin/ 5 µg/ml pepstatin A). Lysates were centrifuged at 10,000 x g at 4°C for 1 hr, and the supernatants were incubated overnight with 100 µl of prewashed streptavidin beads (Pierce, Rockford, IL, USA). After centrifugation at 10,000 x g for 20 s, the pellets were washed sequentially with buffer A (50 mM Tris·HCl, pH 7.4/ 100 mM NaCl/ 5 mM EDTA), buffer B (50 mM Tris·HCl, pH 7.4/ 500 mM NaCl), and buffer C (50 mM Tris·HCl, pH 7.4). Proteins were eluted by addition of 20 µl of 2x loading buffer (containing 60 µg/µl DTT) and incubated at 95°C for 3 min. After centrifugation at 3,000 x g for 10 min, supernatants were loaded on SDS/PAGE, and Western blotting was performed with rabbit anti-NHE3 antibody (1:5000).

Immunohistochemistry

In preparation for immunocytochemistry cells were passaged, disseminated onto coverslips, diluted with Dulbecco's modified Eagle's medium/Ham's F-12 medium (1:1) 1:50 and grown for 48 hours. Slides were washed two times with phosphate buffered saline (PBS) solution to remove medium and fixed with PBS buffer containing 16% paraformaldehyde for 20 min. After washing again with PBS, slides were incubated with 1% SDS for 3 min, washed three times with PBS, and incubated with PBS containing 1% BSA and 0.1% Triton X for 20 min before application of the primary antibodies. The primary antibodies (rabbit anti-OGR1 aff. purified 1:500, mouse monoclonal anti-c-myc 1:500, Invitrogen, Oregon, USA) were diluted in PBS and applied either for 75 min at room temperature or overnight at 4°C. Slides were washed twice for 5

min with PBS + 2.7% NaCl and once with PBS. Hereafter, the respective secondary antibodies (donkey anti-mouse Alexa 488, donkey anti-rabbit Alexa 594 diluted 1:1000, Invitrogen, Basel, Switzerland) and 4',6-Diamidino-2-phenylindole dihydrochloride (DAPI 1mg/ml, 1:500, Sigma) were applied for 1 h at room temperature. Slides were washed twice with PBS + 2.7% NaCl and once with PBS before mounting with VectaMount (Vector Laboratories, Burlingame, CA, USA).

To perform immunohistochemistry on kidney slices, mice were perfused through the left ventricle with PBS followed by a paraformaldehyde-lysine-periodate (PLP) fixative. Kidneys were removed and fixed overnight at 4°C by immersion in PLP. In the following, kidneys were washed three times with PBS, and after cryoprotection with PBS/30% sucrose solution, thin coronal slices were cut, and frozen in liquid propane cooled with liquid nitrogen. The procedure of the immunostaining was carried out as described previously (39-42). In brief, sections were incubated with 1% SDS + 0.1 % Triton-X for 5 min, washed three times with PBS, and incubated with PBS containing 1% BSA and 0.1 % Triton-X for 15 min before application of the primary antibodies. The primary antibodies (rabbit anti-OGR1 aff. purified 1:500, polyclonal anti-human AQP-2 1:400, Santa Cruz Biotechnology, CA, USA) were diluted in PBS + 0.1 % Triton-X and applied either for 75 min at room temperature or overnight at 4°C. Sections were washed twice for 5 min with PBS + 2.7% NaCl, once with PBS, and incubated for 1 h at room temperature with the respective secondary antibodies (donkey anti-rabbit

Alexa 594 and donkey anti-goat Alexa 488 diluted 1:1000, Invitrogen, Basel, Switzerland). Sections were again washed twice with PBS + 2.7% NaCl and once with PBS before mounting with VectaMount (Vector Laboratories, Burlingame, CA, USA).

All sections were viewed using a confocal microscope (Leica CLSM). Pictures were processed (overlaid) using Adobe Photoshop software.

Statistical analysis

All data are presented as means ± SEM. All data were tested for significance using the unpaired *t* Test or one way ANOVA test, and only results with $p < 0.05$ were considered statistically significant.

RESULTS

Activation of OGR1 stimulates NHE and H^+-ATPase activity

OGR1 upregulates NHE activity in cells.

OGR1 was stably expressed in the human renal cell line HEK293 which is known to express various transport proteins involved in renal acid secretion such as the sodium/proton exchanger NHE3 or V-type H^+-ATPases (43). Successful expression of OGR1 was tested by western blotting (Fig. 1A) demonstrating the presence of OGR1 in transfected cells. Two major bands were observed at approx. 70 kDa and 90 kDa.

To examine the effect of OGR1 activation on sodium/proton exchange (NHE) activity, we performed intracellular pH measurement with the pH_i-sensitive dye BCECF in the human renal cell line HEK293 at two different extracellular pH values. Cells were preincubated for 20 min in HEPES buffer at pH 8 to reduce basal OGR1 activity. The Na^+-dependent recovery rate indicating NHE activity was significantly increased in OGR1-transfected cells compared to nontransfected HEK293 cells at baseline pH 8 (0.11 ± 0.007 vs. 0.05 ± 0.002 units pH/ min)(Fig. 1 B). Preincubation of cells for 20 min at pH 7.1 to stimulate OGR1 activity caused an even more pronounced stimulatory effect on NHE activity (0.20 ± 0.010 vs. 0.09 ± 0.003 units pH/ min) (Fig. 1 B, C, table 1).

In contrast, cells expressing the OGR1 mutant (5 extracellular histidines residues mutated to phenylalanine: OGR1-H5Phe) showed the same activity as nontransfected HEK293 cells at pH 8 (0.06 ± 0.006 vs. 0.05 ± 0.002 units pH/

min) that could not be stimulated by changing the pH to 7.1 (0.03 ± 0.001 units pH/ min) (Fig. 1C). Mutation of the 5 histidines residues reduced and left shifted the OGR1 dependent increase in intracellular IP_3 formation (Fig. 1D) as described previously (15).

To determine the affected NHE isoform we used S3226 as a specific inhibitor of the NHE subtype 3 (NHE3) (44). Addition of 100 nM S3226 resulted in a significant decrease of the NHE activity at pH 7.1 in OGR1 transfected cells suggesting NHE3 as the main type of NHE involved (0.20 ± 0.010 units pH/ min in the absence of S3226 vs. 0.05 ± 0.004 units pH/ min in the presence of S3226)).

pH-dependent changes of the H^+-ATPase activity in cells.

In contrast to the NHE activity the Na^+-independent pH_i recovery of OGR1 transfected cells was downregulated at pH 8 compared to HEK control cells (-0.007 ± 0.0009 vs. 0.004 ± 0.0007 units pH/ min, respectively). We have previously shown that this Na^+-independent pH_i-recovery rate is sensitive to the H^+-ATPase inhibitor bafilomycin and is thus due to the activity of V-type H^+-ATPases (35). However, at pH 7.1 H^+-ATPase activity was significantly stimulated versus control (0.013 ± 0.0007 vs. 0.008 ± 0.0009 units pH/ min, respectively). In contrast to the OGR1 transfected clone, OGR1 mutant cells showed a higher H^+-ATPase activity at pH 8 and a downregulation at pH 7.1 (0.009 ± 0.0010 vs. 0.006 ± 0.0009 units pH/ min, respectively) (Fig. 2, table 1).

Inhibitory effect of $ZnCl_2$, $CuCl_2$ but not psychosine on OGR1 dependent stimulation of NHE activity.

Previous data have shown that micromolar concentrations of Zn^{2+} and Cu^{2+} ions inhibited OGR1-dependent IP_3 formation stimulated by lowering extracellular pH (15). Moreover, psychosine has been implicated as an inhibitor of proton-dependent stimulation of OGR1(45) even though the role of lipids in OGR1 stimulation or inhibition is very controversial (16). Thus, we tested whether $ZnCl_2$, $CuCl_2$, and psychosine have an effect on the OGR1 dependent stimulation of NHE and H^+-ATPase activity. $ZnCl_2$ and $CuCl_2$ reduced at 10 μM significantly the OGR1 dependent stimulation of the NHE activity (0.20 ± 0.010 vs. 0.14 ± 0.014 and 0.12 ± 0.008 units pH/ min) (Fig. 3A). Psychosine (10 μM) had no significant effect on NHE stimulation. Higher concentrations of psychosine (100 μM) led frequently to loss of BCECF from cells and detachment of cells suggesting cytotoxicity. In contrast, H^+-ATPase activity was significantly reduced by psychosine but not by $ZnCl_2$ and $CuCl_2$ (Fig. 3B). Higher concentrations of these inhibitors were also tested but resulted in unspecific effects (data not shown).

Intracellular signaling mediating OGR1 dependent pH effects on NHE activity.

OGR1 has been shown to couple to G_q proteins, phospholipase C, and to induce intracellular Ca^{2+} transients in transfected cells (15). Similarly, NHE3 activity can be stimulated by signaling cascades activated by intracellular Ca^{2+} transients involving down-stream signals such as protein kinase C and MAP-

kinases ERK1/2 (30,46-49). As expected, there was a significant increase of intracellular calcium concentration in OGR1 transfected cells compared to HEK control cells when extracellular pH was rapidly switched from pH 8 to pH 7.1 (-1.8 ± 0.75 vs 117.3 ± 17.16 nM Ca^{2+}). ATP (1 mM) was subsequently applied to all cells to confirm viability (Fig. 4B). Chelerythrine (1 μM), an inhibitor of protein kinase C (PKC) completely prevented the OGR1 dependent stimulation of NHE activity. In contrast, inhibition of ERK1/2 activation with PD098059 (20 μM) decreased basal NHE activity but did not prevent the OGR1 dependent stimulation of NHE activity (Fig. 5). Thus, OGR1 activation causes a transient increase of intracellular Ca^{2+} and stimulates NHE activity requiring intact PKC.

OGR1 stimulation reduces NHE3 surface expression

Cells stably transfected with OGR1 or the OGR1-H5Phe mutant were incubated for 1 h at pH 8 and then either left at pH8 or incubated at pH 7.1 for 20 min. Surface expression of the major active NHE isoform in HEK293 cells, NHE3, was assessed by surface biotinylation. Surprisingly, expression of OGR1 reduced NHE3 surface expression at pH 8 as compared to cells expressing inactive receptor. Moreover, activation of the OGR1 receptor at pH 7.1 decreased NHE3 surface erxpression whereas in cells expressing the inactive H5Phe mutant NHE3 surface expression was increased (Fig. 6). Thus, activation of the OGR1 receptor in HEK293 cells reduces NHE3 surface abundance.

Modulation of Na^+/H^+ exchanger and H^+-ATPase activity in proximal tubules. OGR1 mRNA has been detected in most segments of the mouse nephron by real-time PCR, including the proximal tubule and all subsegments of the collecting duct with highest abundance in the outer medullary collecting duct. In order to assess the impact of OGR1 dependent effects of extracellular pH on NHE and H^+-ATPase activity in native tissue, we isolated late proximal tubules from wildtype and *Ogr1*$^{-/-}$ mouse kidneys and measured NHE and H^+-ATPase activity at two different pH_o, pH 8 and pH 7.1. NHE activity in late proximal tubules from wild type mice did not show any significant alteration when changing the extracellular pH from pH 8 to 7.1 (Fig. 7A). In contrast, in late proximal tubules of *Ogr1*$^{-/-}$ mice NHE activity was significantly upregulated at pH 7.1 compared to pH 8 (0.36 ± 0.02 vs. 0.22 ± 0.02 units pH/ min, respectively). H^+-ATPase activity was lower at pH 7.1 in proximal tubules from both wild type and OGR1 deficient mice. However, in *Ogr1*$^{-/-}$ mice H^+-ATPase activity at pH 8 was lower and higher at pH 7.1 when compared to wild type animals (Fig. 7B). Thus, absence of OGR1 in the proximal tubule affects the response of NHE and H^+-ATPase activity to changes in extracellular pH.

H^+-ATPase activity is regulated by OGR1. In the outer medullary collecting duct (OMCD) intercalated cells, H^+-ATPases represent the major acid-extruding pathway (22). Therefore we also tested for the pH and OGR1-dependent regulation of H^+-ATPase activity in intercalated cells in the OMCD. H^+-ATPase activity in OMCD intercalated cells from wild type mice was markedly reduced

when extracellular pH was changed from pH 8 to pH 7.1 (Fig. 8, table 1). Interestingly, H^+-ATPase activity in OMCD intercalated cells from OGR1 deficient mice was much lower at pH 8 and significantly increased at pH 7.1 (Fig. 8).

Intracellular calcium transients in proximal tubule and OMCD of wildtype and OGR1 deficient mice.

In a last series of experiments we tested if OGR1 mediates detectable changes in intracellular Ca^{2+} upon extracellular acidification. Freshly dissected proximal tubule and OMCDs from wildtype and *Ogr1*$^{-/-}$ mice were prepared and intracellular calcium transients measured using FURA-2. In proximal tubule cells changing extracellular pH from 8 to 6.8 did not result in a rise of intracellular Ca^{2+} as observed in OGR1 transfected HEK293 cells. However, in proximal tubule cells from *Ogr1*$^{-/-}$ mice, extracellular acidification significantly decreased intracellular Ca^{2+} which was not observed in wild type proximal tubules (WT 5.9 ± 7.9 vs. *Ogr1*$^{-/-}$ -23.4 ± 8.3 nmol/l) (Fig. 9). Application of ATP (1 mM) elicited intracellular Ca^{2+} transients of similar magnitude in both wild type and OGR1 deficient proximal tubules. In OMCD intercalated cells, no appreciable changes in intracellular calcium concentration could be detected upon switching extracellular pH from 8 to 6.8 in tubules from *Ogr1*$^{+/+}$ and *Ogr1*$^{-/-}$ mice, whereas ATP readily increased intracellular Ca^{2+} (Fig. 9).

DISCUSSION

All (eukaryotic) cells need to regulate intracellular pH and thus be able to sense pH and consecutively activate signaling pathways responsible for the adaptive response such as proton or bicarbonate secretion (22). The role of protons as signaling molecules has been previously discussed in various contexts and a number of proton-activated channels or receptors have been identified (8-14). Recently, Ludwig et al. have demonstrated that the Ovarian Cancer G protein-coupled receptor 1 (OGR1) acts as a proton-activated receptor via IP_3 formation and release of intracellular calcium transients (15).

OGR1 has been initially identified as being differentially expressed in ovarian cancer cells (50) and was later reported to be activated by the lipid messengers sphingosylphosphorylcholine (SPC) and lysophosphatidylcholine (LPC) (51). Similarly, the closely related GPR4 receptor was reported to by activated by SPC and LPC (52). However, these reports could not be substantiated and confirmed by others (16) and the original publications have been retracted in the meantime (51,53). OGR1 deficient mice have recently been described (17) but no specific phenotype could be found. The number of osteoclasts may be slightly reduced, less peritoneal macrophages were observed and LPS-induced ERK phosphorylation in macrophages appeared to be reduced (17). Most importantly, no difference in sphingosylphosphorylcholine and lysophosphatidylcholine induced effects could be observed (17) in line with the notion that OGR1 is not a lipid receptor but may act as a receptor for protons in vivo.

Here we used two different approaches to examine the role of OGR1 in the context of acute regulation of acid-base transport proteins. Renal epithelial cells (HEK293B) cells were stably transfected with active OGR1 and its less active mutant OGR-H5Phe. Secondly, we used native tissues from OGR1 deficient mice.

In the renal epithelial HEK293B cell line, OGR1 acted as a sensor of extracellular pH and stimulated sodium/proton exchange and H^+-ATPase activity. Incubation of cells at pH 7.1 which leads to more than half-maximal activation of the receptor (54) caused a strong stimulation of NHE activity in OGR1 expressing cells but not in cells lacking OGR1 or expressing the H5Phe mutant. This mutant displays activation and IP_3 formation only at much more acidic extracellular pH than the wildtype receptor and demonstrates that not the presence of OGR1 but its activity mediate the effect of extracellular pH on NHE activity.

OGR1 has been shown to couple to G_q proteins, phospholipase C, and to induce intracellular Ca^{2+} transients in transfected cells (15). Of interest, some recent studies have investigated the signaling pathway of acid stimulation of NHE3 and it has been demonstrated that the signaling cascades stimulating NHE3 activity involve/include intracellular Ca^{2+} transients, protein kinase C (PKC) and MAP kinases ERK1/2 (27,29,47,55). In agreement with these data, we found intracellular Ca^{2+} transients in OGR1 transfected cells at pH 7.1, where OGR1 is fully active. Moreover, addition of chelerythrine, an inhibitor of PKC, completely

prevented the OGR1 dependent stimulation of NHE activity. Interestingly, inhibition of the MEK/ERK kinases with PD98059 resulted only in a partial decrease of NHE activity. Regulated trafficking of NHE3 contributes importantly to NHE3 activity regulation. In the renal OKP cell line chronic media acidification results enhanced NHE3 activity, increased apical membrane NHE3 protein abundance, and more NHE3 mRNA and protein abundance (56). Fan et al. studied the role of parathyroid hormone (PTH) on NHE3 activity and protein abundance in parathyroidectomized rats and described that PTH decreases NHE3 activity via a phosphorylation-dependent mechanism followed by a decrease in apical membrane NHE3 protein via changes in protein trafficking (57). In order to test, if the effect of OGR1 on NHE3 is secondary to increased surface protein abundance, were assessed surface expression of NHE3. Surprisingly, activation of OGR1 by acidic pH caused a reduction of NHE3 surface protein expression within 20 mins while NHE3 activity is increased. Thus our data suggest a dual effect of OGR1 on NHE3 membrane abundance and activity.

OGR1 activation stimulates IP_3 formation which is inhibited by micromolar concentrations of $ZnCl_2$ and $CuCl_2$, (54) whereas the role of the lipid messenger psychosine is rather controversial (52) since the data on psychosine have been partly retracted (58). In our study, $ZnCl_2$ and $CuCl_2$ reduced significantly the OGR1 dependent stimulation of NHE activity while psychosine had no effect. In contrast, H^+-ATPase activity was not affected by $ZnCl_2$ and $CuCl_2$ while application of psychosine resulted in lower basal H^+-ATPase activity. Thus,

psychosine does not act as inhibitor of OGR1-mediated stimulation of NHE and H^+-ATPase activity.

To confirm our cell experiment data, we tested the pH dependent effect of OGR1 on NHE and H^+-ATPase activity in isolated proximal tubules and outer medullary collecting ducts of wild type and OGR1 deficient mice. We and others have previously shown that NHE activity in mouse proximal tubule is mainly due to NHE3 activity (59) Acute changes in the extracellular pH of proximal tubules did not affect NHE activity in wild type mice while OGR1 deficient mice demonstrated a significant increase in NHE activity. In contrast, in proximal tubules from OGR1 deficient mice, H^+-ATPase activity was lower at alkaline pH and higher at acidic pH than in the respective wildtype control tubules. These observations indicate that OGR1 is not the only pH-sensing mechanism in mouse proximal tubules and that the effects of OGR1 on NHE and H^+-ATPase activity are distinct. In the case of NHE activity, OGR1 appears to exert an inhibitory effect which is in contrast to our observations in the HEK293B cell model. This may indicate that the effects of OGR1 on transporters may be depending on the cellular context. Clearly, further studies are required to address these questions in more detail.

The intercalated cells of the collecting ducts are the major site of final tuning of urinary acidification (1). . . In parallel to the proximal tubule data, we found that H^+-ATPase activity of wild type mice was higher at pH 8 compared to

OGR1 deficient mice. In contrast, more acidic pH resulted in a decreased H^+-ATPase activity in wild type mice while OGR1 deficient mice showed a stimulation of H^+-ATPase activity. Thus, taken together, our experiments with native OGR1 KO mouse tissue suggest that the presence or absence, respectively, of the OGR1 receptor modulatesthe pH-dependent regulation of both major renal acid-base transport proteins, namely NHE and H^+-ATPase.

Acute stimulation of NHE3 activity by acid has been demonstrated in the renal opossum kidney OKP cell line and a signaling pathway implicated includingc-Src, ERK, and increases in c-fos, c-jun, junB, and egr-1 expression (29,60). Li et al. showed that Pyk2 (prolin-rich kinase 2) is possibly upstream of this pathway and that activation requires calcium (30). The role of this pathway in the regulation of H+-ATPase activity has not been reported to date. Whether OGR1 plays a role in the activation or modulation of the pyk2 dependent pathway remains to be investigated. However, we tested if OGR1 dependent intracellular calcium transients could be detected in isolated proximal tubules and outer medullary collecting ducts. In the proximal tubule, no pH dependent changes in $[Ca^{2+}]_i$ could be observed. Similarly, in the outer medullary collecting duct, no effect of pH was seen in wildtype cells but in cells from OGR1 deficient mice, a significant decrease was observed indicating that OGR1 may be involved in regulating intracellular calcium concentrations.

In summary, OGR1 has an impact on acid regulation of two major proton extruding transporters, NHE3 and H^+-ATPase, in cultured renal cells. The acid-activated signaling pathway of OGR1 involves PKC activity in cells, and a cluster of histidine residues are integral to OGR1 activation. In addition, OGR1 alters the pH-sensitive response of NHE and H^+-ATPase activity in proximal tubules and OMCDs of mice. To our knowledge, this is the first study describing the impact of OGR1 on major renal acid-base transport proteins..

ACKNOWLEDGEMENTS

This study was supported by grants from the Swiss National Science foundation to C.A. Wagner (31-107677). C. Benabbas was supported by a ZIHP PhD student fellowship, N. Mohebbi by a long-term research fellowship from ERA-EDTA.

FIGURE LEGENDS

Table 1. Summary of intracellular pH (pH_i) measurements in cells (HEK293, HEK-OGR1 transfected and the HEK-OGR1-H5PHe mutant) and in proximal tubule and OMCD fragments from wildtype and OGR1 deficient mice. Data are presented as statistical mean ± SEM. If not stated otherwise substances were used at the following concentrations: $ZnCl_2$ 10 µM, $CuCl_2$10 µM; psychosine 10 µM; Chelerythrine 1 µM; PD098059 20 µM. n.d., not determined. † significantly different between HEK and HEK-OGR1 or *Ogr1*$^{+/+}$ and *Ogr1*$^{-/-}$ mouse samples for the same treatment., ‡ significantly different between HEK-OGR1 and HEK-OGR1-H5Phe for the same treatment, # significantly different between HEK and HEK-OGR1-H5Phe for the same treatment, § significantly different between OGR1 pH 7.1 and OGR1 pH 7.1 plus different treatments, & significantly different between *Ogr1*$^{+/+}$ or *Ogr1*$^{-/-}$ pH 8 and *Ogr1*$^{+/+}$ or *Ogr1*$^{-/-}$ pH 7.1, ¶ significantly different between *Ogr1*$^{+/+}$ and *Ogr1*$^{-/-}$ at pH 8 or pH 7.1. * p <0.05, ** p <0.01, *** p <0.0001.

Figure 1. pH-dependent stimulation of the Na^+/H^+ exchanger activity in OGR1 expressing cells.

(A) Expression of myc-tagged human OGR1 was detected and confirmed in transfected cells but not in untransfected cells as two major bands around 65 and 85 kDa, respectively. **(B)** Original pH_i tracing of single representative HEK293 and HEK-OGR1 expressing cells. Removal of NH_4Cl from the bath causes a

rapid intracellular acidification, addition of sodium to the bath realkalinizes cells due to sodium/proton exchanger activity as described previously (61). The initial rate of alkalinization was faster in HEK293B cells expressing OGR1. **(C)** Summary of NHE activities at pH 8 and pH 7.1 in HEK293, HEK293 cells transfected with OGR1 or the H5PHE OGR1 mutant. HEK293 cells untransfected (HEK), HEK293 cells stably transfected with human OGR1 (OGR1) or the OGR1 mutant where 5 histidine residues were mutated to phenylalanine (OGR1-H5Phe) were preincubated for 10 min in HEPES buffer at pH 8 or 7.1 before starting pH_i measurements. Each bar represents measurements from at least 3 different batches of cells, *** p <0.0001. **(D)** IP_3 formation was measured in stably transfected HEK293 cells expressing the OGR1 mutant H5Phe in the absence (0) or presence of lithium (Li). OGR1-H5Phe expressing cells have a markedly reduced IP_3 formation at pH 6.8 where the wild type receptor is fully active (15).

Figure 2. OGR1 stimulates H^+-ATPase activity. (A) Original pH_i tracing of representative HEK293 and OGR1 expressing cells after addition of Na^+ free HEPES buffer. The slow intracellular alkalinization in the absence of sodium is due to H^+-ATPase activity. **(B)** The rate of Na^+-independent pH_i recovery was reduced at pH 8 and increased at pH 7.1 in OGR1 transfected cells. In contrast, OGR1-H5Phe cells demonstrated an increase at pH 8 and decreased activity at pH 7.1. Each bar summarizes data from at least 3 different batches of cells. * p <0.05, ** p <0.01, *** p <0.0001.

Figure 3. $ZnCl_2$ and $CuCl_2$ reduce the OGR1 dependent stimulation of NHE and H^+-ATPase activity. $ZnCl_2$ (100 µM), $CuCl_2$ (10 µM), and psychosine (10 µM) were applied to all solutions. **(A)** $ZnCl_2$ and $CuCl_2$ reduced significantly the OGR1 dependent stimulation of NHE activity whereas psychosine had without effect. **(B)** H^+-ATPase activity was significantly reduced by psychosine only but not by $ZnCl_2$ and $CuCl_2$. However, psychosine and $CuCl_2$ affected also basal H^+-ATPase activity. Each bar summarizes data from at least 3 different batches of cells. * p <0.05, ** p <0.01, *** p <0.0001.

Figure 4. pH-dependent stimulation of intracellular calcium transients in HEK293 and OGR1 expressing cells. (A) HEK293 or OGR1 transfected cells were preincubated 10 min in HEPES buffer at pH 8 before starting calcium measurements. Changing pH to 7.1 induced a significant increase in the intracellular calcium concentration in OGR1 transfected cells compared to HEK cells (shown as FURA-2 340/380 nm fluorescence ratio from a single OGR1 transfected cell compared to a HEK cell). ATP (1 mM) was used as a positive control. **(B)** Summary of data from all experiments. Each bar summarizes data from at least 3 different independent experimentesfrom at least 3 different batches of cells. ** p <0.001, *** p <0.0001

Figure 5. OGR1-dependent stimulation of Na^+/H^+ exchanger activity requires PKC but not ERK1/2. The PKC inhibitor chelerythrine (1 µM) and the ERK1/2 inhibitor PD098059 (20 µM) were added to all solutions. Addition of

chelerythrine resulted in a significant decrease of the Na^+-dependent pH_i recovery in OGR1 transfected cells but not in untransfected HEK293 cells at pH 7.1. Inhibition of the ERK1/2 pathway markedly reduced NHE activity in OGR1 transfected cells. However, the baseline NHE activity was also reduced by PD098059 and could be partly stimulated by OGR1. Each bar represents data from at least 3 different batches of cells. *** p <0.0001.

Figure 6. OGR1 alters NHE3 surface expression. Cells stably transfected with OGR1 or the inactive H5Phe OGR1 mutant were incubated for 20 min in HEPES buffer at pH 8 or pH 7.1. Upon biotinylation and streptavidine precipitation, samples were subjected to SDS PAGE and incubated with an anti-NHE3 antibody. **(A)** The presence of OGR1 increased NHE3 surface expression at pH8 and activation of OGR1 at pH 7.1 reduced NHE3 surface expression. Representative blot from four qualitatively identical experiments. β-actin was probed to exclude biotinylation of cytosolic proteins. **(B)** Summary of four independent experiments based on densitometry of membranes and normalization of bands to OGR1 expressing cells at pH 8. **(C)** Ratio between NHE3 abundance in total lysates and NHE3 abundance in biotinylated proteins. * p < 0.05, **p < 0.01.

Figure 7. pH dependent changes of NHE and H^+-ATPase activity in proximal tubules of OGR1 deficient mice. (A) In freshly isolated mouse proximal tubules

Na^+/H^+ exchanger activity was measured as the rate of Na^+-dependent pH_i-recovery (in the nominal absence of bicarbonate) after preincubation of tubules at pH 8 or 7.1 for 10 min. NHE activity was stimulated in proximal tubules from *Ogr1*$^{-/-}$ but not from wild type mice. **(B)** pH-dependent downregulation of H^+-ATPase activity (Na^+-independent pH_i-recovery rate) in proximal tubules from wild type and OGR1 deficient mice. In parallel to NHE activity, H^+-ATPase activity was lower in *Ogr1*$^{-/-}$ mice at pH 8 compared to control and increased at pH 7.1. Wild type mice showed a significant decrease of the Na^+-independent pH_i recovery at pH 7.1 compared to pH 8. Each bar contains measurements from at least 3 different tubules from 3 different mice. ** *p <0.001,* *** *p* <0.0001

Figure 8. H^+-ATPase activity is stimulated in intercalated cells from the outer medullary collecting duct of OGR1 deficient mice at pH 7.1. Freshly isolated outer medullary collecting ducts (OMCD) of wild type and *Ogr1*$^{-/-}$ mice were preincubated for 10 min in HEPES buffer at pH 8 or pH 7.1 before the experiment. At pH 8 the Na^+-independent pH_i recovery was decreased in *Ogr1*$^{-/-}$ mice compared to wild type animals. In contrast, at pH 7.1 H^+-ATPase activity is significantly increased in *Ogr1*$^{-/-}$ mice compared to wild type mice. Each bar contains measurements from at least 3 different tubules from 3 different mice. *** *p* <0.0001

Figure 9. Intracellular calcium measurements in proximal tubules and medullary collecting ducts of wild type and OGR1 deficient mice. Freshly

hand-dissected proximal tubules or outer medullary collecting ducts (OMCDs) from wild type and *Ogr1*$^{-/-}$ mice were preincubated for 20 min in HEPES buffer at pH 8. **(A)** Original Ca^{2+} tracing of a single proximal tubule cell from a wild type mouse. Changing extracellular pH from 8 to 6.8 did not affect intracellular calcium concentration. Addition of ATP (1 mM) resulted in an increase in the intracellular calcium signal. **(B)** Original fluorescence tracing from a single proximal tubule from an *Ogr1*$^{-/-}$ mice. Switching extracellular pH from 8 to 6.8 resulted in a slight decrease of the intracellular calcium signal. ATP used as control resulted in a distinct rise of the intracellular signal. **(C)** Summary of Ca^{2+} measurements in proximal tubule cells from wild type and *Ogr1*$^{-/-}$ mice. Activation of OGR1 by changing the extracellular pH to 6.8 resulted in a slight (significant or not ?) increase of intracellular calcium in proximal tubules of wild type mice compared to *Ogr1*$^{-/-}$ mice. **(D)** Summary of Ca^{2+} measurement in OMCDs from wild type and *Ogr1*$^{-/-}$ mice. Intracellular calcium signals after changing extracellular pH to 6.8 was decreased in OMCDs from wild type mice compared to OGR1 deficient mice. Each bar represents measurements from at least XX tubules from 3 different mice per group. * p <0.05, ** p <0.01

Table 1.

	Na^+ independent pH_i recovery	No. of cells (tubule fragments)	Na^+ dependent pH_i recovery	No. of cells (tubule fragments)
Cell experiments				
HEK, pH 8	0.004 ± 0.001	100 (6)	0.05 ± 0.002	47 (3)
HEK-OGR1, pH 8	-0.007 ± 0.001***†	119 (8)	0.11 ± 0.007***†	115 (6)
HEK-OGR H5Phe, pH 8	0.009 ± 0.001$^{***\ddagger***\#}$	74 (4)	0.06 ± 0.006***‡	74 (4)
HEK, pH 7.1	0.008 ± 0.001	165 (10)	0.09 ± 0.003	165 (10)
HEK-OGR1, pH 7.1	0.013 ± 0.001***†	270 (16)	0.20 ± 0.010***†	262 (16)
HEK-OGR1 H5Phe, pH 7.1	0.006 ± 0.001***‡	90 (5)	0.03 ± 0.001$^{***\ddagger\#}$	90 (5)
HEK, pH 7.1 + $ZnCl_2$	0.008 ± 0.001	78 (4)	0.07 ± 0.002	78 (4)
HEK-OGR1, pH 7.1 + $ZnCl_2$	0.017 ± 0.006	106 (7)	0.14 ± 0.014**§	80 (7)
HEK, pH 7.1 + $CuCl_2$	0.013 ± 0.002	75 (4)	0.06 ± 0.003	75 (4)
HEK-OGR1, pH 7.1 + $CuCl_2$	0.014 ± 0.001	70 (4)	0.12 ± 0.008***§	74 (4)
HEK, pH 7.1 + psychosine	0.005 ± 0.001	95 (5)	0.08 ± 0.002	95 (5)
HEK-OGR1, pH 7.1 + psychosine	0.005 ± 0.001***§	59 (3)	0.17 ± 0.009	59 (3)
HEK, pH 7.1 + chelerythrine	-0.007 ± 0.001	75 (4)	0.08 ± 0.005	75 (4)
HEK-OGR1, pH 7.1 + chelerythrine	-0.001 ± 0.0003	103 (6)	0.04 ± 0.002***†***§	102 (6)
HEK, pH 7.1 + PD098059	0.003 ± 0.001	76 (5)	0.03 ± 0.006	79 (5)
HEK-OGR1, pH 7.1 + PD098059	0.002 ± 0.0004	49 (3)	0.11 ± 0.007***‡***§	49 (3)
Mouse experiments				
Ogr1$^{+/+}$ proximal tubule, pH 8	0.09 ± 0.002	101 (7)	0.26 ± 0.02	101 (7)
Ogr1$^{-/-}$ proximal tubule, pH 8	0.07 ± 0.003***¶	80 (6)	0.22 ± 0.02	81 (6)
Ogr1$^{+/+}$ proximal tubule, pH 7.1	0.04 ± 0.0002$^{***\&}$	73 (6)	0.31 ± 0.02	73 (6)
Ogr1$^{-/-}$ proximal tubule, pH 7.1	0.05 ± 0.003$^{***\&**\P}$	90 (8)	0.36 ± 0.02$^{***\&}$	90 (8)
Ogr1$^{+/+}$ OMCD, pH 8	0.12 ± 020	34 (6)	n.d.	n.d.
Ogr1$^{-/-}$ OMCD, pH 8	0.05 ± 0.003***¶	73 (11)	n.d.	n.d.
Ogr1$^{+/+}$ OMCD, pH 7.1	0.06 ± 0.008$^{**\&}$	47 (10)	n.d.	n.d.
Ogr1$^{-/-}$ OMCD, pH 7.1	0.10 ± 0.006$^{**\P***\&}$	30 (9)	n.d.	n.d.

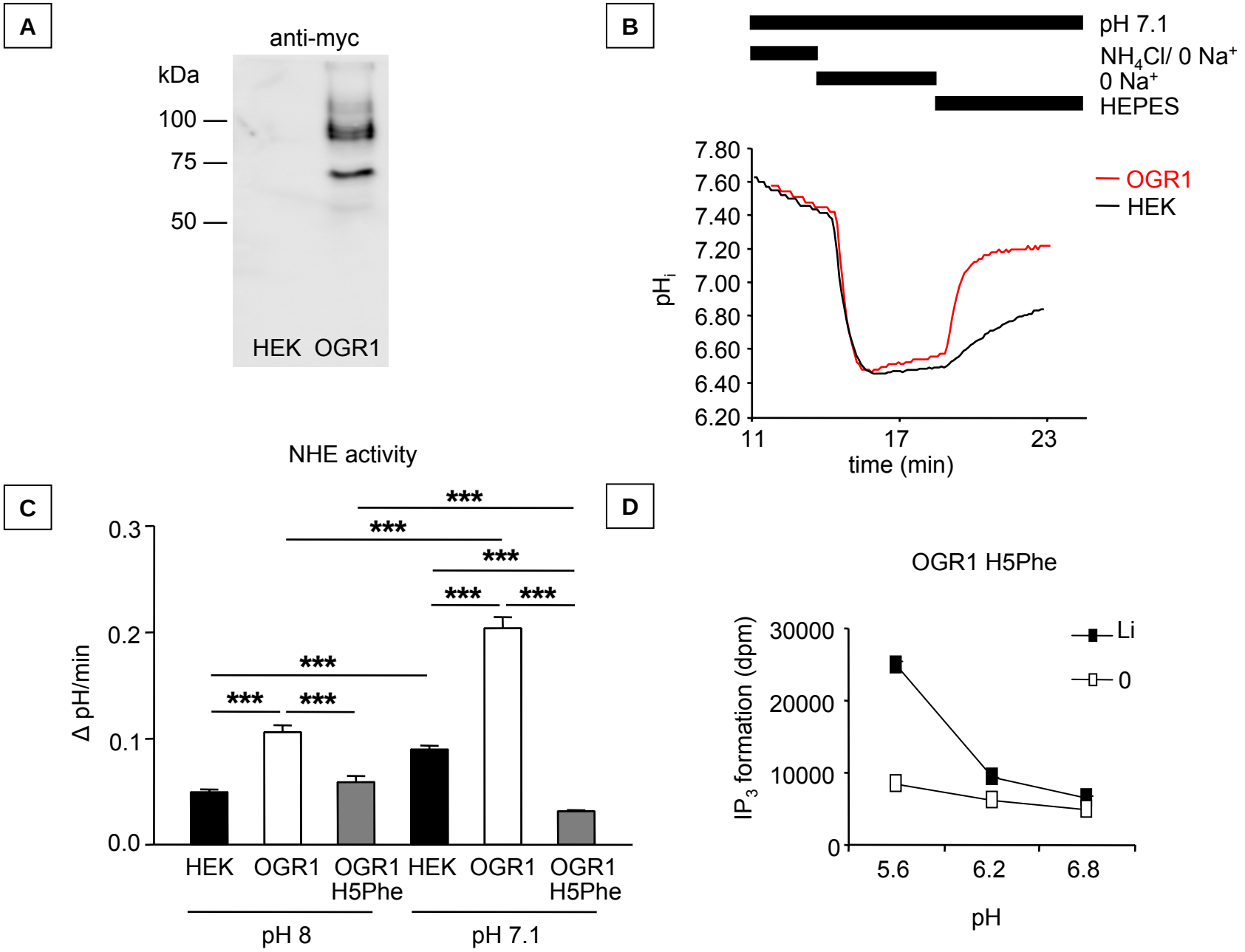
A
anti-myc
kDa
100
75
50
HEK OGR1
B
pH 7.1
NH4Cl/ 0 Na+
0 Na+
HEPES
OGR1
HEK
pHi
7.80
7.60
7.40
7.20
7.00
6.80
6.60
6.40
6.20
11
17
23
time (min)
C
NHE activity
Δ pH/min
0.3
0.2
0.1
0.0
***
HEK
OGR1
OGR1 H5Phe
HEK
OGR1
OGR1 H5Phe
pH 8
pH 7.1
D
OGR1 H5Phe
IP3 formation (dpm)
30000
20000
10000
0
Li
0
5.6
6.2
6.8
pH

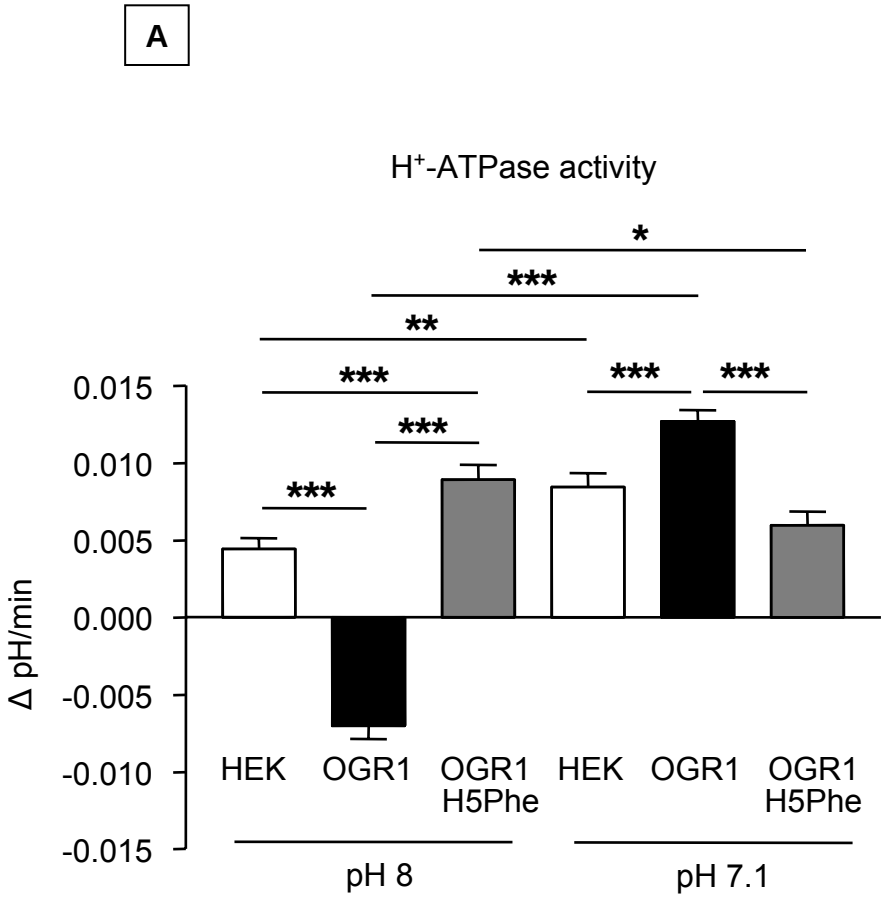
A
H+-ATPase activity
*
***
**
***
***
***
***
***
0.015
0.010
0.005
0.000
-0.005
-0.010
-0.015
Δ pH/min
HEK
OGR1
OGR1 H5Phe
HEK
OGR1
OGR1 H5Phe
pH 8
pH 7.1

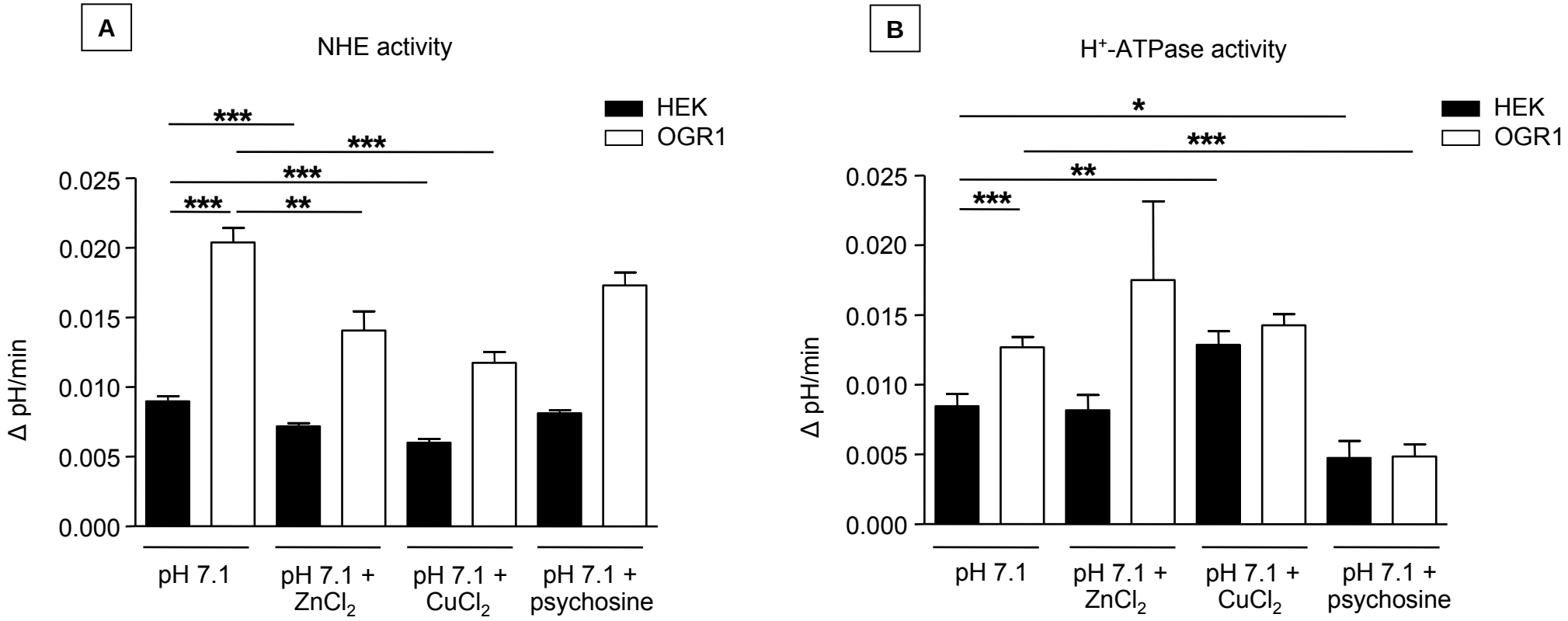
A
NHE activity
HEK
OGR1
***
***
***
***
**
0.025
0.020
0.015
0.010
0.005
0.000
Δ pH/min
pH 7.1
pH 7.1 + ZnCl2
pH 7.1 + CuCl2
pH 7.1 + psychosine
B
H+-ATPase activity
HEK
OGR1
*
***
**
***
0.025
0.020
0.015
0.010
0.005
0.000
Δ pH/min
pH 7.1
pH 7.1 + ZnCl2
pH 7.1 + CuCl2
pH 7.1 + psychosine

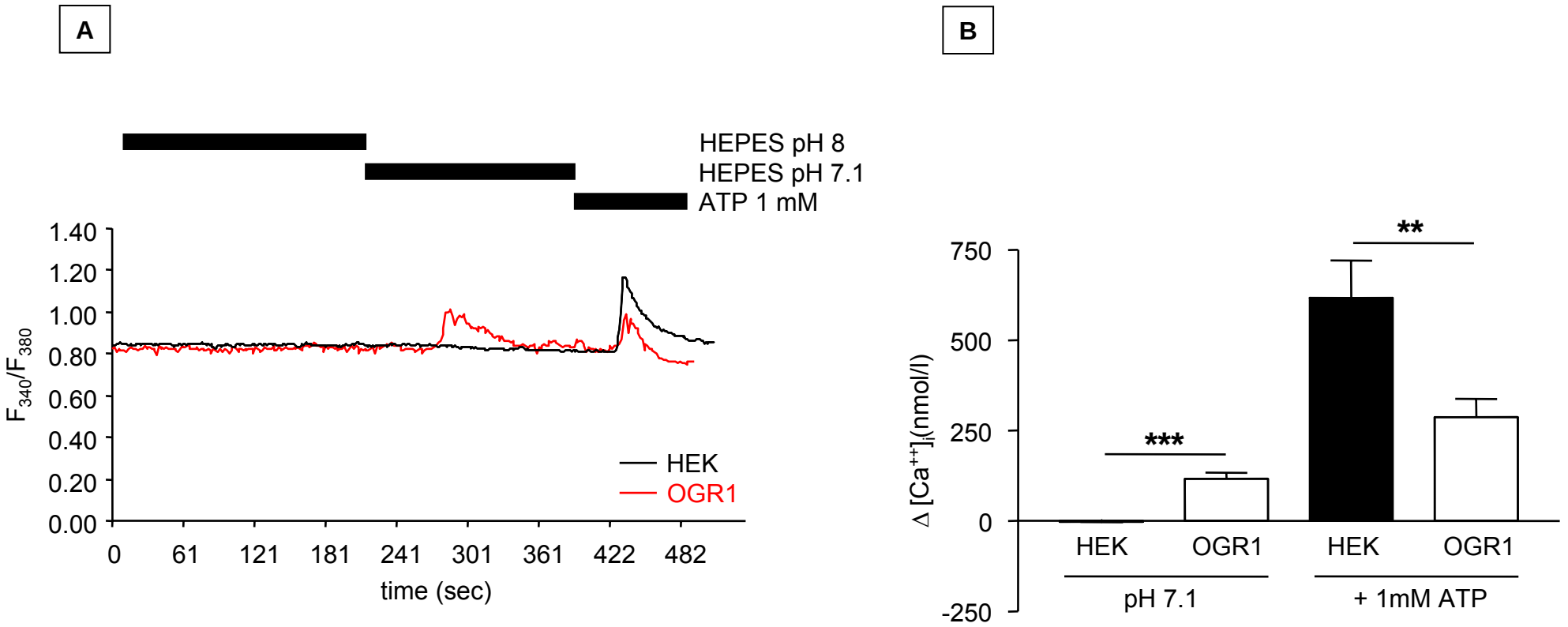
A
HEPES pH 8
HEPES pH 7.1
ATP 1 mM
1.40
1.20
1.00
0.80
0.60
0.40
0.20
0.00
F340/F380
HEK
OGR1
0
61
121
181
241
301
361
422
482
time (sec)
B
750
500
250
0
-250
Δ [Ca++]i(nmol/l)
***
**
HEK
OGR1
HEK
OGR1
pH 7.1
+ 1mM ATP

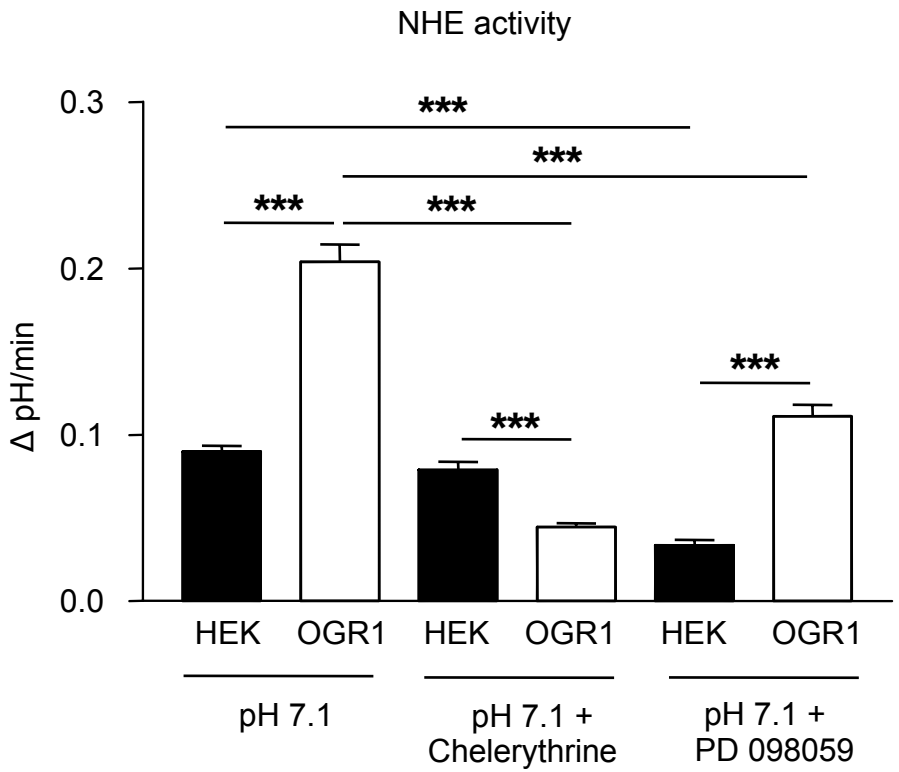
NHE activity
0.3
0.2
0.1
0.0
Δ pH/min
***
***
***
***
***
***
HEK
OGR1
HEK
OGR1
HEK
OGR1
pH 7.1
pH 7.1 +
Chelerythrine
pH 7.1 +
PD 098059

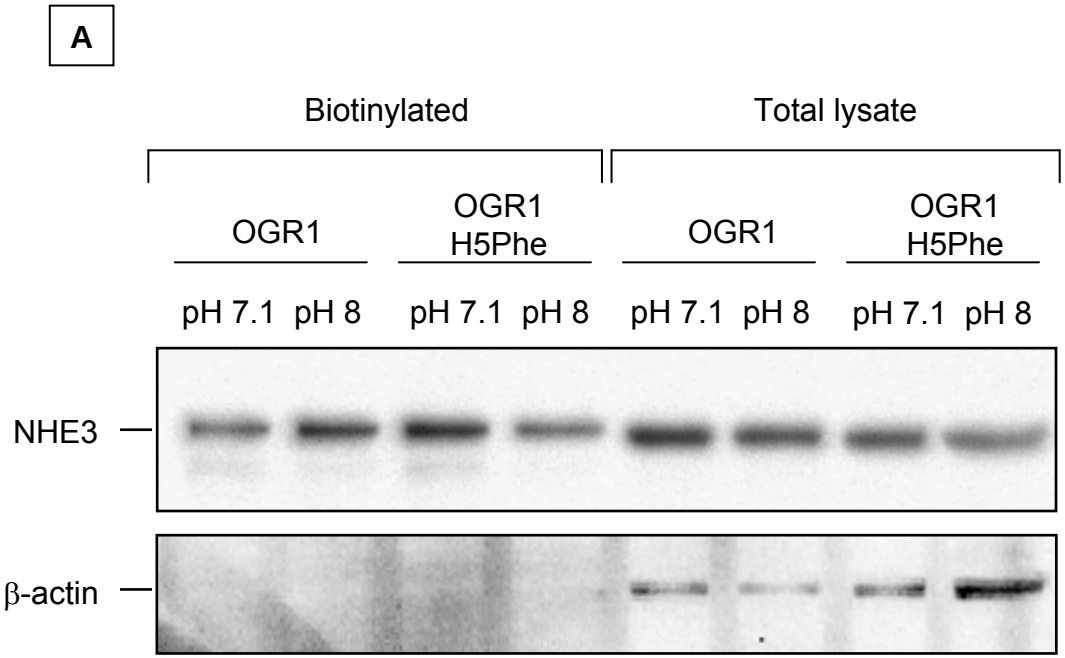
A
Biotinylated
Total lysate
OGR1
OGR1 H5Phe
OGR1
OGR1 H5Phe
pH 7.1 pH 8 pH 7.1 pH 8 pH 7.1 pH 8 pH 7.1 pH 8
NHE3
β-actin

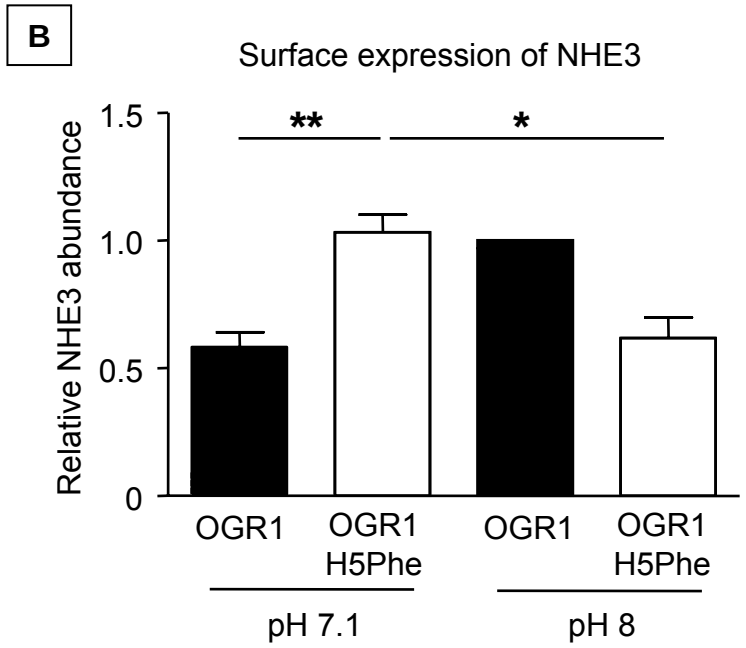
B
Surface expression of NHE3
Relative NHE3 abundance
1.5
1.0
0.5
0
**
*
OGR1
OGR1 H5Phe
OGR1
OGR1 H5Phe
pH 7.1
pH 8

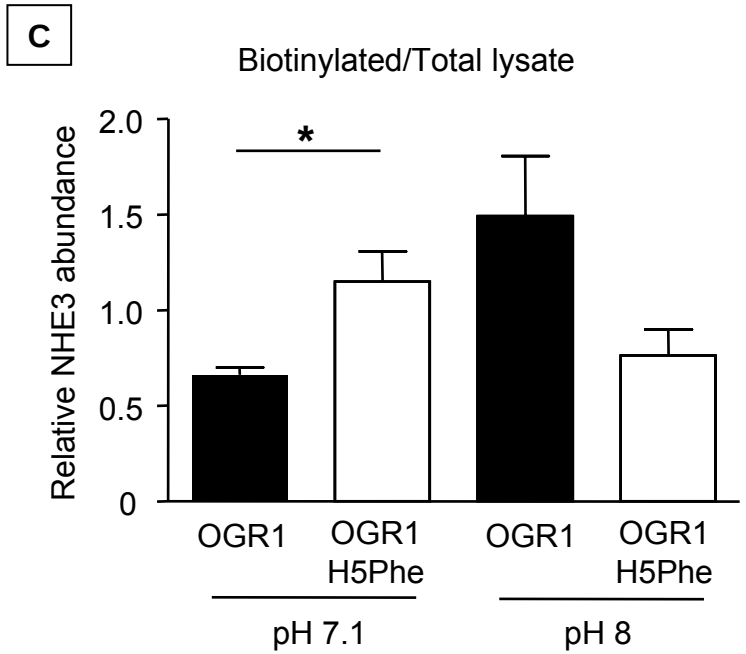
C
Biotinylated/Total lysate
Relative NHE3 abundance
2.0
1.5
1.0
0.5
0
*
OGR1
OGR1 H5Phe
OGR1
OGR1 H5Phe
pH 7.1
pH 8

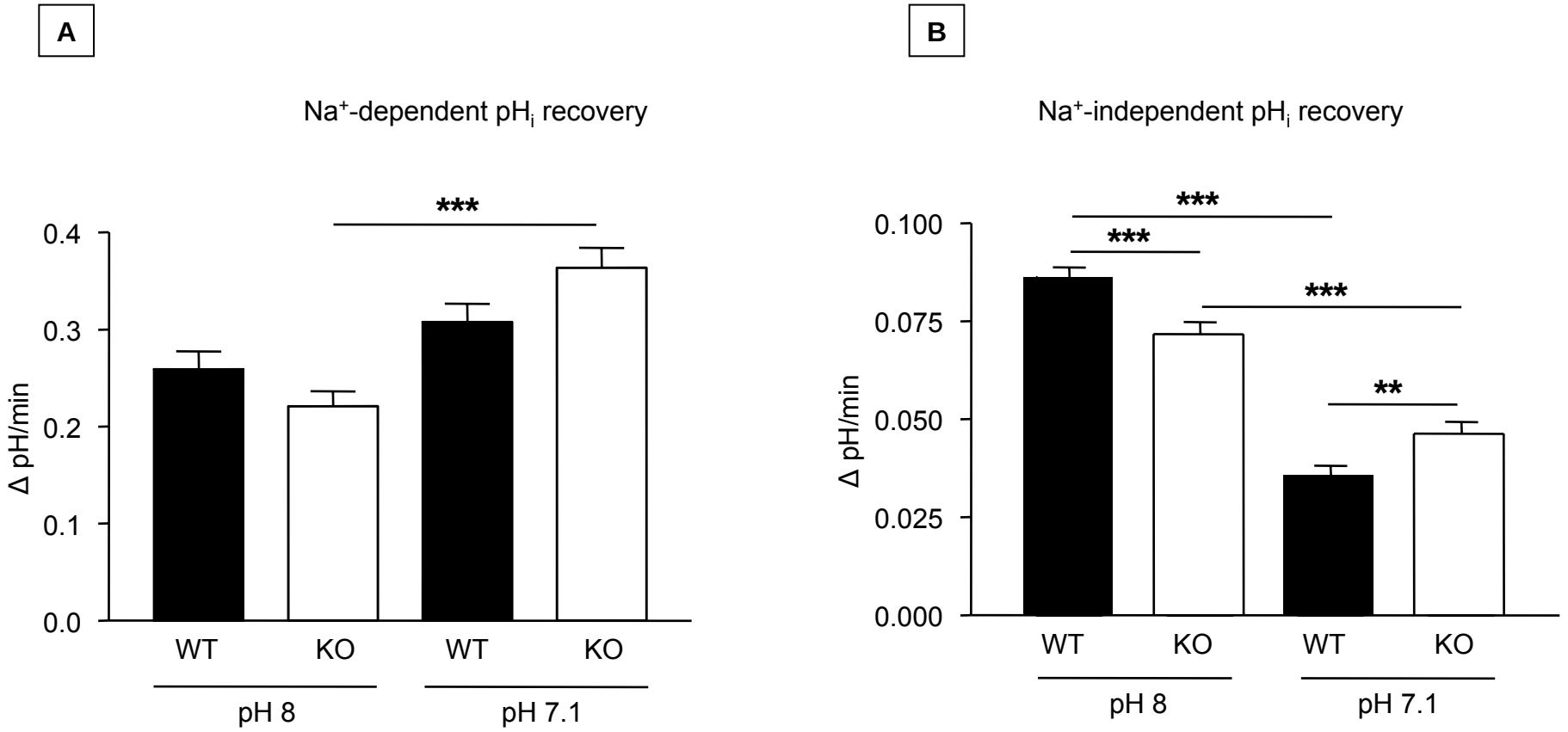
A
Na+-dependent pHi recovery
***
0.4
0.3
0.2
0.1
0.0
Δ pH/min
WT
KO
WT
KO
pH 8
pH 7.1
B
Na+-independent pHi recovery
***
***
***
**
0.100
0.075
0.050
0.025
0.000
Δ pH/min
WT
KO
WT
KO
pH 8
pH 7.1

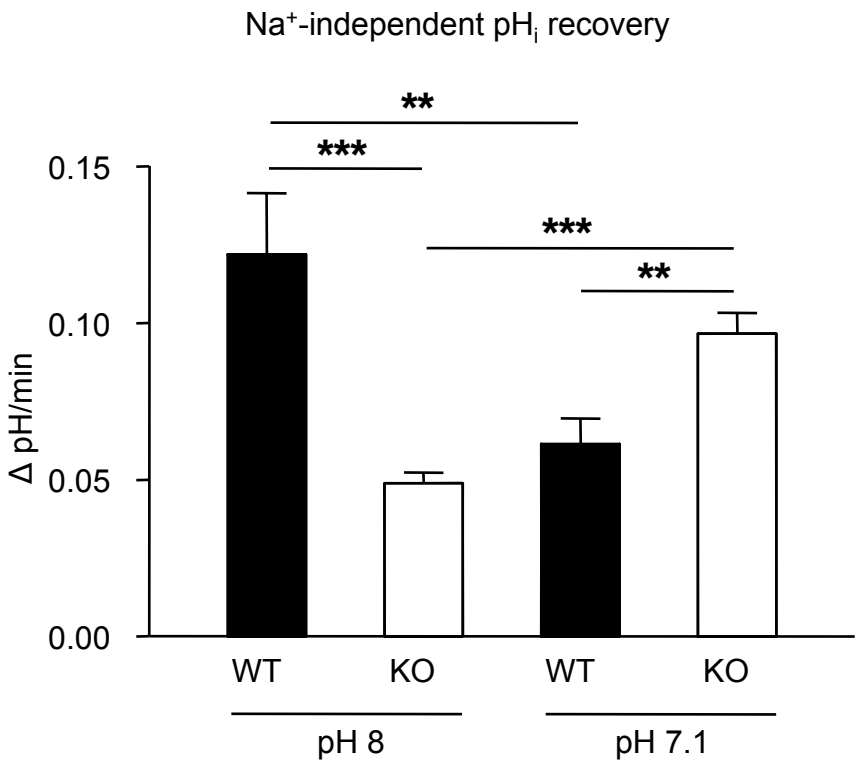
Na+-independent pHi recovery
**
***
***
**
0.15
0.10
0.05
0.00
Δ pH/min
WT
KO
WT
KO
pH 8
pH 7.1

A

Tracing from WT PT

B

Tracing from KO PT

Nilufar is this from PT or OMCD ?

C

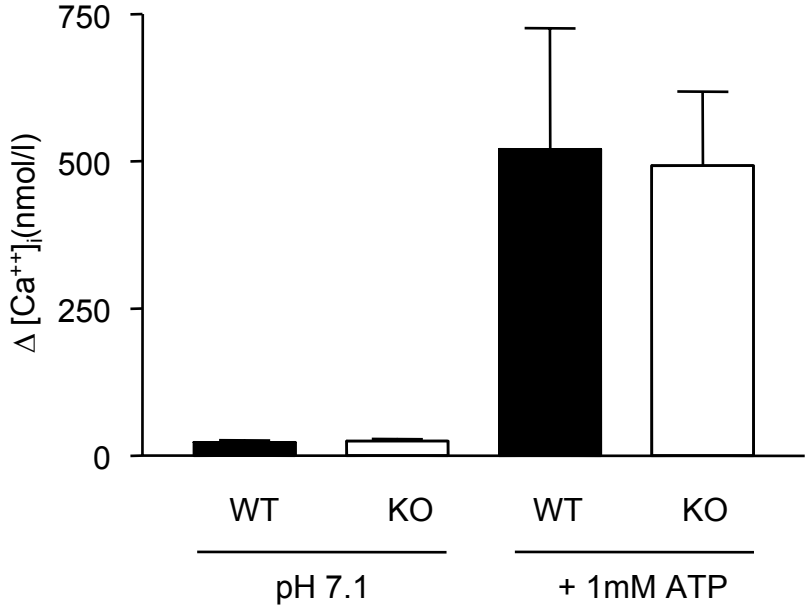

D

Summary of PT or OMCD missing

References

1. Wagner, C. A., Devuyst, O., Bourgeois, S., and Mohebbi, N. (2009) *Pflugers Arch* **458**, 137-156

2. Malo, M. E., and Fliegel, L. (2006) *Canadian journal of physiology and pharmacology* **84**, 1081-1095

3. Brown, D., and Sabolic, I. (1993) *Journal of cell science* **17**, 49-59

4. Moore, H. P., Andresen, J. M., Eaton, B. A., Grabe, M., Haugwitz, M., Wu, M. M., and Machen, T. E. (2002) *Archives of physiology and biochemistry* **110**, 16-25

5. Van Dyke, R. W. (1990) *Journal of internal medicine* **732**, 41-46

6. Brown, D., and Breton, S. (2000) *The Journal of experimental biology* **203**, 137-145

7. Halestrap, A. P., and Price, N. T. (1999) *The Biochemical journal* **343 Pt 2**, 281-299

8. Beg, A. A., Ernstrom, G. G., Nix, P., Davis, M. W., and Jorgensen, E. M. (2008) *Cell* **132**, 149-160

9. Pfeiffer, J., Johnson, D., and Nehrke, K. (2008) *Curr Biol* **18**, 297-302

10. Lingueglia, E. (2007) *The Journal of biological chemistry* **282**, 17325-17329

11. Venkatachalam, K., and Montell, C. (2007) *Annual review of biochemistry* **76**, 387-417

12. Adebanjo, O. A., Shankar, V. S., Pazianas, M., Zaidi, A., Simon, B., Huang, C. L., and Zaidi, M. (1994) *Biochemical and biophysical research communications* **199**, 742-747

13. Doroszewicz, J., Waldegger, P., Jeck, N., Seyberth, H., and Waldegger, S. (2005) *Kidney international* **67**, 187-192

14. Quinn, S. J., Bai, M., and Brown, E. M. (2004) *The Journal of biological chemistry* **279**, 37241-37249

15. Ludwig, M. G., Vanek, M., Guerini, D., Gasser, J. A., Jones, C. E., Junker, U., Hofstetter, H., Wolf, R. M., and Seuwen, K. (2003) *Nature* **425**, 93-98

16. Seuwen, K., Ludwig, M. G., and Wolf, R. M. (2006) *J Recept Signal Transduct Res* **26**, 599-610

17. Li, H., Wang, D., Singh, L. S., Berk, M., Tan, H., Zhao, Z., Steinmetz, R., Kirmani, K., Wei, G., and Xu, Y. (2009) *PLoS One* **4**, e5705

18. Aronson, P. S., Nee, J., and Suhm, M. A. (1982) *Nature* **299**, 161-163

19. Gluck, S. L., Iyori, M., Holliday, L. S., Kostrominova, T., and Lee, B. S. (1996) *Kidney Int* **49**, 1660-1664

20. Gluck, S. L., Underhill, D. M., Iyori, M., Holliday, L. S., Kostrominova, T. Y., and Lee, B. S. (1996) *Annu Rev Physiol* **58**, 427-445

21. Breton, S., and Brown, D. (2007) *Am J Physiol Renal Physiol* **292**, F1-10

22. Wagner, C. A., Finberg, K. E., Breton, S., Marshansky, V., Brown, D., and Geibel, J. P. (2004) *Physiological reviews* **84**, 1263-1314

23. Winter, C., Schulz, N., Giebisch, G., Geibel, J. P., and Wagner, C. A. (2004) *Proc Natl Acad Sci U S A* **101**, 2636-2641

24. Ambuhl, P. M., Amemiya, M., Danczkay, M., Lotscher, M., Kaissling, B., Moe, O. W., Preisig, P. A., and Alpern, R. J. (1996) *The American journal of physiology* **271**, F917-925

25. Wu, M. S., Biemesderfer, D., Giebisch, G., and Aronson, P. S. (1996) *The Journal of biological chemistry* **271**, 32749-32752

26. Licht, C., Laghmani, K., Yanagisawa, M., Preisig, P. A., and Alpern, R. J. (2004) *Kidney international* **65**, 1320-1326

27. Moe, O. W. (1999) *J Am Soc Nephrol* **10**, 2412-2425

28. Moe, O. W., Miller, R. T., Horie, S., Cano, A., Preisig, P. A., and Alpern, R. J. (1991) *The Journal of clinical investigation* **88**, 1703-1708

29. Tsuganezawa, H., Sato, S., Yamaji, Y., Preisig, P. A., Moe, O. W., and Alpern, R. J. (2002) *Kidney Int* **62**, 41-50

30. Li, S., Sato, S., Yang, X., Preisig, P. A., and Alpern, R. J. (2004) *J Clin Invest* **114**, 1782-1789

31. Avraham, H., Park, S. Y., Schinkmann, K., and Avraham, S. (2000) *Cellular signalling* **12**, 123-133

32. Schlaepfer, D. D., and Hunter, T. (1998) *Trends in cell biology* **8**, 151-157

33. Wagner, C. A., Lukewille, U., Valles, P., Breton, S., Brown, D., Giebisch, G. H., and Geibel, J. P. (2003) *Pflugers Arch* **446**, 623-632

34. Geibel, J., Giebisch, G., and Boron, W. F. (1990) *Proc Natl Acad Sci U S A* **87**, 7917-7920

35. Wagner, C. A., Giebisch, G., Lang, F., and Geibel, J. P. (1998) *Proc Natl Acad Sci U S A* **95**, 9665-9668

36. Roos, A., and Boron, W. F. (1981) *Physiol Rev* **61**, 296-434

37. Thomas, J. A., Buchsbaum, R. N., Zimniak, A., and Racker, E. (1979) *Biochemistry* **18**, 2210-2218

38. Grynkiewicz, G., Poenie, M., and Tsien, R. Y. (1985) *J Biol Chem* **260**, 3440-3450

39. Stehberger, P. A., Shmukler, B. E., Stuart-Tilley, A. K., Peters, L. L., Alper, S. L., and Wagner, C. A. (2007) *J Am Soc Nephrol* **18**, 1408-1418

40. Finberg, K. E., Wagner, C. A., Stehberger, P. A., Geibel, J. P., and Lifton, R. P. (2003) *Gene* **318**, 25-34

41. Smith, A. N., Finberg, K. E., Wagner, C. A., Lifton, R. P., Devonald, M. A., Su, Y., and Karet, F. E. (2001) *J Biol Chem* **276**, 42382-42388

42. Brown, D., Lydon, J., McLaughlin, M., Stuart-Tilley, A., Tyszkowski, R., and Alper, S. (1996) *Histochem Cell Biol* **105**, 261-267

43. Lang, K., Wagner, C., Haddad, G., Burnekova, O., and Geibel, J. (2003) *Cell Physiol Biochem* **13**, 257-262

44. Schwark, J. R., Jansen, H. W., Lang, H. J., Krick, W., Burckhardt, G., and Hropot, M. (1998) *Pflugers Arch* **436**, 797-800

45. Wang, J. Q., Kon, J., Mogi, C., Tobo, M., Damirin, A., Sato, K., Komachi, M., Malchinkhuu, E., Murata, N., Kimura, T., Kuwabara, A., Wakamatsu, K., Koizumi, H., Uede, T., Tsujimoto, G., Kurose, H., Sato, T., Harada, A., Misawa, N., Tomura, H., and Okajima, F. (2004) *J Biol Chem* **279**, 45626-45633

46. Oliver, R., 3rd, Friday, E., Turturro, F., Lacy, A., and Welbourne, T. (2005) *Am J Physiol Renal Physiol* **288**, F1257-1266

47. Wiederkehr, M. R., Zhao, H., and Moe, O. W. (1999) *Am J Physiol* **276**, C1205-1217

48. Watts, B. A., 3rd, George, T., and Good, D. W. (2006) *Am J Physiol Renal Physiol* **291**, F1005-1013

49. Liu, F., and Gesek, F. A. (2001) *Am J Physiol Renal Physiol* **280**, F415-425

50. Xu, Y., and Casey, G. (1996) *Genomics* **35**, 397-402

51. Xu, Y., Zhu, K., Hong, G., Wu, W., Baudhuin, L. M., Xiao, Y., and Damron, D. S. (2000) *Nat Cell Biol* **2**, 261-267

52. Zhu, K., Baudhuin, L. M., Hong, G., Williams, F. S., Cristina, K. L., Kabarowski, J. H., Witte, O. N., and Xu, Y. (2001) *J Biol Chem* **276**, 41325-41335

53. Zhu, K., Baudhuin, L. M., Hong, G., Williams, F. S., Cristina, K. L., Kabarowski, J. H. S., Witte, O. N., and Xu, Y. (2005) *J Biol Chem* **280**, 43280

54. Ludwig, M. G., Vanek, M, Guerini, D, Gasser, J A, Jones, C E, Junker, U, Hofstetter, H, Wolf, R M, Seuwen, K. (2003) *Nature* **425**, 93-98

55. Slotki, I. N., Schwartz, J. H., and Alexander, E. A. (1990) *Am J Physiol* **259**, F666-671

56. Yang, X., Amemiya, M., Peng, Y., Moe, O. W., Preisig, P. A., and Alpern, R. J. (2000) *Am J Physiol Cell Physiol* **279**, C410-419

57. Fan, L., Wiederkehr, M. R., Collazo, R., Wang, H., Crowder, L. A., and Moe, O. W. (1999) *J Biol Chem* **274**, 11289-11295

58. (2005) *J Biol Chem* **280**, 43280

59. Wagner, C. A., Lukewille, U, Valles, P, Breton, S, Brown, D, Giebisch, G H, Geibel, J P. (2003) *Pflugers Arch* **446**, 623-632

60. Yamaji, Y., Tsuganezawa, H., Moe, O. W., and Alpern, R. J. (1997) *Am J Physiol* **272**, C886-893

61. Lang, K., Wagner, C A, Haddad, G, Burnekova, O, Geibel, J. (2003) *Cell Physiol Biochem* **13**, 257-262

14.2. The pH-Receptor GPR4 is Critical for Renal and Respiratory Control of Acid-base Balance

(Manuscript in preparation)

Ana Velic[1,2], **Chahira Benabbas**[1,]2, Jorge Soliz[2,3], Dominique Eladari[4], , Max Gassmann[2,3], Thomas Suply[5], Marie-Gabrielle Ludwig[5], Klaus Seuwen[5], Carsten A. Wagner[1,2]

1 Institute of Physiology, University of Zürich, Switzerland
2 Centre for Integrative Human Physiology, University of Zürich, Switzerland
3 Institute of animal Physiology, University of Zürich, Switzerland
4 INSERM U652, IFR58, Institut des Cordeliers, Paris, France
5 Novartis Institute of biomedical research, Basel, Switzerland

Corresponding author:
Carsten A. Wagner
Institute of Physiology and Zurich Center for
Integrative Human Physiology (ZIHP)
University of Zurich
Winterthurerstrasse 190
CH-8057 Zurich
Switzerland
Phone: +41-44-63 50659
Fax: +41-44-63 56814
E-Mail: Wagnerca@access.uzh.ch

14.3. Renal Acid-Base Transport: Old and New Players

Wagner CA, Kovacikova J, Stehberger PA, Winter C, **Benabbas C**, Mohebbi N.

Nephron Physiol. 2006;103(1):p1-6

KARGER

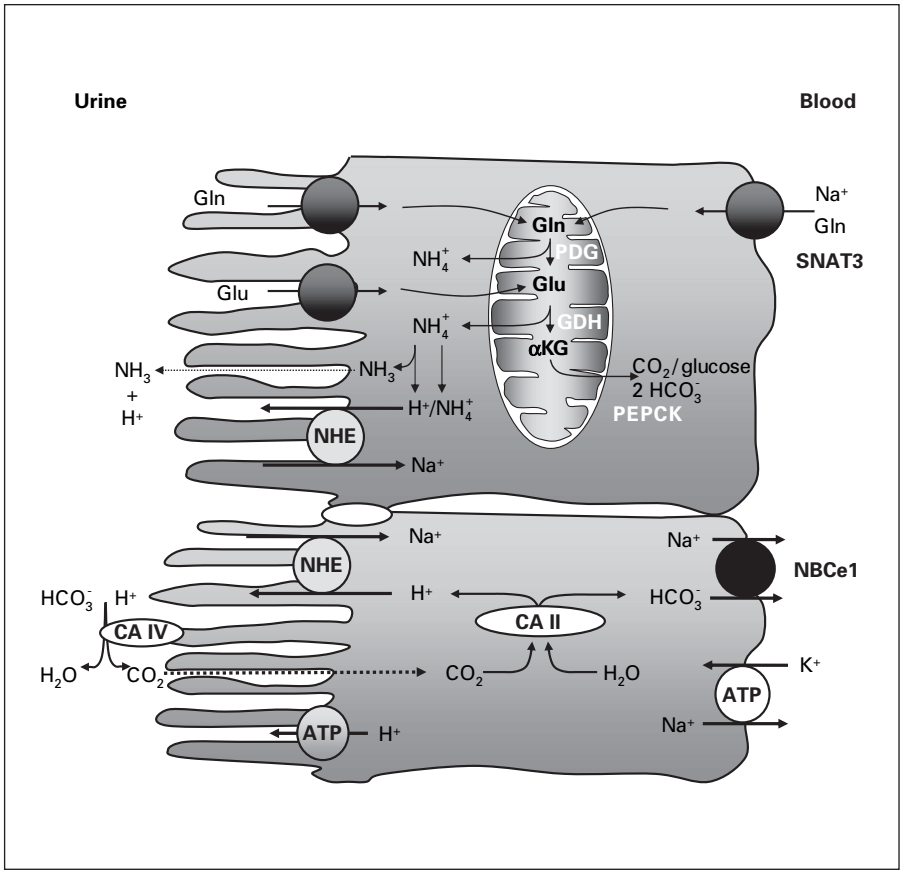

Fig. 1. Transport mechanisms involved in acid-base transport and ammoniagenesis in the proximal tubule. For clarity processes are depicted in two different cells but occur in all cells of the proximal tubule. Bicarbonate absorption is mediated by apical Na^+/H^+ exchangers (NHE) and vacuolar H^+-ATPases in concert with extracellular and cytosolic carbonic anhydrases (CAII and CAIV). Bicarbonate is released into blood via the basolateral electrogenic Na^+/HCO_3^- cotransporter (NBCe1). Ammoniagenesis takes place in the proximal tubule during normal conditions mainly in the S3 segment. It involves uptake of glutamine (Gln) from urine and blood via several apical and basolateral Na^+-dependent amino acid transporters. Gln is converted to glutamate (Glu) by the action of the mitochondrial phosphate-dependent glutaminase (PDG) and further metabolized to α-ketoglutarate (α-KG) via the glutamine dehydrogenase (GDH). Eventually, glucose and CO_2 are produced by the cytosolic phosphoenolpyruvate carboxykinase (PEPCK). During this process HCO_3^- and NH_3/NH_4^+ are formed. NH_3 diffuses into the lumen whereas NH_4^+ is transported via NHE into urine. During acidosis ammoniagenesis is increased and the expression of the basolateral glutamine transporter SNAT3 stimulated.

thick ascending limb accounting for about 20% of the filtered bicarbonate [2].

The proximal tubule also plays an important role in the synthesis of the major titratable acid, NH_3/NH_4^+, synthesized from glutamine yielding two HCO_3^- and NH_3 molecules as well as glucose. The synthesis of NH_3/H_4^+ is highly regulated and stimulated during metabolic acidosis and requires the extraction of glutamine from blood across the basolateral membrane [3]. The amino acid transporter responsible for glutamine uptake into proximal tubular cells has been identified as SNAT3 (SLC38A3) and is upregulated both on mRNA and protein levels during metabolic acidosis [4, 5; Moret, Dave, Schulz, Verrey, Wagner, own unpublished observations]. Interestingly, SNAT3 is localized only in the late proximal tubule under normal conditions but its expression spreads to earlier proximal segments during acidosis. The second important titratable acid, phosphate, is also regulated by the proximal tubule as most phosphate is reabsorbed at this site via the apical Na^+/phosphate cotransporter NaPi-IIa. During acidosis renal phosphate excretion is increased. In rats, but not in mice, acidosis downregulates NaPi-IIa activity and expression in the kidney [6, 7]. Interestingly, phosphate uptake from diet and expression of the intestinal NaPi-IIb phosphate transporter are stimulated during acidosis in mice [7]. This could provide phosphate for renal excretion and help to protect bone from massive phosphate loss during acidosis.

Secretion of Protons or Bicarbonate from Intercalated Cells

The final tuning of urinary acidification occurs in the late distal tubule, the connecting segment, the cortical and medullary collecting duct mainly through the action of intercalated cells [8]. At least two types of intercalated cells have been described based on morphological and functional criteria: acid-secretory type-A intercalated cells (A-IC) and bicarbonate-excreting type-B intercalated cells (B-IC). A-IC express vacuolar H^+-ATPases on the luminal membrane excreting protons into urine which

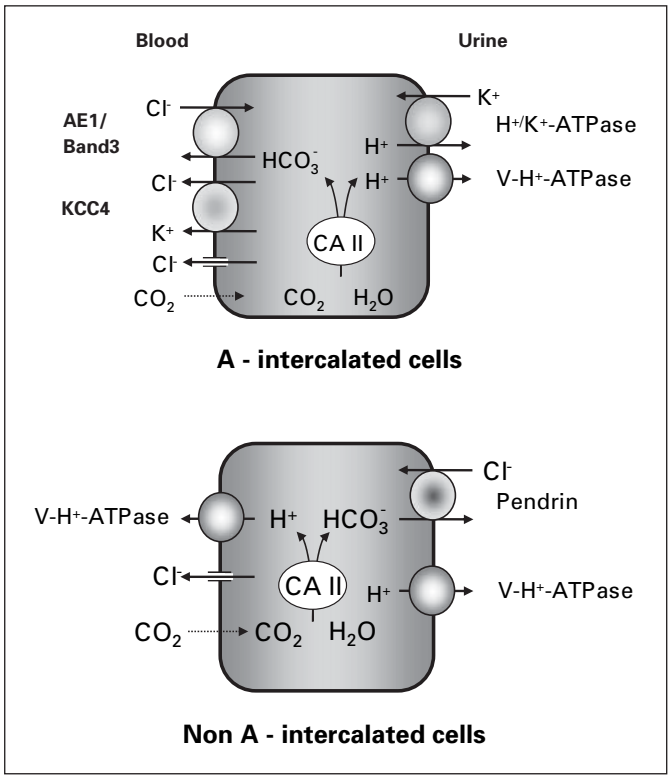

Fig. 2. Transport schemes for type A and non-type A intercalated cells. Type A intercalated express an apical H^+-ATPase secreting protons into urine and a basolateral Cl^-/HCO_3^- exchanger, AE1, releasing bicarbonate into blood. Protons and bicarbonate are provided by a cytosolic carbonic anhydrase (CAII). Basolateral Cl^- channels and a K^+/Cl^- symporter (KCC4) may be involved in recycling chloride ions for AE1 activity. Non-type A intercalated cells express a vacuolar H^+-ATPase on the basolateral side (type B IC) or on both sides (non-A/non-B IC). Both subtypes, however, express the Cl^-/HCO_3^- exchanger pendrin on their luminal side.

stem from the hydration of CO_2 and subsequent formation of protons and bicarbonate by the cytosolic CAII isoform. The bicarbonate is released into blood via the basolaterally expressed chloride-bicarbonate exchanger AE1 (band 3). In contrast, B-IC express an apical chloride-bicarbonate exchanger excreting bicarbonate into urine. Protons are secreted into blood by basolateral H^+-ATPases. The apical Cl^-/HCO_3^- exchanger is most likely represented by pendrin. The function and regulation of pendrin has recently gained much attention because of its regulated expression in response to dietary chloride intake and the fact that pendrin-deficient mice are more sensitive to dietary salt restriction and do not increase blood pressure in response to aldosterone analogues [9–11]. These findings suggest a role of pendrin in chloride conservation by the kidneys and blood pressure regulation. Pendrin may also be important for protecting the body from the development of metabolic alkalosis as evident from pendrin-deficient mice and a mouse model lacking the B1 subunit of the basolateral proton pump of B-IC and reduced pendrin abundance. Both mouse models are more prone to the development of metabolic alkalosis [10, 12]. An additional Cl^-/HCO_3^- exchanger, AE4, has been identified in non-type A-IC. The subcellular localization of AE4 appears to be species specific. In the rabbit AE4 is localized in the apical membrane whereas in the rat and mouse AE4 is found on the basolateral side [13, 14].

Regulation of Renal Acid-Base Transport

The renal excretion of acid and base equivalents by the kidney is influenced by many factors such as diet, electrolyte status, physical activity, and drugs. Several hormones have been identified that could link metabolism and renal acid-base transport such as aldosterone, angiotensin II, endothelin, insulin-like growth factor 1, antidiuretic hormone, and thyroid hormones.

The vasoconstrictor endothelin has appeared over the last years as an important factor regulating renal acid secretion. Endothelin production in arteries and proximal tubules is increased during metabolic acidosis [15, 16]. The stimulatory effect of endothelin on Na^+/H^+ exchanger(s) and vacuolar H^+-ATPases in the proximal and distal tubules is mostly mediated by ET-B receptors [17, 18]. Furthermore, the increased urinary acid excretion in animals on a diet rich in protein depends on endothelin.

The importance of aldosterone for final urinary acidification has been known for decades and insufficiency of aldosterone synthesis, excretion or signaling underlies the hyperkalemic type of distal renal tubular acidosis (dRTA) [19]. Two findings have shed new light on aldosterone. First, a high-protein diet providing a dietary acid load stimulates renal acid excretion via endothelin, increasing aldosterone secretion [20]. Blocking either the endothelin or aldosterone pathway results in an inappropriate urinary acidification. Second, aldosterone stimulates vacuolar H^+-ATPase activity also in a way distinct from the classic route (i.e. via the mineralocorticoid receptor and subsequent regulation of transcription). In freshly isolated mouse and human outer medullary collecting ducts, aldosterone directly stimulates insertion of proton pumps into the membrane in a rapid non-genomic manner. This

effect is mediated by a complex signaling cascade via small G proteins, phospholipase C, protein kinase C, ERK1/2 kinases as well as elements of the protein kinase A-dependent pathway [21].

Besides these hormonal pathways, a novel concept of local pH sensing and regulation of acid-base transporters has emerged. Incubation of the renal OK cell line with an acid medium increases Na^+/H^+-exchange activity via a src-like tyrosine kinase and pyk2 [22, 23]. Pyk2 is activated in vitro in a slightly acidic buffer and phosphorylates and activates src [22]. However, it is unclear if pyk2 is the pH sensor itself. A novel subfamily of G protein-coupled receptors may contain such pH sensors. Three members of this subfamily, OGR1, GPR4 and TDAG8, are activated by extracellular protons with half-maximal activation occurring in the pH range of 7.4–7.0. Activation of OGR1 increases intracellular calcium and IP_3 levels, known stimuli for Na^+/H^+-exchange activity [24]. GPR4 and TDAG8 couple to cAMP- and PKA-dependent pathways. Both OGR1 and GPR4 are expressed in the kidney and at least in the case of OGR1 its localization in the basolateral membrane of almost all nephron segments appears ideally suited for an extracellular pH sensor [Mohebbi, Benabbas and Wagner, unpublished observations]. In addition to direct proton sensing, also sensors for CO_2 and HCO_3^- may exist. The recently discovered soluble adenylate cyclase is expressed in several HCO_3^--transporting epithelia including the kidney and is activated in the physiological HCO_3^- concentration range [25]. In addition, evidence from isolated perfused proximal tubules suggest that basolateral HCO_3^- or CO_2 sensors exist and regulate fluid and bicarbonate fluxes [26].

Inherited Disorders of Renal Acid-Base Transport

Genes responsible for several rare inherited disorders of renal acid-base transport have been identified [27]. Mutations in two genes, the Na^+/HCO_3^--cotransporter NBCe1 (SLC4A4) and CAII, cause defective bicarbonate absorption in the proximal tubule. The gene encoding the electrogenic Na^+/HCO_3^- cotransporter (SLC4A4) underlies proximal renal tubular acidosis associated with blindness. Patients suffer from excessive urinary bicarbonate wasting and severe metabolic acidosis. The transporter is not only expressed on the basolateral side of the proximal tubule but also in the eye. Functional analysis of a number of mutants revealed that some mutants are retained in the endoplasmic reticulum, others are inserted into the membrane but show reduced function, and at least in the case of one mutant aberrant trafficking to the apical membrane in polarized cells was found [28, 29]. Mutations in the CAII gene cause a mixed type of proximal and dRTA due to its expression in both segments. Patients also suffer from cerebral calcification and osteopetrosis [30].

Inherited forms of dRTA can be caused by mutations either in two different subunits of the vacuolar H^+-ATPase (ATP6V1B1 (B1 subunit), ATP6V0A4 (a4 subunit)) or the Cl^-/HCO_3^--exchanger AE1 (Band 3, SLC4A1) [1, 27]. All forms are clinically characterized by hyperchloremic metabolic acidosis and hypokalemia and are often associated with retarded growth in infants with rickets. In adults, osteomalacia develops with high urinary calcium and nephrocalcinosis and nephrolithiasis. dRTA due to mutations in proton pump subunits is transmitted in an autosomal recessive way, whereas dRTA caused by AE1 mutations mostly follows an autosomal dominant inheritance. In rare cases, AE1 mutations can also cause autosomal recessive dRTA which has been detected in several patients in Southeast Asia [27].

Patients with mutations in the B1 proton pump subunit often also suffer from sensorineural deafness due to its expression in the inner ear. A mouse model deficient for the *Atp6v1b1* gene has been generated and shown to develop an incomplete dRTA [31]. Due to the expression of the B1 subunit also in bicarbonate-secretory type B intercalated cells, mice lacking the B1 subunit are susceptible to more severe metabolic alkalosis [12]. Thus proton pumps containing the B1 subunit are involved in both acid secretion as well as in bicarbonate secretion during metabolic acidosis or alkalosis, respectively.

The AE1 chloride-bicarbonate exchanger is expressed both in red blood cells (RBC) and in acid-secretory type A-IC. Due to this expression pattern, mutations in the AE1 gene cause spherocytosis, Southeast Asian ovalocytosis and dRTA. However, with rare exceptions, only either RBC or the kidney are affected. This may be partially explained by two different observations. AE1 interacts in RBC with glycophorinA and this interaction functionally rescues many mutations observed in dRTA [32]. However, glycophorin A is not present in intercalated cells [32] and its absence may thus cause a renal defect, whereas the mutations have less functional consequences in RBC. Second, wild-type AE1 has to be sorted to the basolateral side of type-A intercalated cells in order to mediate the vectorial transport of bicarbonate into blood. Some dRTA mutations when expressed in polarized cell lines appear at the apical membrane or are retained intracellularly [33, 34]. Missorting would obvious-

ly not affect AE1 function in non-polarized RBC but reverse the physiological direction of transport in kidney. However, it remains to be clarified if the mistargeting of mutant AE1 also occurs in vivo. dRTA caused by mutations in AE1 is mostly inherited in an autosomal dominant way in contrast to other genetic forms of dRTA. It has been suggested that the formation of functional heterodimers of normal and mutant AE1 may explain this pattern of inheritance. This interpretation is partly supported by two observations. A common mutant found in Southeast Asian ovalocytosis is functionally inactive and decreases transport activity in RBC without giving rise to dRTA [35]. Secondly, a mouse model lacking AE1 both in RBC and the kidney. Mice lacking one allele (heterozygotes) show no sign of metabolic acidosis whereas homozygotes completely lacking AE1 show a severe phenotype with high postnatal lethality, very low hematocrit and hemoglobin levels. Surviving mice suffer from dRTA, severe hyperchloremic metabolic acidosis, growth retardation, nephrocalcinosis with high urinary calcium and phosphate levels and low urinary citrate. In addition, mice are unable to concentrate urine and are dehydrated. However, the vasopressin-regulated AQP2 water channel is found predominantly in intracellular vesicles in the inner medulla pointing to a deranged regulation and possibly explaining the concentrating defect also seen in dRTA patients [36]. The defective AQP2 regulation may at least in part be explained by the concomitant hypercalciuria that may activate calcium-sensing receptors inhibiting AQP2 trafficking [37].

Conclusion and Outlook

Work over the last few years has identified a number of novel transport proteins that contribute directly or indirectly to the kidney's ability to excrete acid or bicarbonate, respectively. Rare mutations found in patients with several forms of renal tubular acidosis in some of these transport proteins have made it possible to gain deeper insight into mechanisms of renal acid-base transport. Newly developed genetic animal models facilitate the examination of transport processes and their regulation, and identify compensatory mechanisms activated by loss of function. However, little is known at present about the signals by which kidney cells sense systemic or local changes in acid-base balance. Hormones such as endothelin and the angiotensin-aldosterone system contribute to regulation. Novel putative proton-sensing receptors may also be involved in this task, however, their physiological role remains to be proven. The cellular events triggered by changes in acid-base homeostasis have only begun to be unraveled. Their elucidation will deepen our understanding of how cells in general and kidney cells in particular regulate intra- and extracellular pH homeostasis.

Acknowledgements

We thank J. Biber, J.P. Geibel, G. Giebisch, H. Murer, and F. Verrey for many discussions. Work in the authors' laboratory was supported by the Swiss National Research Foundation and the 6th EU frame work projects EUGINDAT and EuReGene (005085).

References

1 Wagner CA, Finberg KE, Breton S, Marshansky V, Brown D, Geibel JP: Renal vacuolar H^+-ATPase. Physiol Rev 2004;84:1263–1314.

2 Capasso G, Unwin R, Rizzo M, Pica A, Giebisch G: Bicarbonate transport along the loop of Henle: molecular mechanisms and regulation. J Nephrol Suppl 2002;5:S88–S96.

3 Nagami GT: Renal ammonia production and excretion; in Seldin D, Giebisch G (eds): The Kidney. Physiology and Pathophysiology, ed 3. Philadelphia, Lippincott Williams & Wilkins, 2000, pp 1995–2013.

4 Karinch AM, Lin CM, Wolfgang CL, Pan M, Souba WW: Regulation of expression of the SN1 transporter during renal adaptation to chronic metabolic acidosis in rats. Am J Physiol Renal Physiol 2002;283:F1011–F1019.

5 Solbu TT, Boulland JL, Zahid W, Lyamouri Bredahl MK, Amiry-Moghaddam M, Storm-Mathisen J, Roberg BA, Chaudhry FA: Induction and targeting of the glutamine transporter SN1 to the basolateral membranes of cortical kidney tubule cells during chronic metabolic acidosis suggest a role in pH regulation. J Am Soc Nephrol 2005;16:869–877.

6 Ambuhl PM, Zajicek H K, Wang H, Puttaparthi K Levi M: Regulation of renal phosphate transport by acute and chronic metabolic acidosis in the rat. Kidney Int 1998;53:1288–1298.

7 Stauber A, Radanovic T, Stange G, Murer H, Wagner CA, Biber J: Regulation of intestinal phosphate transport II. Metabolic acidosis stimulates Na^+-dependent phosphate absorption and expression of the Na^+-P_i cotransporter NaPi-IIb in small intestine. Am J Physiol Gastrointest Liver Physiol 2005;288:G501–G506.

8 Wagner CA, Geibel J P: Acid-base transport in the collecting duct. J Nephrol Suppl 2002;5:S112–S127.

9 Quentin F, Chambrey R, Trinh-Trang-Tan MM, Fysekidis M, Cambillau M, Paillard M, Aronson PS, Eladari D: The Cl^-/HCO_3^- exchanger pendrin in the rat kidney is regulated in response to chronic alterations in chloride balance. Am J Physiol Renal Physiol 2004;287:F1179–F1188.

10 Verlander JW, Hassell KA, Royaux IE, Glapion DM, Wang ME, Everett LA, Green ED, Wall SM: Deoxycorticosterone upregulates PDS (Slc26a4) in mouse kidney: role of pendrin in mineralocorticoid-induced hypertension. Hypertension 2003;42:356–362.

11 Wall SM, Kim YH, Stanley L, Glapion DM, Everett LA, Green ED, Verlander JW: NaCl restriction upregulates renal Slc26a4 through subcellular redistribution: role in Cl^- conservation. Hypertension 2004;44:982–987.

12 Kovacikova J, Paunescu T, Bacic D, Finberg KE, Lifton RP, Breton S, Brown D, Wagner CA: B-intercalated cell function is deficient in mice lacking the B1 subunit of the H^+-ATPase (abstract). J Am Soc Nephrol 2004;15:F-PO025.

13 Ko SBH, Xiang L, Hager H, Rojek A, Choi JY, Licht C, Suzuki M, Muallem S, Nielsen S, Ishibashi K: AE4 is a DIDS-Sensitive Cl^-/HCO_3^- exchanger in the basolateral membrane of the rat and mouse renal CCD and the SMG duct. Am J Physiol Cell Physiol 2002;283:C1206–C1218.

14 Tsuganezawa H, Kobayashi K, Iyori M, Araki T, Koizumi A, Watanabe S, Kaneko A, Fukao T, Monkawa T, Yoshida T, Kim DK, Kanai Y, Endou H, Hayashi M, Saruta T: A new member of the HCO_3^- transporter superfamily is an apical anion exchanger of beta-intercalated cells in the kidney. J Biol Chem 2001;276:8180–8189.

15 Licht C, Laghmani K, Yanagisawa M, Preisig PA, Alpern RJ: An autocrine role for endothelin-1 in the regulation of proximal tubule NHE3. Kidney Int 2004;65:1320–1326.

16 Wesson DE, Simoni J, Green DF: Reduced extracellular pH increases endothelin-1 secretion by human renal microvascular endothelial cells. J Clin Invest 1998;101:578–583.

17 Laghmani K, Preisig PA, Moe OW, Yanagisawa M, Alpern RJ: Endothelin-1/endothelin-B receptor-mediated increases in NHE3 activity in chronic metabolic acidosis. J Clin Invest 2001;107:1563–1569.

18 Wesson DE, Dolson GM: Endothelin-1 increases rat distal tubule acidification in vivo. Am J Physiol 1997;273:F586–F594.

19 DuBose TD Jr, Alpern RJ: Renal tubular acidosis; in Scriver CR, Beaudet AL, Sly WS, Valle D (eds): The Metabolic and Molecular Bases of Inherited Disease, ed 8. New York, McGraw-Hill, 2001, pp 4983–5021.

20 Khanna A, Simoni J, Wesson DE: Endothelin-induced increased aldosterone activity mediates augmented distal nephron acidification as a result of dietary protein. J Am Soc Nephrol, 2005;16:1929–1935.

21 Winter C, Schulz N, Giebisch G, Geibel JP, Wagner CA: Nongenomic stimulation of vacuolar H^+-ATPases in intercalated renal tubule cells by aldosterone. Proc Nat Acad Sci USA 2004;101:2636–2641.

22 Li S, Sato S, Yang X, Preisig PA, Alpern RJ: Pyk2 activation is integral to acid stimulation of sodium/hydrogen exchanger 3. J Clin Invest 2004;114:1782–1789.

23 Tsuganezawa H, Sato S, Yamaji Y, Preisig PA, Moe OW, Alpern RJ: Role of c-SRC and ERK in acid-induced activation of NHE3. Kidney Int 2002;62:41–50.

24 Ludwig MG, Vanek M, Guerini D, Gasser JA, Jones CE, Junker U, Hofstetter H, Wolf RM, Seuwen K: Proton-sensing G-protein-coupled receptors. Nature 2003;425:93–98.

25 Chen Y, Cann MJ, Litvin TN, Iourgenko V, Sinclair ML, Levin LR, Buck J: Soluble adenylyl cyclase as an evolutionarily conserved bicarbonate sensor. Science 2000;289:625–628.

26 Zhou Y, Zhao J, Bouyer P, Boron WF: Evidence from renal proximal tubules that HCO_3^- and solute reabsorption are acutely regulated not by pH but by basolateral HCO_3^- and CO_2. Proc Nat Acad Sci USA 2005;102:3875–3880.

27 Alper SL: Genetic diseases of acid-base transporters. Annu Rev Physiol 2002;64:899–923.

28 Dinour D, Chang MH, Satoh J, Smith BL, Angle N, Knecht A, Serban I, Holtzman EJ, Romero MF: A novel missense mutation in the sodium bicarbonate cotransporter (NBCe1/SLC4A4) causes proximal tubular acidosis and glaucoma through ion transport defects. J Biol Chem 2004;279:52238–52246.

29 Li HC, Szigligeti P, Worrell RT, Matthews JB, Conforti L, Soleimani M: Missense mutations in Na^+:HCO_3^- cotransporter NBC1 show abnormal trafficking in polarized kidney cells: a basis of proximal renal tubular acidosis. Am J Physiol Renal Physiol 2005;289:F61–F71.

30 Sly WS, Shah GN: The carbonic anhydrase II deficiency syndrome: osteopetrosis with renal tubular acidosis and cerebral calcification; in Scriver CR, Beaudet AL, Sly WS, Valle D (eds): The Metabolic and Molecular Bases of Inherited Disease. New York, McGraw-Hill, 2001, pp 5331–5343.

31 Finberg KE, Wagner CA, Bailey MA, Paunescu TG, Breton S, Brown D, Giebisch G, Geibel JP, Lifton RP: The B1-subunit of the H^+-ATPase is required for maximal urinary acidification. Proc Natl Acad Sci 2005;102:13616–13621.

32 Tanphaichitr VS, Sumboonnanonda A, Ideguchi H, Shayakul C, Brugnara C, Takao M, Veerakul G, Alper SL: Novel AE1 mutations in recessive distal renal tubular acidosis. Loss-of-function is rescued by glycophorin A. J Clin Invest 1998;102:2173–2179.

33 Devonald MA, Smith AN, Poon JP, Ihrke G, Karet FE: Non-polarized targeting of AE1 causes autosomal dominant distal renal tubular acidosis. Nat Genet 2003;33:125–127.

34 Toye AM, Banting G, Tanner MJ: Regions of human kidney anion exchanger 1 (kAE1) required for basolateral targeting of kAE1 in polarised kidney cells: mis-targeting explains dominant renal tubular acidosis (dRTA). J Cell Sci 2004;117:1399–1410.

35 Bruce LJ, Wrong O, Toye AM, Young MT, Ogle G, Ismail Z, Sinha AK, McMaster P, Hwaihwanje I, Nash GB, Hart S, Lavu E, Palmer R, Othman A, Unwin RJ, Tanner MJ: Band 3 mutations, renal tubular acidosis and South-East Asian ovalocytosis in Malaysia and Papua New Guinea: loss of up to 95% band 3 transport in red cells. Biochem J 2000;350:41–51.

36 Stehberger PA, Stuart-Tilley AK, Shmukler BE, Alper SL, Wagner CA: Impaired distal renal acidification in a mouse model for distal renal tubular acidosis lacking the AE1 (Band 3) Cl^-/HCO_3^- exchanger (Slc4a1) (abstract). J Am Soc Nephrol 2004;15:F-PO008.

37 Sands JM, Naruse M, Baum M, Jo I, Hebert SC, Brown EM, Harris HW: Apical extracellular calcium/polyvalent cation-sensing receptor regulates vasopressin-elicited water permeability in rat kidney inner medullary collecting duct. J Clin Invest 1997;99:1399–1405.

14.4. Essential role for collectrin in renal amino acid transport

Danilczyk U, Sarao R, Remy C, **Benabbas C**, Stange G, Richter A, Arya S, Pospisilik JA, Singer D, Camargo SM, Makrides V, Ramadan T, Verrey F, Wagner CA, Penninger JM.

Nature. 2006 Dec 21;444(7122):1088-91

Vol 444|21/28 December 2006|doi:10.1038/nature05475

LETTERS

Essential role for collectrin in renal amino acid transport

Ursula Danilczyk[1], Renu Sarao[1], Christine Remy[2], Chahira Benabbas[2], Gerti Stange[2], Andreas Richter[3], Sudha Arya[4], J. Andrew Pospisilik[1], Dustin Singer[2], Simone M. R. Camargo[2], Victoria Makrides[2], Tamara Ramadan[2], Francois Verrey[2], Carsten A. Wagner[2] & Josef M. Penninger[1]

Angiotensin -converting enzyme 2 (ACE2) is a regulator of the renin angiotensin system involved in acute lung failure, cardiovascular functions and severe acute respiratory syndrome (SARS) infections in mammals[1–3]. A gene encoding a homologue to ACE2, termed collectrin (Tmem27), has been identified in immediate proximity to the *ace2* locus[4]. The *in vivo* function of collectrin was unclear. Here we report that targeted disruption of *collectrin* in mice results in a severe defect in renal amino acid uptake owing to downregulation of apical amino acid transporters in the kidney. Collectrin associates with multiple apical transporters and defines a novel group of renal amino acid transporters. Expression of collectrin in *Xenopus* oocytes and Madin–Darby canine kidney (MDCK) cells enhances amino acid transport by the transporter B^0AT1. These data identify collectrin as a key regulator of renal amino acid uptake.

ACE2 is a chimaeric protein that has emerged from the duplication of two genes: homology with ACE at the catalytic domain and homology with collectrin in the membrane proximal domain (Fig. 1a). In the mouse, *collectrin* is expressed in the kidneys[4] and pancreas[5,6] and to a lesser extent in the intestine (duodenum, jejunum and ileum), liver, heart and stomach (Supplementary Fig. 1). To assess the *in vivo* function of collectrin, we generated *collectrin* knockout mice (Fig. 1b). Mice were crossed with the transgenic Cre *deleter* strain to ubiquitously delete *collectrin*[7] (Supplementary Fig. 2a). The null mutation of *collectrin* was verified by the absence of *collectrin* messenger RNA transcripts and protein (Supplementary Fig. 2b, c). ACE2 expression in the kidneys was not altered in *collectrin* mutant mice (Supplementary Fig. 2c). *Collectrin* null mice were born at the expected mendelian frequency, indistinguishable from their heterozygous and wild-type littermates. *Collectrin* mutant males ($collectrin^{-/y}$) and females ($collectrin^{-/-}$) were fertile and we failed to observe any overt morphological alterations in all organs analysed, including kidney, for up to six months of age (Fig. 1c).

Collectrin was originally reported to be expressed in collecting ducts[4] and β-islet cells of the pancreas[5,6]. We therefore assessed whether collectrin is involved in renal salt and/or glucose balance. Na^+ excretion in urine was comparable in $collectrin^{+/y}$ and $collectrin^{-/y}$ mice. Loss of collectrin also did not affect the levels of calcium, potassium, phosphate, chloride, urea, uric acid or creatinine in urine and blood (Supplementary Table 1). *collectrin* mutant mice had the same glucose concentration as their wild-type littermates in serum and urine. Surprisingly, storage of the urine samples collected from mutant mice at 4 °C resulted in the formation of large white precipitates (Fig. 1d). Morphological analysis revealed large needle-like crystals in the urine of the *collectrin* null mice whereas such crystals were never observed in wild-type mice (Fig. 1e). Biochemically, these crystals were not composed of common urinary crystal components such as ammonium urate, sodium urate, calcium oxalate dihydrate or calcium phosphate. High performance liquid chromatography (HPLC) analyses showed that these crystals contained ~10% phenylalanine (Phe) and 90% tyrosine (Tyr) (see Fig. 1f). When animals were fed a tyrosine-free and phenylalanine-free diet or when the animals were fasting, no crystals were formed in the urine of *collectrin* null mice (Fig. 1d), indicating that the observed changes are not caused by tyrosinaemia[8,9]. Thus, loss of collectrin expression results in the formation of tyrosine/phenylalanine crystals in the urine.

To determine whether collectrin deficiency caused a more general defect in amino acid handling in the kidneys, we assessed urinary amino acid contents. Whereas in wild-type mice almost all amino acids are reabsorbed from the urine, deletion of *collectrin* resulted in severe leakage of all amino acids (Fig. 1g). Concentrations of the amino acids were also lower in the serum of mutant mice, although amino acids were still present (Supplementary Fig. 3). Urinary output was higher in $collectrin^{-/y}$ mice (3.31 ± 0.25 ml urine per 24 h) as compared to $collectrin^{+/y}$ littermates (1.65 ± 0.28 ml urine per 24 h) which may be owing to the higher concentration of osmotically active solutes in urine from *collectrin*-deficient mice. Water restriction for 24 h demonstrated that *collectrin*-deficient mice were not able to concentrate urine to the same degree, confirming that the higher urinary output is due to a primarily renal defect (Supplementary Fig. 4). Thus, collectrin is critical for normal amino acid reabsorption in the kidney.

Amino acid reabsorption occurs in the proximal tubules of the kidney[10]. Immunohistochemical staining showed that collectrin is indeed expressed at the luminal side of brush border membranes in proximal tubules (Fig. 2a), which is a specialized microenvironment involved in amino acid reabsorption[11]. Biochemically, we confirmed specific expression of collectrin in brush border membrane vesicles (BBMV) isolated from the kidney of $collectrin^{+/y}$, but not $collectrin^{-/y}$ mice (Fig. 2b). BBMV isolates were free from contamination (assessed by the absence of the collecting duct marker aquaporin 2; Fig. 2b). In addition, collectrin mRNA was found to be highly expressed in proximal tubules (Fig. 2c). Thus, collectrin is localized in brush border membranes of proximal tubules.

Because collectrin is predicted to be a type I transmembrane protein having only one transmembrane helix[4], it was unlikely that collectrin itself forms an amino acid transport pore. Because collectrin expression parallels that of the B^0 cluster of the solute carrier SLC6 proteins B^0AT1, XT3s1/SIT1, XT2 and XT3, a recently identified subfamily of Na^+-dependent transporters of neutral amino acids[12–17], we assessed whether loss of collectrin may affect these

[1]IMBA, Institute for Molecular Biotechnology of the Austrian Academy of Sciences, Dr. Bohr-Gasse 3, A-1030, Vienna, Austria. [2]Institute of Physiology and Center for Integrative Human Physiology, University of Zurich, Winterthurerstrasse 190, 8057 Zurich, Switzerland. [3]Department of Chemical Ecology and Ecosystem Research, Center of Ecology, University of Vienna, Althanstrasse 14, A-1090 Vienna, Austria. [4]The Hospital for Sick Children, 555 University Avenue, Toronto, Ontario M5G 1X8, Canada.

amino acid transporters. Immunoblots of BBMVs revealed that the neutral amino acid transporter B^0AT1 was markedly downregulated in *collectrin*$^{-/y}$ mice (Fig. 2d and Supplementary Fig. 5a, b). Protein expression of the three other members of the SLC6 family XT3s1/SIT1, XT2 and XT3, and expression of EAAC1, the apical transporter responsible for glutamate/aspartate reabsorption[18], was also markedly downregulated (Fig. 2e). By contrast, expression of $b^{0,+}AT$ (also known as slc7a9) (Fig. 2e), the exchanger mediating apical uptake of cystine, arginine, lysine and ornithine[19], and expression of the basolateral amino acid transporter subunits 4F2hc and LAT2 (ref. 10) remained unchanged (Supplementary Fig. 5b). Expression of the sodium/phosphate co-transporter Na^+/Pi IIa was also not affected in *collectrin* null mice (Fig. 2d). mRNA expression of all these transporters was comparable in *collectrin*$^{+/y}$ and *collectrin*$^{-/y}$ mice (Supplementary Fig. 6). Immunoblotting of total kidney membranes demonstrated that the abundance of these amino acid transporters was also decreased to a similar extent as observed in BBMVs (Supplementary Fig. 5b).

To test whether reduced expression resulted in decreased amino acid transport activity, we isolated BBMVs and measured Na^+-dependent amino acid uptake rates. As expected from the urinary loss of B^0AT1 substrates, the uptake rate of glutamine and phenylalanine in BBMV from kidneys of *collectrin* null mice was decreased compared to control littermates, whereas uptake of phosphate was not affected (Fig. 2f). These data show that loss of collectrin is associated with reduced expression and impaired activity of apical, Na^+-dependent amino acid transporters in the kidney.

To identify the molecular pathway by which collectrin regulates amino acid transporters, we first examined whether collectrin can associate with B^0AT1 and/or other transporters. Immunoprecipitations from BBMV lysates showed direct binding between collectrin and B^0AT1, XT2 and XT3 in *collectrin*$^{+/y}$, but not *collectrin*$^{-/y}$ mice (Fig. 3a). Moreover, collectrin co-localized with B^0AT1 in the early proximal S1 tubule (Fig. 3b). As a control, collectrin did not associate with $b^{0,+}AT$ (Fig. 3a). The specificity of the collectrin band was confirmed by pre-incubation with the antigenic peptide (Supplementary Fig. 7a, b). Renal amino acid transporters such as LAT2 or y^+LAT1 form functional heterodimers with a second subunit, 4F2hc (ref. 10). In all known instances, this heterodimerization is stabilized by disulphide bonds[20]. Under reducing conditions (+DTT), collectrin appears as a single band with gel mobility of ~44 kDa, whereas B^0AT1 can be detected as a single band that corresponds to a monomeric form of

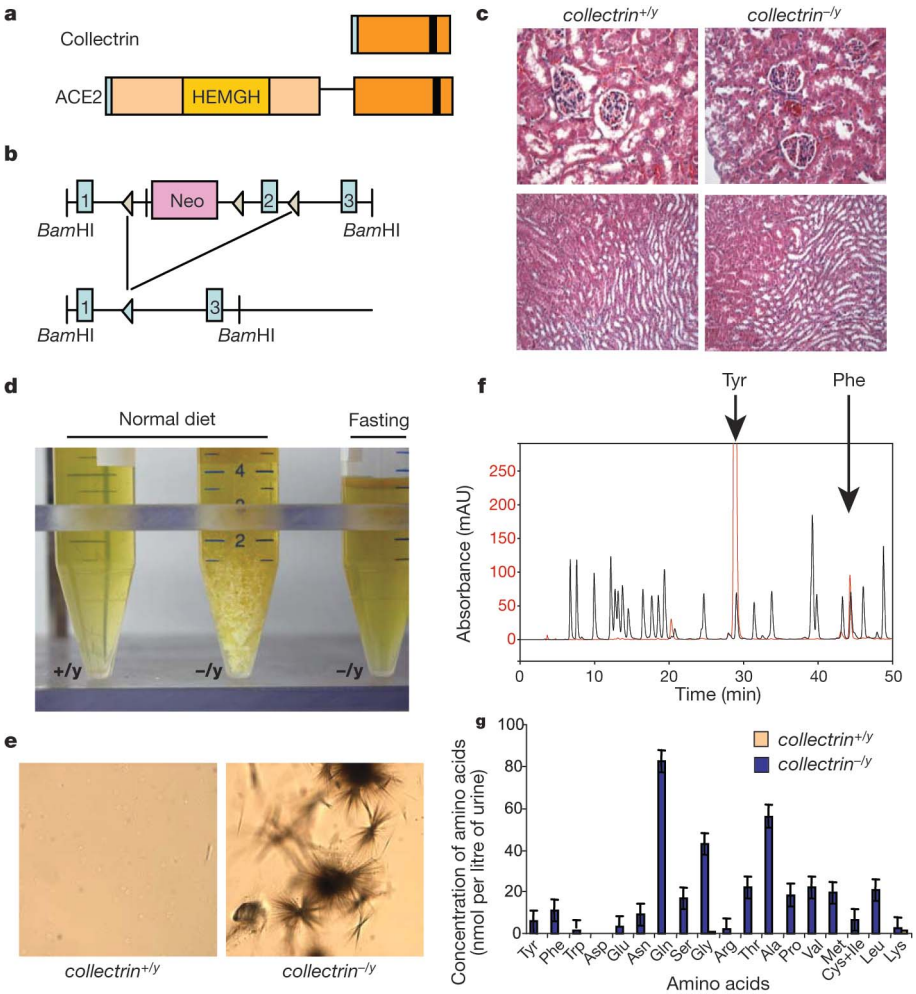

Figure 1 | Tyrosine crystals and renal amino acid loss in *collectrin*$^{-/y}$ mice. **a**, Schematic outline of homologous regions between collectrin and ACE2. Collectrin lacks the HEMGH carboxypeptidase domain. The black boxes indicate the transmembrane domains. Leader peptides are shown in light blue. **b**, Gene targeting (flox-and-delete) strategy for the generation of *collectrin* mutant alleles. Upon breeding with Cre *deleter* mice, animals with excision of exon 2 were selected. **c**, H&E-stained sections of kidney isolated from six-month-old *collectrin*$^{+/y}$ and *collectrin*$^{-/y}$ mice. Top panels, overview over cortex; bottom panels, normal medullary structures. **d**, At 4 °C, large white precipitates form in the urine of *collectrin* null (−/y) but not control wild-type (+/y) mice. These precipitates disappear upon fasting for 24 h. **e**, Formation of needle-like crystals in the urine of *collectrin* null mice. **f**, HPLC analysis of crystals isolated from the urine of *collectrin*$^{-/y}$ mice. The crystals co-elute with tyrosine and phenylalanine. mAU, milli-absorbance units. **g**, Excretion of all amino acids tested in *collectrin*$^{-/y}$ mice. Urine was collected from four-month-old *collectrin*$^{+/y}$ and *collectrin*$^{-/y}$ littermates and analysed by HPLC. Values are mean ± s.e.m. of ten mice per group. $P < 0.05$ (Student's *t*-test and analysis of variance, ANOVA).

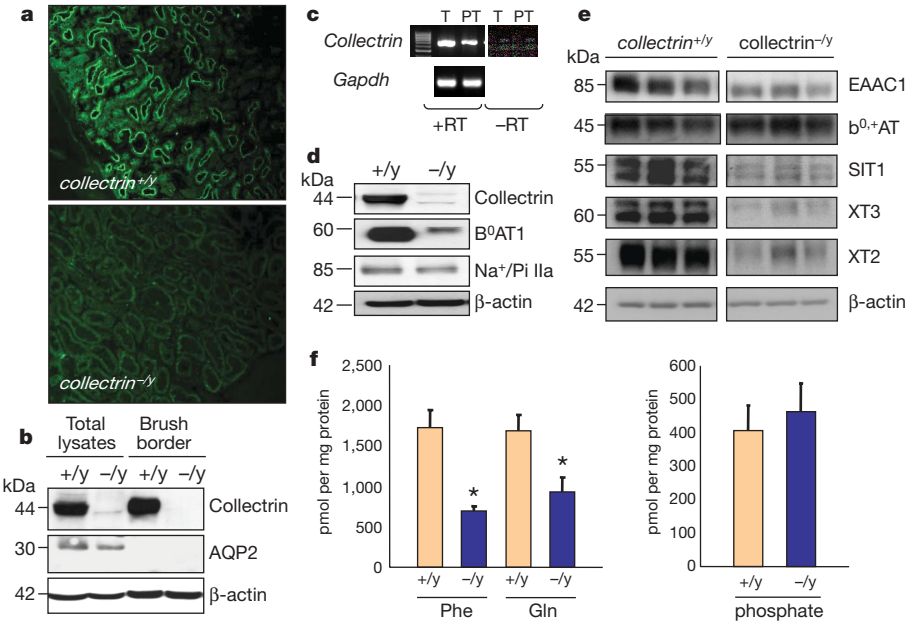

Figure 2 | Defective expression of amino acid transporters in *collectrin* mutant mice. **a**, Immunodetection of collectrin (green) in kidneys of *collectrin*$^{+/y}$ and *collectrin*$^{-/y}$ mice. Note that collectrin localizes to proximal tubules. **b**, Western blot analysis of brush border membranes from *collectrin*$^{+/y}$ and *collectrin*$^{-/y}$ mice. Protein extracts from total lysates (50 μg per lane) and renal brush border membranes (10 μg per lane) were analysed using antibodies to collectrin, aquaporin (AQP2), and β-actin. **c**, Collectrin mRNA expression in proximal tubules (PT) and total kidneys (T). RNA was isolated from wild-type mice and reverse transcribed (+RT). Equal loading was confirmed by Gapdh. **d**, **e**, Western blot analysis of proteins (50 μg) from brush border membranes isolated from *collectrin*$^{+/y}$ and *collectrin*$^{-/y}$ mice. In **d** and **e**, data from three different mice are shown for each genotype. Molecular sizes are indicated in kDa. **f**, Na^+-dependent uptake of the amino acids phenylalanine (Phe) and glutamine (Gln) and uptake of phosphate into BBMVs from *collectrin*$^{+/y}$ and *collectrin*$^{-/y}$ mice. All experiments were done in triplicates from each kidney. Values are mean ± s.e.m. of four mice per group. $^*P < 0.001$ (Student's *t*-test).

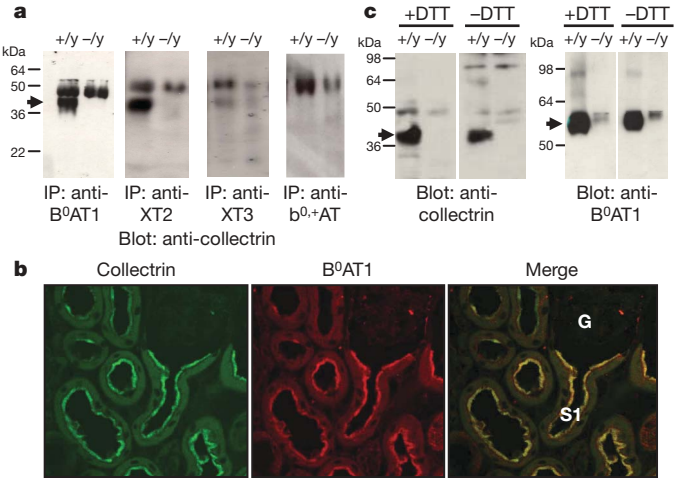

Figure 3 | Collectrin associates with apical amino acid transporters through non-covalent interactions. **a**, Renal brush border membrane proteins (100 μg) from *collectrin*$^{+/y}$ and *collectrin*$^{-/y}$ mice were incubated overnight with anti-B^0AT1, anti-XT2, and anti-XT3 and anti-$b^{0,+}AT$ antibodies. Immunoprecipitated (IP) complexes were analysed by western blot using an anti-collectrin antibody (arrow). **b**, Collectrin co-localizes with B^0AT1 in kidney proximal tubules. Kidney sections from wild-type mice were stained with antibodies to collectrin (green) and B^0AT1 (red). Yellow indicates co-localization. S1, initial part of the proximal tubule. G, glomerulus. Magnifications, ×400. **c**, Western blot analysis of isolated renal brush border membranes under reducing (+DTT; 100 mM) and non-reducing (−DTT) conditions from *collectrin*$^{+/y}$ and *collectrin*$^{-/y}$ mice using antibodies directed against collectrin and B^0AT1. Under reducing as well as under non-reducing conditions collectrin and B^0AT1 appear as bands of ~44 and ~60 kDa, respectively (arrows). Molecular sizes are indicated in kDa.

B^0AT1 (Fig. 3c). Unlike 4F2hc and its catalytic subunits, B^0AT1 and collectrin migrate under non-reducing (no dithiothreitol, −DTT) conditions with the same mobility as under reducing conditions (Fig. 3c), indicating that the association between collectrin and B^0AT1 as well as other transporters occurs through non-covalent interactions. Thus, collectrin co-localizes and specifically associates with a subgroup of renal amino acid transporters.

To define the molecular mechanism of collectrin-regulated amino acid transport, we examined the effect of collectrin on B^0AT1 function using *Xenopus laevis* oocytes and polarized MDCK cells. Two days of expression of B^0AT1 alone in *Xenopus* oocytes conferred only a low transport activity for the B^0AT1 substrate L-isoleucine[16] (Fig. 4a). Collectrin alone did not exhibit any transport activity. However, co-expression of B^0AT1 with collectrin resulted in a striking increase in L-isoleucine uptake (Fig. 4a). As a control, co-expression of collectrin with the Na^+/phosphate IIa co-transporter in oocytes did not affect the rates and kinetics of phosphate uptake (Fig. 4b). To assess whether collectrin changes binding of L-isoleucine to its transporter B^0AT1, we measured the apparent affinity (K_m) for L-isoleucine uptake (Fig. 4c). Co-transport of L-isoleucine with Na^+ generated a saturable, reversible inward current with an apparent K_m for L-isoleucine of 0.99 ± 0.17 mM when B^0AT1 was expressed alone, and of 0.78 ± 0.10 mM when B^0AT1 was co-expressed with collectrin. Thus, the collectrin-induced increase in L-isoleucine transport is not due to a change in apparent affinity, but due to an increase in the maximal transport rate of B^0AT1, probably as a result of increased surface expression. Indeed, expression of collectrin allowed functional surface expression of B^0AT1 and apical uptake of L-isoleucine in polarized kidney MDCK cells (Fig. 4d). Thus, collectrin enhances functional surface expression of the SLC6 family transporter B^0AT1.

We conclude that genetic inactivation of *collectrin* in mice results in a major defect in renal amino acid reabsorption. Collectrin controls protein expression and function of apical amino acid transporters in the brush border membranes of proximal tubules.

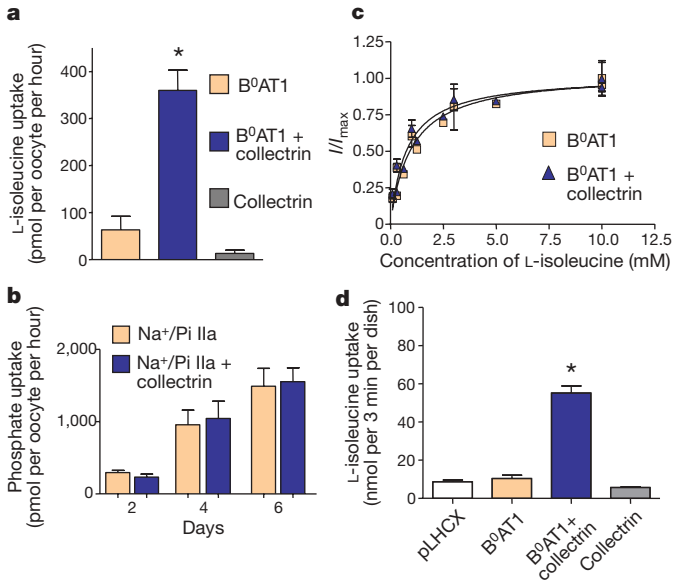

Figure 4 | Collectrin enhances B^{0}AT1 transport activity. **a**, *Xenopus laevis* oocytes were injected with murine B^{0}AT1, collectrin, or B^{0}AT1 plus collectrin RNA. L-isoleucine transport was determined two days after injection. Each bar represents mean transport activity ± s.d. ($n = 15$ oocytes analysed). **b**, *Xenopus laevis* oocytes were injected with murine Na^+/Pi IIa alone or Na^+/Pi IIa plus collectrin; phosphate transport (mean ± s.d.) was then determined at the indicated time points. $n = 7$ oocytes per sample. **c**, The half-maximal uptake rate K_m of L-isoleucine by B^{0}AT1 at six days of expression in the absence or presence of collectrin. K_m was determined using two electrode voltage clamps at −50 mV using 0–10 mM of L-isoleucine in the presence of 100 mM Na^+. Data was normalized to 10 mM L-isoleucine for $n = 11$ oocytes per group. **d**, MDCK cells were transduced with murine B^{0}AT1, collectrin, B^{0}AT1 plus collectrin, or empty vector (pLHCX). Bars represent the mean uptake of 300 μM L-isoleucine in 3 min ± s.d. *$P < 0.001$ (Student's *t*-test).

Mechanistically, collectrin associates with several amino acid transporters, enhances their surface expression, and thereby increases amino acid transport function. These data identify the ACE2 homologue collectrin as a regulator of renal amino acid uptake and may provide a molecular explanation for aminoaciduria in Hartnup disease, Fanconi syndrome, or diabetes.

METHODS

***collectrin* knockout mice.** A gene-targeting vector containing three *loxP* sites flanking exon 2 and a Neo selection cassette was constructed. Chimaeric progeny were crossed to the C57BL/6J Cre *deleter* line[7] to generate complete null animals.

mRNA and protein analyses. Real-time polymerase chain reaction (PCR) was performed as described[12]. For protein analyses, total cell lysates and BBMVs of adult mouse kidney were prepared[21] and probed with antibodies to mouse b$^{0,+}$AT, NaPi IIa, aquaporin 2, collectrin, XT2, XT3, SIT1, B^{0}AT1, ACE2, LAT2 and 4F2. For immunoprecipitations, brush border membrane proteins were probed with antibodies to B^{0}AT1, XT2, XT3 and b$^{0,+}$AT.

Urine and plasma analyses. Urine was collected over 24 h in a metabolic cage. Urinary crystals were observed under a magnification of ×1,000. For HPLC analysis[19], crystals were dissolved in 0.1 M HCl. Na^+, K^+ and Cl^- were assayed by indirect potentiometry. Phosphate was determined using the phosphomolybdate method. Calcium levels were obtained by cresolphthalein. Glucose, urea and uric acid were measured using Reflovet (Roche).

Histology and immunohistochemistry. Paraffin sections were stained with haematoxylin and eosin (H&E). Immunohistochemistry was performed with an affinity purified anti-collectrin antibody. B^{0}AT1 was detected using a rabbit anti-mouse B^{0}AT1 antibody.

Amino acid transporter activities. Uptake of ^{3}H-Phe, ^{14}C-Gln and $^{32}PO_4$ was determined in BBMVs at 60 s. The final amino acid concentration was 1 mM. Measurements were done in parallel in the presence of either Na^+ or K^+. Expression studies and uptake measurements in *Xenopus laevis* oocytes and kidney MDCK cells were performed as described[22,23].

Received 5 May; accepted 23 November 2006.
Published online 13 December 2006.

1. Imai, Y. *et al.* Angiotensin-converting enzyme 2 protects from severe acute lung failure. *Nature* **436,** 112–116 (2005).
2. Crackower, M. A. *et al.* Angiotensin-converting enzyme 2 is an essential regulator of heart function. *Nature* **417,** 822–828 (2002).
3. Kuba, K. *et al.* A crucial role of angiotensin converting enzyme 2 (ACE2) in SARS coronavirus-induced lung injury. *Nature Med.* **11,** 875–879 (2005).
4. Zhang, H. *et al.* Collectrin, a collecting duct-specific transmembrane glycoprotein, is a novel homolog of ACE2 and is developmentally regulated in embryonic kidneys. *J. Biol. Chem.* **276,** 17132–17139 (2001).
5. Fukui, K. *et al.* The HNF-1 target Collectrin controls insulin exocytosis by SNARE complex formation. *Cell Metabol.* **2,** 373–384 (2005).
6. Akpinar, P., Kuwajima, S., Krutzfeldt, J. & Stoffel, M. Tmem27: A cleaved and shed plasma membrane protein that stimulates pancreatic β cell proliferation. *Cell Metabol.* **2,** 385–397 (2005).
7. Schwenk, F., Baron, U. & Rajewsky, K. A cre-transgenic mouse strain for the ubiquitous deletion of *loxP*-flanked gene segments including deletion in germ cells. *Nucleic Acids Res.* **23,** 5080–5081 (1995).
8. Bergeron, A., Jorquera, R. & Tanguay, R. M. Hereditary tyrosinemia: an endoplasmic reticulum stress disorder? *Med. Sci.* **10,** 976–980 (2003).
9. Endo, F. *et al.* Animal models reveal pathophysiologies of tyrosinemias. *J. Nutr.* **3,** 2063S–2067S (2003).
10. Verrey, F. *et al.* Novel renal amino acid transporters. *Annu. Rev. Physiol.* **67,** 557–572 (2005).
11. Kenny, A. J. & Maroux, S. Topology of microvillar membrance hydrolases of kidney and intestine. *Physiol. Rev.* **62,** 91–128 (1982).
12. Romeo, E. *et al.* Luminal kidney and intestine SLC6 amino acid transporters of B0AT-cluster and their tissue distribution in *Mus musculus*. *Am. J. Physiol. Renal Physiol.* **290,** F376–F383 (2006).
13. Broer, A. *et al.* Molecular cloning of mouse amino acid transport system B0, a neutral amino acid transporter related to Hartnup disorder. *J. Biol. Chem.* **279,** 24467–24476 (2004).
14. Kleta, R. *et al.* Mutations in SLC6A19, encoding B0AT1, cause Hartnup disorder. *Nature Genet.* **6,** 999–1002 (2004).
15. Seow, H. F. *et al.* Hartnup disorder is caused by mutations in the gene encoding the neutral amino acid transporter SLC6A19. *Nature Genet.* **6,** 1003–1007 (2004).
16. Camargo, S. M., Makrides, V., Virkki, L. V., Forster, I. C. & Verrey, F. Steady-state kinetic characterization of the mouse BoAT1 sodium-dependent neutral amino acid transporter. *Eur. J. Physiol.* **451,** 338–348 (2005).
17. Kowalczuk, S. *et al.* Molecular cloning of the mouse IMINO system: an Na^+- and Cl^--dependent proline transporter. *Biochem. J. Mar.* **15,** 417–422 (2005).
18. Peghini, P., Janzen, J. & Stoffel, W. Glutamate transporter EAAC-1-deficient mice develop dicarboxylic aminoaciduria and behavioral abnormalities but no neurodegeneration. *EMBO J.* **16,** 3822–3832 (1997).
19. Feliubadalo, L. *et al.* Slc7a9-deficient mice develop cystinuria non-I and cystine urolithiasis. *Hum. Mol. Genet.* **12,** 2097–2108 (2003).
20. Wagner, C. A., Lang, F. & Broer, S. Function and structure of heterodimeric amino acid transporters. *Am. J. Physiol. Cell Physiol.* **81,** C1077–C1093 (2001).
21. Malathi, P., Preiser, H., Fairclough, P., Mallett, P. & Crane, R. K. A rapid method for the isolation of kidney brush border membranes. *Biochim. Biophys. Acta* **554,** 259–263 (1979).
22. Ristic, Z. *et al.* Neutral amino acid transport mediated by ortholog of imino acid transporter SIT1/SLC6A20 in opossum kidney cells. *Am. J. Physiol. Renal Physiol.* **290,** F880–F887 (2006).
23. Bauch, C., Forster, N., Loffing-Cueni, D., Summa, V. & Verrey, F. Functional cooperation of epithelial heteromeric amino acid transporters expressed in Madin–Darby canine kidney cells. *J. Biol. Chem.* **278,** 1316–1322 (2003).

Supplementary Information is linked to the online version of the paper at www.nature.com/nature.

Acknowledgements We thank M. J. Crackower, A. Leibbrandt, Y. Imai, K. Kuba and many others for their contributions. Supported by grants from The National Bank of Austria, The Austrian Ministry of Science and Education, IMBA, an EU Marie Curie Excellence grant, and EUGeneHeart to J.M.P., from the Swiss National Science Foundation to F.V. and EUGINDAT to F.V. and C.A.W.

Author Contributions U.D, R.S., C.R., C.B., G.S., A.R., S.A., J.A.P., D.S., S.M.R.C., V.M., T.R. and C.A.W. performed experiments. U.D., F.V., C.A.W. and J.M.P. planned experiments and wrote the manuscript.

Author Information Reprints and permissions information is available at www.nature.com/reprints. The authors declare no competing financial interests. Correspondence and requests for materials should be addressed to J.M.P. (josef.penninger@imba.oeaw.ac.at) or C.A.W. (wagnerca@access.unizh.ch).

REFERENCES

1. **Perez DM**. From plants to man: the GPCR "tree of life". *Mol Pharmacol* 2005; 67: 1383-4

2. **Vassilatis DK, Hohmann JG, Zeng H, Li F, Ranchalis JE, Mortrud MT, *et al*.** The G protein-coupled receptor repertoires of human and mouse**.** *Proc Natl Acad Sci USA* 2003; 100: 4903-8

3. **Kostenis E.** A glance at G-protein-coupled receptors for lipid mediators: a growing receptor family with remarkably diverse ligands. *Pharmacol Ther* 2004; 102: 243-57

4. **Ishii S, Kihara Y and Shimizu T**. Identification of T cell death-associated gene 8 (TDAG8) as a novel acid sensing G-protein-coupled receptor. *J Biol Chem* 2005 ;11;280(10):9083-7

5. **Ludwig MG, Vanek, M, Guerini, D, Gasser, J A, Jones, C E, Junker, U, Hofstetter, H, Wolf, R M, Seuwen, K**. Proton-sensing G-protein-coupled receptors. *Nature* 2003; 425: 93-98

6. **Murakami N, Yokomizo T, Okuno T and Shimizu T**. G2A is a proton-sensing G-protein-coupled receptor antagonized by lysophosphatidylcholine. *J Biol Chem* 2004; 279: 42484-42491

7. **Wang JQ, Kon J, Mogi C, Tobo M, Damirin A, Sato K, Komachi M, Malchinkhuu E, Murata N, Kimura T, Kuwabara A, Wakamatsu K, Koizumi H, Uede T, Tsujimoto G, Kurose H, Sato T, Harada A, Misawa N, Tomura H and Okajima F**. TDAG8 is a proton-sensing and psychosine-sensitive G-protein-coupled receptor. *J Biol Chem* 2004; 279: 45626-45633

8. **Xu Y and Casey G.** Identification of human OGR1, a novel G protein-coupled receptor that maps to chromosome 14. *Genomics* 1996; 35: 397-402

9. **Zhu K, Baudhuin LM, Hong G, Williams FS, Cristina KL, Kabarowski JH, Witte ON and Xu Y**. Sphingosylphosphorylcholine and lysophosphatidylcholine are ligands for the G protein-coupled receptor GPR4. *J Biol Chem* 2001; 276: 41325-41335. Retraction in: *J Biol Chem* 2005; 30;280(52):43280.

10. **Z. Weng, A.C. Fluckiger, S. Nisitani, M.I. Wahl, L.Q. Le, C.A. Hunter, A.A. Fernal, M.M. Le Beau and O.N. Witte.** A DNA damage and stress inducible G protein-coupled receptor blocks cells in G_2/M *Proc. Natl. Acad. Sci U. S. A.* 1998; 95, p. 12334

11. **I.E. Zohn, M. Klinger, X. Karp, H. Kirk, M. Symons, M. Chrzanowska-Wodnicka, C.J. Der and R.J.** Kay. G2A is an oncogenic G protein-coupled receptor *Oncogene* 2000; 19, p. 3866

12. **J.W. Choi, S.Y. Lee and Y. Choi.** Identification of a Putative G Protein-Coupled Receptor Induced during Activation-Induced Apoptosis of T Cells *Cell. Immunol.* 1996; 168, p. 78

13. **H. Kyaw, Z. Zeng, K. Su, P. Fan, B.K. Shell, K.C. Carter and Y. Li,** *DNA* Cloning, characterization, and mapping of human homolog of mouse T-cell death-associated gene, *Cell Biol* 1998; 17 p. 493

14**. N. Tosa, M. Murakami, W.Y. Jia, M. Yokoyama, T. Masunaga, C. Iwabuchi, M. Inobe, K. Iwabuchi, T. Miyazaki, K. Onoe, M. Iwata and T.** Critical function of T cell death-associated gene 8 in glucocorticoid-induced thymocyte apoptosis. Uede, *Int. Immunol.* 2003; 15, p. 741

15. **Radu CG, Nijagal A, McLaughlin J, Wang L, Witte ON.** Differential proton sensitivity of related G protein-coupled receptors T cell death-associated gene 8 and G2A expressed in immune cells. *Proc Natl Acad Sci U S A* 2005; 102: 1632-7

15-1. **Seuwen K, Ludwig MG, Wolf RM.** Receptors for protons or lipid messengers or both? *J Recept Signal Transduct Res.* 2006; 26(5-6):599-610

16. **Kabarowski JH, Zhu K, Le LQ, Witte ON and Xu Y**. Lysophosphatidylcholine as a ligand for the immunoregulatory receptor G2A. *Science* 2001; 293: 702-705. Retraction in: *Science* 2005 Jan 14;307(5707):206

17. **Kostenis E**. Novel clusters of receptors for sphingosine-1-phosphate, sphingosylphosphorylcholine, and (lyso)-phosphatidic acid: new receptors for "old" ligands. *J Cell Biochem* 2004; 92: 923-936

18. **Xu Y, Zhu K, Hong G, Wu W, Baudhuin LM, Xiao Y and Damron DS**. Sphingosylphosphorylcholine is a ligand for ovarian cancer G-protein-coupled receptor 1. *Nat Cell Biol* 2000; 2: 261-267. Retraction in: *Nat Cell Biol* 2006; 8(3):299

19. **Bektas M, Barak LS, Jolly PS, Liu H, Lynch KR, Lacana E, Suhr KB, Milstien S and Spiegel S**. The G protein-coupled receptor GPR4 suppresses ERK activation in a ligand-independent manner. *Biochemistry* 2003; 42: 12181-12191

20. **J.L. Wike-Hooley, J. Haveman and H.S. Reinhold**. The relevance of tumour pH to the treatment of malignant disease. *Radiother. Oncol* 1984; 2, p. 343

21**. H. Izumi, T. Torigoe, H. Ishiguchi, H. Uramoto, Y. Yoshida, M. Tanabe, T. Ise, T. Murakami, T. Yoshida, M. Nomoto and K. Kohno.** Cellular pH regulators: potentially promising molecular targets for cancer chemotherapy. *Cancer Treat. Re.* 2003; 29, p. 541.

22. **Singh LS, Berk M, Oates R, Zhao Z, Tan H, Jiang Y, Zhou A, Kirmani K, Steinmetz R, Lindner D, Xu Y.** Ovarian Cancer G Protein–Coupled Receptor 1, a New Metastasis Suppressor Gene in Prostate Cancer. *JNCI Journal of the National Cancer Institute* 2007; 99(17):1313-1327

23. **W. Huang, P. Swietach, R. Vaughan-Jones, O. Ansorge, M. Glitsch.** Extracellular Acidification Elicits Spatially and Temporally Distinct Ca^{2+} Signals. *Current Biology* 2008;18 (10), P 781-785

24. **Sin WC, Zhang Y, Zhong W, Adhikarakunnathu S, Powers S, Hoey T, An S and Yang J**. G protein-coupled receptors GPR4 and TDAG8 are oncogenic and overexpressed in human cancers. *Oncogene* 2004; 23: 6299-6303

25. **Yang M, Mailhot G, Birnbaum MJ, MacKay CA, Mason-Savas A, Odgren PR.** Expression of and role for ovarian cancer G-protein-coupled receptor 1 (OGR1) during osteoclastogenesis. *J Biol Chem* 2006 18;281(33):23598-605

26. **Komarova SV, Pereverzev A, Shum JW, Sims SM, Dixon SJ.** Convergent signaling by acidosis and receptor activator of NF-κB ligand (RANKL) on the calcium/calcineurin/NFAT pathway in osteoclasts. *Proc Natl Acad Sci U S A*. 2005; 15;102(7):2643-8

27. **Kevin K Frick, Nancy S Krieger, Keith Nehrke, David A Bushinsky.** Metabolic Acidosis Increases Intracellular Calcium in Bone Cells Through Activation of the Proton Receptor OGR1. *Journal of Bone and Mineral Research* 2009;:24:305-313

28. **Tomura H, Wang JQ, Liu JP, Komachi M, Damirin A, Mogi C, Tobo M, Nochi H, Tamoto K, Im DS, Sato K, Okajima F.** Cyclooxygenase-2 Expression and Prostaglandin E_2 Production in Response to Acidic pH Through OGR1 in a Human Osteoblastic Cell Line. *J Bone Miner Res*. 2008 ;23(7):1129-39.

29**. J.M. Hyvelin, C. O'Connor and P. McLoughlin.** Effect of changes in pH on wall tension in isolated rat pulmonary artery: role of the RhoA/Rho-kinase pathway. *Am. J. Physiol. Lung Cell Mol. Physiol.* 2004; 287, p. L673

30. **W.I. Rosenblum.** ATP-Sensitive Potassium Channels in the Cerebral Circulation *Stroke* 2003; 34(6), p. 1547-52

31. **J.E. Brayden**. Functional Roles Of K_{ATP} Channels In Vascular Smooth Muscle. *Clin. Exp. Pharmacol. Physiol.* 2002; 29, p. 312.

32. **X. Wang, J. Wu, L. Li, F. Chen, R. Wang and C. Jiang.** Hypercapnic Acidosis Activates K_{ATP} Channels in Vascular Smooth Muscles. *Circ. Res* 2003; 92, p. 1225.

33. **H. Xu, J. Wu, N. Cui, L. Abdulkadir, R. Wang, J. Mao, L.R. Giwa, S. Distinct Chanchevalap and C. Jiang.** Histidine Residues Control the Acid-induced Activation and Inhibition of the Cloned K_{ATP} Channel. *J. Biol. Chem*2001; 276, p. 38690

34. **Tomura H, Wang JQ, Komachi M, Damirin A, Mogi C, Tobo M, Kon J, Misawa N, Sato K, Okajima F.** Prostaglandin I(2) production and cAMP accumulation in response to acidic extracellular pH through OGR1 in human aortic smooth muscle cells. *J Biol Chem*. 2005 14;280(41):34458-64

35. **Hoenderop JG, Nilius B, Bindels RJ.** Calcium absorption across epithelia. *Physiol Rev* 2005; 85: 373–422

36. **Hoenderop JG, and René J. M. Bindels** Calciotropic and Magnesiotropic TRP Channels. *Physiology* 2008; 23: 32-40

37. **Suki WN.** Calcium transport in the nephron. *Am J Physiol (Lond)* 1079; 237: F1–F6

38. **Joost G.J. Hoenderop and René J.M. Bindels.** Epithelial Ca^{2+} and Mg^{2+} Channels in Health and Disease. *J Am Soc Nephrol* 2005; 16: 15-26

39. **Hoenderop JG, Nilius B, Bindels RJ.** Molecular mechanisms of active Ca^{2+} reabsorption in the distal nephron. *Annu Rev Physiol* 2002; 64: 529–549

40. **Bindels RJ, Hartog A, Timmermans J, Van Os CH.** Active Ca^{2+} transport in primary cultures of rabbit kidney CCD: Stimulation by 1,25-dihydroxyvitamin D_3 and PTH. *Am J Physiol (Lond)* 1991; 261: F799–F807

41. **Friedman PA, Coutermarsh BA, Kennedy SM, Gesek FA.** Parathyroid hormone stimulation of calcium transport is mediated by dual signaling mechanisms involving protein kinase A and protein kinase C. *Endocrinology* 1996; 137: 13–20

42. **Van Cromphaut SJ, Dewerchin M, Hoenderop JG, Stockmans I, Van Herck E, Kato S, Bindels RJ, Collen D, Carmeliet P, Bouillon R, Carmeliet G.** Duodenal calcium absorption in vitamin D receptor-knockout mice: Functional and molecular aspects. *Proc Natl Acad Sci U S A* 2001; 98: 13324–13329

43. **Friedman PA, Gesek FA.** Vitamin D_3 accelerates PTH-dependent calcium transport in distal convoluted tubule cells. *Am J Physiol (Lond)* 1993; 265: F300–F308

44. **Hoenderop JG, Chon H, Gkika D, Bluyssen HA, Holstege FC, St-Arnaud R, Braam B, Bindels RJ.** Regulation of gene expression by dietary Ca^{2+} in kidneys of 25-hydroxyvitamin D_3-1α-hydroxylase knockout mice. *Kidney Int* 2004; 65: 531–539

45. **Gesek FA, Friedman PA.** Calcitonin stimulates calcium transport in distal convoluted tubule cells. *Am J Physiol (Lond)* 1993; 264: F744–F751

46. **Van Abel M, Hoenderop JG, Dardenne O, St Arnaud R, Van Os CH, Van Leeuwen HJ, Bindels RJ.**1,25-dihydroxyvitamin D_3-independent stimulatory effect of estrogen on the expression of ECaC1 in the kidney. *J Am Soc Nephrol* 2002; 13: 2102–2109

47. **Van Cromphaut SJ, Rummens K, Stockmans I, Van Herck E, Dijcks FA, Ederveen AG, Carmeliet P, Verhaeghe J, Bouillon R, Carmeliet G.** Intestinal calcium transporter genes are upregulated by estrogens and the reproductive cycle through vitamin D receptor-independent mechanisms. *J Bone Miner Res* 2003; 18: 1725–1736

48. **Peng JB, Zhuang L, Berger UV, Adam RM, Williams BJ, Brown EM, Hediger MA, Freeman MR.** CaT1 expression correlates with tumor grade in prostate cancer. *Biochem Biophys Res Commun* 2001; 282: 729–734

49. **Hoenderop JG, Dardenne O, van Abel M, van der Kemp AW, Van Os CH, St-Arnaud R, Bindels RJ.** Modulation of renal Ca^{2+} transport protein genes by dietary Ca^{2+} and 1,25-dihydroxyvitamin D_3 in 25-hydroxyvitamin D_3-1α-hydroxylase knockout mice. *FASEB J* 2002; 16: 1398–1406

50. **Dai LJ, Ritchie G, Kerstan D, Kang HS, Cole DE, Quamme GA.** Magnesium transport in the renal distal convoluted tubule. *Physiol Rev* 2001; 81: 51–84

51. **Quamme GA, Dirks JH.** Magnesium transport in the nephron. *Am J Physiol (Lond)* 239: F393–F401, 1980.

52. **Quamme GA, Dirks JH.** Intraluminal and contraluminal magnesium on magnesium and calcium transfer in the rat nephron. *Am J Physiol (Lond)* 1980; 238: F187–F198

53. **Lemann J Jr, Bushinsky DA, Hamm LL.** Bone buffering of acid and base in humans. *Am J Physiol Renal Physiol* 2003; 285 : F811 –F832

54 . **Nijenhuis T, Renkema KY, Hoenderop JG, and Bindels RJ.** Acid-base status determines the renal expression of Ca2+ and Mg2+ transport proteins. *J Am Soc Nephrol* 2006; 17: 617-626

55. **Rizzo M, Capasso G, Bleich M, Pica A, Grimaldi D, Bindels RJ, and Greger R.** Effect of chronic metabolic acidosis on calbindin expression along the rat distal tubule. *J Am Soc Nephrol* 2000; 11: 203-210

56. **Lemann J, Jr, Bushinsky, D A, Hamm, L L.** Bone buffering of acid and base in humans. *Am J Physiol Renal Physiol* 2003; 285: F811-832

58. **Stehberger PA, Shmukler BE, Stuart-Tilley AK, Peters LL, Alper SL, and Wagner CA.** Distal renal tubular acidosis in mice lacking the AE1 (band3) Cl^-/HCO_3^- exchanger (slc4a1). *J Am Soc Nephrol* 2007; 18: 1408-1418

59. **Laghmani K, Borensztein P, Ambuhl P, Froissart M, Bichara M, Moe OW, Alpern RJ, and Paillard M**. Chronic metabolic acidosis enhances NHE-3 protein abundance and transport activity in the rat thick ascending limb by increasing NHE-3 mRNA. *The Journal of clinical investigation* 1997; 99: 24-30

60. **Faroqui S, Sheriff S, and Amlal H**. Metabolic acidosis has dual effects on sodium handling by rat kidney. *American journal of physiology* 2006; 291: F322-331

61. **Nowik M, Lecca MR, Velic A, Rehrauer H, Brandli AW, and Wagner CA.** Genome-wide gene expression profiling reveals renal genes regulated during metabolic acidosis. *Physiol Genomics* 2008; 32: 322-334

62. **Wang T, Egbert AL, Jr., Aronson PS, and Giebisch G**. Effect of metabolic acidosis on NaCl transport in the proximal tubule. *The American journal of physiology* 1998; 274: F1015-1019

63. **Frische S, Kwon TH, Frokiaer J, Madsen KM, and Nielsen S**. Regulated expression of pendrin in rat kidney in response to chronic NH4Cl or NaHCO3 loading. *American journal of physiology* 2003; 284: F584-593

64. **Jara A, Felsenfeld AJ, Bover J, Kleeman CR.** Chronic metabolic acidosis in azotemic rats on a high-phosphate diet halts the progression of renal disease. *Kidney Int.* 2000;58(3):1023-32

65. **Tashima Y, Kohda Y, Nonoguchi H, Ikebe M, Machida K, Star RA, and Tomita K**. Intranephron localization and regulation of the V1a vasopressin receptor during chronic metabolic acidosis and dehydration in rats. *Pflugers Arch* 2001; 442: 652-661

66. **Kim GH, Martin SW, Fernandez-Llama P, Masilamani S, Packer RK, and Knepper MA**. Long-term regulation of renal Na-dependent cotransporters and ENaC: response to altered acid-base intake. *American journal of physiology* 2000; 279: F459-467

67. **Seaton B and Ali A.** Simplified manual high performance clinical chemistry methods for developing countries. *Med Lab Sci* 1984; 41: 327-336

68. **Berthelot M.** Violet d'aniline. *Rep Chim App* 1859; 1: 284

69. **McLean IW, Nakane, P K.** Periodate-lysine-paraformaldehyde fixative. A new fixation for immunoelectron microscopy. *J Histochem Cytochem* 1974; 22: 1077-1083

70. **Wagner CA, Finberg, K E, Stehberger, P A, Lifton, R P, Giebisch, G H, Aronson, P S, Geibel, J P.** Regulation of the expression of the Cl^-/anion exchanger pendrin in mouse kidney by acid-base status. *Kidney Int* 2002; 62: 2109-2117,

71. **Loffing J, Loffing-Cueni, D, Valderrabano, V, Klausli, L, Hebert, S C, Rossier, B C, Hoenderop, J G, Bindels, R J, Kaissling, B.** Distribution of transcellular calcium and sodium transport pathways along mouse distal nephron. *Am J Physiol Renal Physiol* 2001; 281: F1021-1027

72. **Li S, Sato S, Yang X, Preisig PA, and Alpern RJ.** Pyk2 activation is integral to acid stimulation of sodium/hydrogen exchanger 3. *J Clin Invest* 2004; 114: 1782-1789

73. **Bagnis C, Marshansky V, Breton S, Brown D.** Remodeling the cellular profile of collecting ducts by chronic carbonic anhydrase inhibition. *Am J Physiol Renal Physiol* 2001; 280: F437–F448

74. **Eckardt KU, Kurtz A, Bauer C.** Regulation of erythropoietin production is related to proximal tubular function. *Am J Physiol Renal Fluid Electrolyte Physiol* 1989; 256: F942–F947

75. **Hafner P, Grimaldi R, Capuano P, Capasso G, Wagner CA.** Pendrin in the mouse kidney is primarily regulated by Clexcretionbut also by systemic metabolic acidosis. Am J Physiol Cell Physiol 2008; 295:C1658–C1667

76. **Simon DB, Lu Y, Choate KA, Velazquez H, Al-Sabban E, Praga M, Casari G, Bettinelli A, Colussi G, Rodriguez-Soriano J, McCredie D, Milford D, Sanjad S, and Lifton RP.** Paracellin-1, a tight junction protein required for paracellular Mg^{2+} resorption. *Science* 1999; 285: 103-106

77. **Voets T, Nilius B, van der Kemp AW, Droogmans G, Bindels RJ, Hoenderop JG.** TRPM6 forms the Mg2+ influx channel involved in Mg2+ reabsorption. *J Biol Chem* 2004; 279 : 19 –25

78. **Walder RY, Landau D, Meyer P, Shalev H, Tsolia M, Borochowitz Z, Boettger MB, Beck GE, Englehardt RK, Carmi R, Sheffield VC.** Mutation of TRPM6 causes familial hypomagnesemia with secondary hypocalcemia. *Nat Genet* 2002; 31: 171 –174

79. **Preisig PA, Alpern RJ:** Chronic metabolic acidosis causes an adaptation in the apical membrane Na/H antiporter and basolateral membrane Na(HCO3) symporter in the rat proximal convoluted tubule. *J Clin Invest* 1988; 82 : 1445 –1453

80. **Laghmani K, Preisig PA, Moe OW, Yanagisawa M, Alpern RJ:** Endothelin-1/endothelin-B receptor-mediated increases in NHE3 activity in chronic metabolic acidosis. *J Clin Invest* 2001; 107 : 1563 –1569

81.**Vennekens R, Prenen J, Hoenderop JG, Bindels RJ, Droogmans G, Nilius B**: Modulation of the epithelial Ca2+ channel ECaC by extracellular pH. *Pflugers Arch* 2001; 442 : 237 –242

82. **Yeh BI, Sun TJ, Lee JZ, Chen HH, Huang CL:** Mechanism and molecular determinant for regulation of rabbit transient receptor potential type 5 (TRPV5) channel by extracellular pH. *J Biol Chem* 2003; 278 : 51044 – 51052

83. **Lambers TT, Oancea E, de Groot T, Topala CN, Hoenderop JG, Bindels RJ** Extracellular pH dynamically controls cell surface delivery of functional TRPV5 channels. *Mol Cell Biol* 2007; 27:1486–1494

84. **van de Graaf SF, Hoenderop JG, Gkika D, Lamers D, Prenen J, Rescher U, Gerke V, Staub O, Nilius B, Bindels RJ** Functional expression of the epithelial Ca^{2+} channels (TRPV5 and TRPV6) requires association of the S100A10–annexin 2 complex. *Embo J 2003*; 22:1478–1487

85. **Gerke V, Creutz CE, Moss SE** Annexins: linking Ca^{2+} signalling to membrane dynamics. *Nat Rev Mol Cell Biol* 2005; 6:449–461

86. **van de Graaf SF, Chang Q, Mensenkamp AR, Hoenderop JG, Bindels RJ** Direct interaction with Rab11a targets the epithelial Ca^{2+} channels TRPV5 and TRPV6 to the plasma membrane. *Mol Cell Biol* 2006; 26:303–312

87. **Casanova JE, Wang X, Kumar R, Bhartur SG, Navarre J, Woodrum JE, Altschuler Y, Ray GS, Goldenring JR** Association of Rab25 and Rab11a with the apical recycling system of polarized Madin–Darby canine kidney cells. *Mol Biol Cell* 1999; 10:47–61

88. **Xi Q, Hoenderop JG, Bindels RJ**. Regulation of magnesium reabsorption in DCT. *TRANSPORT PHYSIOLOGY* 2009; 458(1):89-98

89. **Ikari A, Okude C, Sawada H, Takahashi T, Sugatani J, Miwa M** (2007) Down-regulation of TRPM6-mediated magnesium influx by cyclosporin A. *Naunyn Schmiedebergs Arch Pharmacol* 2007; 377(4–6):333–343

90. **Nijenhuis T, Hoenderop JG, Bindels RJ** Downregulation of Ca^{2+} and Mg^{2+} transport proteins in the kidney explains tacrolimus (FK506)-induced hypercalciuria and hypomagnesemia. *J Am Soc Nephrol 2004*; 15:549–557

91. **Loffing J, Vallon V, Loffing-Cueni D, Aregger F, Richter K, Pietri L, Bloch-Faure M, Hoenderop JG, Shull GE, Meneton P, Kaissling B** Altered renal distal tubule structure and renal Na^{+} and Ca^{2+} handling in a mouse model for Gitelman's syndrome. *J Am Soc Nephrol* 2004; 15:2276–2288

92. **Nijenhuis T, Vallon V, van der Kemp AW, Loffing J, Hoenderop JG, Bindels RJ** Enhanced passive Ca^{2+} reabsorption and reduced Mg^{2+} channel abundance explains thiazide-induced hypocalciuria and hypomagnesemia. *J Clin Invest* 2005; 115:1651–1658

93. **Cairo ER, Friedrich T, Swarts HG, Knoers NV, Bindels RJ, Monnens LA, Willems PH, De Pont JJ, Koenderink JB** Impaired routing of wild type FXYD2 after oligomerisation with FXYD2-G41R might explain the dominant nature of renal hypomagnesemia. *Biochim Biophys Acta* 2008; 1778:398–404

94. **Meij IC, Koenderink JB, van Bokhoven H, Assink KF, Groenestege WT, de Pont JJ, Bindels RJ, Monnens LA, van den Heuvel LP, Knoers NV** Dominant isolated renal magnesium loss is caused by misrouting of the Na^+,K^+-ATPase gamma-subunit*. Nat Genet* 2000; 6:265–266

95. **Schlingmann KP, Weber S, Peters M, Niemann Nejsum L, Vitzthum H, Klingel K, Kratz M, Haddad E, Ristoff E, Dinour D, Syrrou M, Nielsen S, Sassen M, Waldegger S, Seyberth HW, Konrad M** Hypomagnesemia with secondary hypocalcemia is caused by mutations in TRPM6, a new member of the TRPM gene family. *Nat Genet* 2002; 31:166–170

96. **Reilly RF, Ellison DH Mammalian distal tubule:** physiology, pathophysiology, and molecular anatomy. *Physiol Rev* 2000; 80:277–313

97. **Sutton RA, Dirks JH (1975) The renal excretion of calcium: a review of micropuncture data.** *Can J Physiol Pharmacol* 1975; 53:979–988

98. **Biner HL, Arpin-Bott MP, Loffing J, Wang X, Knepper M, Hebert SC, Kaissling B Human cortical distal nephron:** distribution of electrolyte and water transport pathways. *J Am Soc Nephrol* 2002; 13:836–847

99. **Costanzo LS, Windhager EE, Ellison DH.** (2000) Calcium and sodium transport by the distal convoluted tubule of the rat. *J Am Soc Nephrol* 1978; 11:1562–1580

100. **Brown EM, Gamba G, Riccardi D, Lombardi M, Butters R, Kifor O, Sun A, Hediger MA, Lytton J, Hebert SC** Cloning and characterization of an extracellular Ca^{2+}-sensing receptor from bovine parathyroid. *Nature* 1993; 366:575–580

101. **Riccardi D, Lee WS, Lee K, Segre GV, Brown EM, Hebert**. SC Localization of the extracellular Ca^{2+}-sensing receptor and PTH/PTHrP receptor in rat kidney. *Am J Physiol* 1996; 271:F951–956

102. **van Abel M, Hoenderop JG, van der Kemp AW, Friedlaender MM, van Leeuwen JP, Bindels RJ**. Coordinated control of renal Ca^{2+} transport proteins by parathyroid hormone. *Kidney Int* 2005; 68:1708–1721

103. **Sutton RA, Wong NL, Dirks JH**.Effects of metabolic acidosis and alkalosis on sodium and calcium transport in the dog kidney. *Kidney Int* 1979; 15:520–533

104. **Groenestege WM, Thebault S, van der Wijst J, van den Berg D, Janssen R, Tejpar S, van den Heuvel LP, van Cutsem E, Hoenderop JG, Knoers NV, Bindels RJ:** Impaired basolateral sorting of pro-EGF causes isolated recessive renal hypomagnesemia. *J Clin Invest* 2007; 117 : 2260–2267

105. **Groenestege WM, Hoenderop JG, van den Heuvel L, Knoers N, Bindels RJ:** The epithelial Mg2+ channel transient receptor potential melastatin 6 is regulated by dietary Mg2+ content and estrogens. *J Am Soc Nephrol* 2006; 17 : 1035 –1043, 2006

106. **Wagner CA, Kovacikova J, Stehberger PA, Winter C, Benabbas C, Mohebbi:** N. Renal acid-base transport: old and new players. Nephron *Physiol.* 2006; 103(1):p1-6

107. **Wagner CA, Devuyst O, Bourgeois S, Mohebbi N.** Regulated acid–base transport in the collecting duct. *European Journal of Physiology*. 2009 ;458(1):137-56

108. **Gluck SL**. Acid sensing in renal epithelial cells. *J Clin Invest* 2004; 114: 1696-1699

109. **Aronson, P.S., J. Nee, and M.A. Suhm,** *Modifier role of internal H+ in activating the Na+-H+ exchanger in renal microvillus membrane vesicles. Nature* 1982; 299(5879): p. 161-3

110. **Wagner, C.A., et al.,** *Renal vacuolar H+-ATPase. Physiol Rev* 2004; 84(4): p. 1263-314.

111. **Wong NL, Quamme GA, Dirks JH:** Effects of acid-base disturbances on renal handling of magnesium in the dog. *Clin Sci (Lond)* 1986; 70 : 277 –284

112. **Wouter M. Tiel Groenestege, Joost G. Hoenderop, Lambertus van den Heuvel, Nine Knoers and René J. Bindels**: The Epithelial Mg^{2+} Channel Transient Receptor Potential Melastatin 6 Is Regulated by Dietary Mg^{2+} Content and Estrogens *J Am Soc Nephrol* 2006; 17: 1035-1043

113. **Brown EM, MacLeod RJ:** Extracellular calcium sensing and extracellular calcium signaling. *Physiol Rev* 2001; 81: 239–297

114. **WardDT and Riccardi D.** Renal physiology of the extracellular calcium-sensing receptor. *Pflügers Arch* 2002; 445: 169–176

115. **Van AbelM, Hoenderop JG, van Leeuwen HJ, and Bindels R.** Down-regulation of calcium transporters in kidney and duodenum by the calcimimetic compound NPS R-467 (Abstract). *J Am Soc Nephrol* 2003; 14: 459A

116. **Ritchie G, Kerstan D, Dai LJ, Kang HS, Canaff L, Hendy GN, and Quamme GA.** 1,25(OH)(2)D(3) stimulates Mg^{2+} uptake into MDCT cells: modulation by extracellular Ca^{2+} and Mg^{2+}. *Am J Physiol Renal Physiol* 2001; 280: F868–F878

117. **Muallem S, Moe OW** When EGF is offside, magnesium is wasted. *J Clin Invest* 2007; 117:2086–2089

118. **Thébault S, Alexander RT, Groenestege WM, Bindels RJ, Hoenderop JG.** EGF activates TRPM6 via a Src kinase and Rac1 mediated increase in plasma membrane expression. *J Am Soc Nephrol* 2008; 283:19999–20007

119. **Buck J, Sinclair, M L, Schapal, L, Cann, M J, Levin, L R**. Cytosolic adenylyl cyclase defines a unique signaling molecule in mammals. *Proc Natl Acad Sci U S A* 1999; 96: 79-84

120. **Chen Y, Cann, M J, Litvin, T N, Iourgenko, V, Sinclair, M L, Levin, L R, Buck, J**. Soluble adenylyl cyclase as an evolutionarily conserved bicarbonate sensor. *Science* 2000; 289: 625-628

121. **Wuttke MS, Buck, J, Levin, L R**. Bicarbonate-regulated soluble adenylyl cyclase. *JOP* 2001; 2: 154-158

122. **Zippin JH, Levin, L R, Buck, J**. CO_2/HCO_3^--responsive soluble adenylyl cyclase as a putative metabolic sensor. *Trends Endocrinol Metab* 2001; 12: 366-370

123. **Litvin, T. N., Kamenetsky, M., Zarifyan, A., Buck, J. and Levin, L. R.** Kinetic properties of `soluble' adenylyl cyclase: synergism between calcium and bicarbonate. *J. Biol. Chem.* 2003; 278,15922 -15926

124. **Paunescu, T. G., Da Silva, N., Russo, L. M., McKee, M., Lu, H. A., Breton, S. and Brown, D.** Association of soluble adenylyl cyclase with the V-ATPase in renal epithelial cells. *Am. J. Physiol. Renal Physiol.* 2008; 294,F130 -F138

125. **Li S, Sato S, Yang X, Preisig PA and Alpern RJ**. Pyk2 activation is integral to acid stimulation of sodium/hydrogen exchanger 3. *J Clin Invest* 2004; 114: 1782-1789

126. **Li H, Wang D, Singh LS, Berk M, Tan H, Zhao Z, Steinmetz R, Kirmani K, Wei G, Xu Y.** Abnormalities in osteoclastogenesis and decreased tumorigenesis in mice deficient for ovarian cancer G protein-coupled receptor 1. *PLoS One* 2009; 28;4(5)

127. **Tsukamoto Y.** Chronic kidney disease (CKD) and bone. From renal osteodystrophy to CKD-MBD: new disease entity. *Clin Calciu*. 2009;19(4):479-84

128. **Krieger NS**, **Frick KK**, **Bushinsky DA**. Mechanism of acid-induced bone resorption. *Curr Opin Nephrol Hypertens* 2004;13(4):423-36

ACKNOWLEDGMENTS

I dedicate this thesis to my parents,
for encouraging and supporting me all my life…

This work was supported by many people. I acknowledge and feel very thankful for their contributions which were at various stages a prerequisite for this work.

I am indebted to Prof. Dr. Carsten A. Wagner for offering me a unique chance to enter the world of science, for maintaining a creative atmosphere and encouraging independence. I am particularly grateful for many chances to attend conferences and set-up collaborations.

I would like to thank the members of my thesis committee, Prof. Dr. Jürg Biber, Prof. Dr. Johannes Loffing and Prof. Dr. Dominique Eladari for their insightful feedback and words of encouragement.

The realization of this project gave me the opportunity to collaborate with several people whom I would like to thank here: Dr. Klaus Seuwen, Dr. Marie-Gabrielle Ludwig and Dr. Jürg Gasser from Novartis in Basel; Prof. Dr. Rene Bindels and Dr. Joost Hoenderop from the department of physiology, Nijmegen Centre for Molecular Life Sciences, Netherlands.

Many thanks to all my lab colleagues and members of our group for their comments, discussions and contributions, special thanks to Stephanie Busque and Nilufar Mohebbi for help and ideas. Many thanks to all people at the J floor for creating and maintaining a cheerful atmosphere.

Last but not least, special thanks to my family for the support they provided me through my entire life and in particular I must acknowledge my husband and best friend, Ahmed, without whose love and encouragement I would not have finished my thesis.

CURRICULUM VITAE

Name: BENABBAS

First Name: Chahira

Date of birth: 27.11.1978 Algiers

PROFESIONAL EXPERIENCE

2004 – 2009: PhD student at the Institute of Physiology, University of Zurich. PhD thesis under supervision of Prof. Dr. CA. Wagner.

Role of the H^+-Activated Ovarian Cancer G Protein-Coupled Receptor 1 (OGR1) in the Renal Handling of Calcium and Magnesium.

2003 – 2004: Master of Pharmacology and Cellular and Molecular Biology, University of Nice, Sophia-Antipolis, (UNSA) France.

Creation of CMV-LOX-STOP-LOX-GFP mouse allowing the characterization of transgenic mice expressing the Cre recombinase specifically at the renal and pulmonary levels.

2004 – 2004: Practical training, Laboratory of Genomic Instability, Faculty of Medicine University of Nice, Sophia-Antipolis, (UNSA) France.

Research topic: V-ATPase.

2002 – 2002: Practical training, Laboratory of Microbiology, University of Nice Sophia-Antipolis, (UNSA) France.

EDUCATION:

2004: **DEA (Master)** of Pharmacology and Cellular and Molecular Biology University of Nice Sophia-Antipolis, (UNSA) France.

2003: **Maitrise** of Biochemistry, UNSA France.

2001: **Licence** of Biochemistry, UNSA France.

2000: **DEUG** Science, UNSA France.

1999: **DEUG** Cellular Biology and Physiology, University of Sciences, Algiers.

1997: **High school diploma** science section, Algiers.

PUBLICATION LIST:

Articles:

Essential role for collectrin in renal amino acid transport.
Danilczyk U, Sarao R, Remy C, **Benabbas C**, Stange G, Richter A, Arya S, Pospisilik JA, Singer D, Camargo SM, Makrides V, Ramadan T, Verrey F, Wagner CA, Penninger JM. Nature. 2006 Dec 21;444(7122):1088-91.

Renal acid-base transport: old and new players.
Wagner CA, Kovacikova J, Stehberger PA, Winter C, **Benabbas C**, Mohebbi N. Nephron Physiol 2006 Jan;103(1):1-6.

Abstracts:

Role of the proton-activated receptor OGR1 in the Regulation of ion transport and acid-base balance.
Benabbas C, Mohebbi N, Velic A, Ludwig MG, Gasser J, Seuwen K, Wagner CA. Opening Symposium of the Center for Integrative Human Physiology (CIHP), Zurich-Switzerland September 2005.

The pH-sensitive G-Protein coupled receptor OGR1 is expressed in kidney.
Mohebbi N, Ludwig MG, **Benabbas C**, Seuwen K, Wagner CA. J Am Soc Nephrol 2005, October; Vol. 16, Th-PO023.

Role of the proton-activated receptor OGR1 in the regulation of ion transport and acid-base balance.
Benabbas C, Mohebbi N, Velic A, Ludwig MG, Seuwen K, Wagner CA. Acta Physiologica 2006; Vol. 188, Suppl. 651:P23.

The pH-sensing receptor GPR4 is required for normal acid-base and electrolyte balance.
Velic A, **Benabbas C**, Suply T, Seuwen K, Wagner CA. 2nd Symposium of the Center for Integrative Human Physiology (CIHP), Zurich, Switzerland September 2006.

Regulation of renal ion transport by the proton-activated receptor OGR1.
Benabbas C, Mohebbi N, Velic A, Ludwig MG, Gasser J, Seuwen K, Wagner CA. 2nd Symposium of the Center for Integrative Human Physiology (CIHP), Zurich, Switzerland September 2006.

Regulation of ion transport by the proton-activated receptor OGR1.
Benabbas C, Velic A, Mohebbi N, Ludwig MG, Gasser J, Seuwen K, Wagner CA. JASN 2006 November; Vol. 17, F-PO1031.

The putative proton sensing receptor GPR4 is required for normal acid-base and electrolyte balance.
Velic A, **Benabbas C**, Suply T, Seuwn K, Wagner CA:, JASN 2006 November; Vol. 17, SA-PO004.

The ovarian cancer G-protein coupled receptor 1 (OGR1) modulates the activity of the vacuolar H+-ATPase and Na+/H+ exchangers.
Mohebbi N, **Benabbas C**, Velic A, Ludiwg MG, Seuwen K, Wagner CA.
Meeting German Physiological Society, Hannover, Germany 2007.

The proton-activated receptor OGR1 regulates renal magnesium handling.
Chahira Benabbas, Mohebbi N, Velic A, Ludwig MG, Gasser J, Seuwen K, Wagner CA. Asher-Hess competition, the Swiss Physiological Society, in Bern, Switzerland July, 2007.

Oral presentation:

87th Annual Meeting German Physiological Society, Hannover, Germany March 2007.
Regulation of renal ion transport by the proton-activated receptor OGR1.

Asher-Hess competition, the Swiss Physiological Society, in Bern, Switzerland July, 2007.
The proton-activated receptor OGR1 regulates renal magnesium handling.